# A QUANTITATIVE ANALYSIS OF SWIMMING POOL RECIRCULATION SYSTEM EFFICIENCY IN RETURNING WATER TO THE TREATMENT SYSTEM

by

Nathan Thomas Madding

A thesis submitted to the faculty of
The University of North Carolina at Charlotte
in partial fulfillment of the requirements
of the degree of Master of Science in
Civil Engineering

Charlotte

2015

Approved by:

_____
Dr. James E. Amburgey

_____
Dr. James D. Bowen

_____
Dr. Olya S. Keen

# ABSTRACT

NATHAN THOMAS MADDING. A quantitative analysis of swimming pool recirculation system efficiency in returning water to the treatment system. (Under the direction of DR. JAMES E. AMBURGEY)

While chemical reactors have been studied extensively, little work had been done in understanding the recirculation system efficiency of swimming pools. It was proposed by Gage and Bidwell (1926) that recirculation in swimming pools was described by their "Law of Dilution". They stated that the recirculation efficiency (or contaminant removal efficiency) in a swimming pool followed an ideal exponential decay model. The recirculation efficiency is defined as the percentage of the pool volume and contaminant load that reaches the treatment system during a "turnover" period. Following the Gage and Bidwell model, a pool would only remove approximately 63% of the initial contaminant concentration during any turnover period when using a 100% efficient filter since only 63% of the water is filtered per turnover period. Recent research has shown that sand and cartridge filtration are only able to achieve *Cryptosporidium* removal rates of 25 to 50% under normal US operating conditions. This has led designers and regulators to look more closely at newer treatment options like UV, membranes, and regenerative media filters that boast of removal efficiencies from 99 to 99.9999+%. Despite significant increases in both cost and complexity for many new treatment technologies, the recirculation system efficiency would limit the removal per turnover to 63% for a perfect (100% efficient) filter system according to Gage and Bidwell. Quantifying the recirculation efficiency of swimming pools allows for a more efficient overall design of pools as well as accurate prediction of contaminant removal over time.

Two bench-scale swimming pools were systematically evaluated using dye studies and salt tracer experiments. Each pool was investigated using a two-phased approach. The first phase included triplicate non-recirculating salt tracer studies in order to calculate the residence time distribution and hydraulic characteristics of each pool. Short-circuiting and mixing behavior were also visually assessed via dye studies. Triplicate salt tracer studies were performed with alternate pool flowrates and/or flow patterns to assess changes in the recirculation efficiency. In the second phase, triplicate salt tracer experiments were performed while operating the system in a recirculating mode like normal swimming pools. Pools were allowed to come to a steady-state condition to quantify the initial mixing.

Non-recirculating salt tracer studies indicated that in all experimental operating conditions salt tracer removal trends agreed with the Gage and Bidwell model with approximately 63% of the salt being removed during the first turnover. Regardless of the internal flow pattern and/or turnover rate, the hydraulic efficiency was not significantly altered. In all cases while operating the system in a non-recirculating mode, greater than 98% of the salt was removed from the system and/or conductivity detection limits were reached within 4 turnover periods. In operational modes with 1 hour or 6 hour turnovers, the exit age distribution followed a predictable exponential decay model as described by Gage and Bidwell. The exponential decay of the salt removal was approximately proportional to the flowrate divided by the system volume, multiplied by a fitting parameter of $1.00 \pm 0.11$.

In characterizing the bench-scale swimming pools, it was also important to characterize the salt tracer distribution. Describing the time and uniformity of tracer distribution emulates the time to distribute chlorine in an actual pool system. In all cases,

the time to distribute the salt tracer was less than 12% of the turnover period. During a standard 6 hour turnover period operations, the tracer typically reached peak concentration in less than 30 minutes. While operating the systems in recirculation mode, in all cases (n=6) a steady state condition was reached within 10% of the turnover period (or less than 36 minutes for a 6 hour turnover). All dye studies were performed using a standard 6 hour turnover period. Dye studies showed initial short-circuiting and uneven initial mixing. However, in all cases (n=6) the pool reached a uniform dye saturation within 2% of the turnover interval or 7 minutes.

A model was developed to determine the time needed to reach a pathogen removal goal. Pool flowrate, volume, and treatment system efficiency were used to predict the time required to obtain a specific removal percentage goal. Combined filter and UV systems of 1 to 4 $\log_{10}$ (90%, 99%, and 99.99%,) efficiency were found to reach 3 $\log_{10}$ pathogen removal at 48 hours ± 3 hours when operated using a 6 hour turnover period. This indicates that increasing the filter and UV system efficiency between 90 and 99.9% has almost no effect on overall pathogen removal efficiency for a pool despite significant increases in cost.

The overall results demonstrate that bench-scale pools recirculate in a predictable manner that is controlled by the pool's volume and flowrate. The recirculation efficiency is a bottleneck that controls the treatment system rate of removal. The required time for any given removal goal can be calculated using the recirculation model and treatment system efficiency. Pool treatment systems (e.g., UV, Ozone, and filtration) with an efficiency of greater than 90% are unlikely to justify the cost of the upgraded treatment

system since changing from 90% efficiency to 99.99% or greater would only decrease time required for the entire pool to reach 99.9% removal goal approximately 10%.

In terms of practical recommendations for future pool designers, the design of inlets and outlets has little effect on recirculation system efficiency or overall contaminant removal rates, as long as current U.S. or European design standards are met. The combined efficiencies of filtration and disinfection systems of greater than 90% ($1\log_{10}$) have little impact on contaminant removal rates due to inherent inefficiencies of the recirculation systems. Increasing the removal efficiency of current technologies such as sand and cartridge filters from 25% to 90% would provide valuable improvements. Decreasing pool turnover times (as opposed to more efficient disinfection or filter systems) appears to be the most practical means of increasing the rate of contaminant removal from pools using existing technology with removal rates of at least 90% efficiency.

# DEDICATION

This is dedicated to my wife Brooklyn and all of my family and friends. Thank you for all of your support throughout this entire journey.

# ACKNOWLEDGEMENTS

I would like to acknowledge the direction and guidance of my advisor and committee chair, Dr. James Amburgey. His guidance was vital in many aspects throughout this process. I would also like to thank my committee members, Dr. James Bowen and Dr. Olya Keen for their input and time.

A special acknowledgement goes to Amir AlAnsari. Without his assistance and input, this project would have suffered. I would like to thank Charles Murphy for his direction during the initial phase of the project and Ted Brown for his continual assistance in the many construction projects needed to complete my research. Finally, I would like to thank the National Swimming Pool Foundation for funding this project.

# TABLE OF CONTENTS

# LIST OF TABLES

# LIST OF FIGURES

# CHAPTER 1: INTRODUCTION

## 1.1 Background

Recreational water illnesses (RWIs) are a source for great concern in the recreational water industry. The inactivation and removal of *Cryptosporidium* is one of the main challenges facing pool operators today. While chlorination inactivates many of the harmful bacteria and viruses that can cause recreational water illnesses, the effects of harmful chlorine byproducts are under scrutiny (Helenius et al., 1998). Some of the more troublesome RWIs are resistant to chlorination. The protozoa *Cryptosporidium* can remain active in properly chlorinated pools for up to 10 days (Amburgey et al., 2012) *Cryptosporidium* in recreational water venues is a leading cause of cryptosporidiosis, a severe illness that can cause death in children and those who are immunocompromised (Goodgame et al., 1993). Infections from "Crypto" can be caused by as few as 10 oocysts while an infected person can shed from $6 \times 10^6$ to $1.2 \times 10^9$ oocysts a day with infections lasting up to 21 days (Chappell et al., 2006; Goodgame et al., 1993; Yoder et al., 2012). Due to its chlorine resistance, Crypto is a frequent culprit for outbreaks in recreational aquatic venues (Chappell et al., 2006; Okhuysen et al., 1999). The CDC reports a 16.9% increase in cases of Cryptosporidiosis from 2009 to 2010 with 8,951 cases reported in 2010 (Yoder et al., 2012).

To remove these chlorine-resistant pathogens, aquatic venues typically use methods of treatment such as diatomaceous earth, cartridge, or sand filtration, as a primary treatment

system. Even when properly operated and maintained, these treatment systems provide 25% to 99.9% of *Cryptosporidium* oocyst removal per filter pass (Amburgey et al., 2009; Amburgey et al., 2012; Croll et al., 2007; Hayes et al., 2009). In order to provide another level of safety, many venues have begun using secondary treatment systems to their primary treatment systems. UV treatment has been an attractive option, promising removal rates of over 99.9%. However, even properly maintained venues using effective UV systems as secondary treatment are still susceptible to outbreaks of Crypto (Boehmer et al., 2009). To remove harmful pathogens from the pool and enhance pool clarity current pool regulations advocate that pools have a maximum turnover time of 6 hours (CDC MAHC, 2014). Ideally, during the turnover period, the entire volume of the pool would be recycled through the treatment system. The removal rates advertised for treatment systems are based only on the volume of water that actually passes through the treatment devices. These current removal rates are based on the assumption that all of the pool system water reaches the treatment system. The prevalent theory (since 1926) has been that only 63% of a pools volume actually reaches the treatment system during a turnover period. Gage and Bidwell's "Law of Dilution" states that only 63% of the pool's water reaches the treatment system during any given turnover period (Gage et al., 1926). This reduces the efficiency of the overall treatment system to the efficiency of the pool to deliver water to the system for treatment. Since 1926, pool design and treatment has progressed using only a passing mention of Gage and Bidwell's work to form regulations. Very little work has been done to investigate the efficiency of the recirculation system of pools in delivering water to the treatment system. Understanding pool recirculation efficiency has great implications for treatment system operation and the handling of RWI incidence.

## 1.2 Research Objective

The primary objective of this research project was to conduct a quantitative analysis of the hydraulic efficiencies of swimming pools to better understand the implications of turnover period and interior mixing as it applies to returning water to the treatment system. The individual project objectives are listed below.

- Quantify how efficiently water is returned to the treatment system of two 1:25 scale swimming pools.
- Determine whether the recirculation efficiency of a given swimming pool can be changed by modifying the turnover period or flow pattern.
- Evaluate the impact of recirculation efficiency on the choice of filtration system and/or UV system design
- Provide pool owners and operators with a quantifiable model of treatment efficiency of swimming pools to promote the selection of cost-effective treatment system components.

## 1.3 Research Approach

A study of swimming pool hydraulics was systematically carried out using two bench-scale pools. Two phases were carried out for each bench-scale pool. The first phase consisted of tracer studies without recirculation of the system to quantify the hydraulic efficiency of moving water to the treatment system and evaluate the hydraulics of the pool system. In the second phase, recirculation was introduced to the system to simulate normal pool operating conditions and describe the initial distribution of the salt tracer.

# CHAPTER 2: LITERATURE REVIEW

## 2.1 Tracer Studies

Tracer studies using compounds that change the conductivity of water can be performed efficiently with online instruments. Experiments using salts must take care not to over dose and create density gradients. Salt tracers must be adequately mixed into the reactor flow to avoid density currents, and the injection time should be as quick as possible to accurately produce a pulse input (Teefy, 1996; Terashima et al., 2013). Temperature can also significantly affect conductivity and must be corrected for (Teefy, 1996). Salt tracers with significantly different densities can influence the flow patterns with the denser tracer flowing into deeper regions due to gravity effects. Ideally, tracer solutions should be mixed to be equal to the density of the reactor fluid (Terashima et al., 2013). Density differences can also deform the residence time distribution curve and impact quantifying the reactor. (Chen et al., 2012; Teefy, 1996). In comparing salt tracers, Chen (2012) found highly-concentrated salt pulse tracers appeared earlier and peaked higher than calculated in residence time distribution (RTD) curves. This result suggests a density current of tracer that flowed directly to the drain, short-circuiting the main volume of the reactor. The high concentration tracer also created a "stair-step" decay in the RTD curve that degraded the ability to accurately analyze the RTD curve (Chen et al., 2012). A dimensionless tracer amount (DTA) was developed as the ratio of tracer to total volume (Chen et al., 2012). The DTA for KCl is shown in Table 2.1.

The comparison of tracers also found that properly dosed KCl tracers more closely followed calculated RTD curves than properly dosed NaCl tracers (Chen et al., 2012).

Table 2.1: KCl tracer range (DTA) (Chen et al., 2012)

| KCl | Low | Optimal | High |
|---|---|---|---|
| Dimensionless Tracer Amount | $0.191 \times 10^{-3}$ | $0.202 \times 10^{-3}$ | $1.053 \times 10^{-3}$ |

Test duration should be performed for at least three to four times the mean residence time as calculated in equation 2.1. Typically, three detention times should allow for a quick determination of dead zones and experiment length can be adjusted if need. During tracer studies, the volume and flow rate should remain constant (Teefy, 1996).

$$\tau = \frac{V}{Q} \tag{2.1}$$

where: $\tau$ = mean residence time
V = reactor Volume
Q = volumetric flow rate

## 2.2 RTD Models

To quantify and understand swimming pool hydraulics, it is often useful to think of pools as reactors. A reactor is a vessel or container in which a reaction takes place. Compounds like chlorine and urea constantly react while in swimming pools. The kinetics of chemicals like chlorine can be understood by applying reactor theory and models. The flow pattern of a swimming pool can be compared to a continuous flow reactor, where a continuous flow of treated water enters the pool while a continuous flow of water exits the pool to the treatment system. Compounds and chemicals are introduced to the pool via

treatment systems and bathers. The behavior of these reactors is affected by many factors. Inlets, skimmers, drains, and bather activity are all parameters that can be used to quantify and predict contaminant fate and transport in swimming pools using mixed reactor models. The shape and design of the reactor as well as the position of the inlets and outlets can have a great effect on the hydraulics and mixing of the reactor (Kjellstrand et al., 2005). There are many mathematical reactor models that quantify the flow patterns, kinetics and molecular reactions in reactors (Crittenden et al., 2012). The application of reactor models can be applied to swimming pools to quantify hydraulic efficiency, mixing, short-circuiting, dead volumes, and to predict reaction kinetics.

One method of describing reactors is by the flow characteristics. Batch reactors are mixed, performed to completion, and then emptied. Conversely, continuous flow reactors operate with a continuous flow into and out of the reactor. A reactor in continuous flow operation has the reactants added to the reactor without interrupting the flow. Continuous flow reactors may be further broken down to describe their hydraulic characteristics (Crittenden et al., 2012; Fogler, 2005; Levenspiel, 1972). Laminar flow reactors, plug flow reactors, and completely mixed reactors are often used to describe most reactor types.

Reactors can also be described as ideal or non-ideal. In an ideal reactor, assumptions are made regarding mixing, dispersion, and flow. Ideal reactors are often possible in laboratory settings. Non-ideal reactors are typically more complex than ideal reactors, and the same assumptions cannot be made about their operation. Continuously stirred tank reactors (CSTR) and plug-flow reactors (PFR) describe the mixing in the reactor and configuration (Crittenden et al., 2012). The mixing in an ideal CSTR is completely mixed throughout the entire reactor while a PFR is completely unmixed. In a

PFR particles move through the reactor as a slug, with no mixing. Combinations of CSTRs and plug-flow reactors are possible, as are multiple inline CSTRs, called CSTRs in series (Fogler, 2005; Levenspiel, 1972).

A completely mixed reactor in which no reaction occurs, such as with an inert tracer, can be defined mathematically as the change in concentration over time as equal to the system mass balance:

$$\left[\frac{\partial(C \cdot V)}{\partial t}\right] = Q \cdot C_{in} - Q \cdot C \tag{2.2}$$

Where: C = concentration leaving the reactor
V = Volume of reactor
$C_{in}$ = Concentration entering the reactor
Q = Reactor flow

Aside from a simple mass balance, not much was understood regarding reactors prior to the 1930's. In the 1930's the concept of the residence time distribution (RTD) was described by MacMullin and Weber (1935) as a method of quantifying the reactor. The RTD function quantifies the amount of time a particle spends inside a reactor. The concept of the RTD was further refined and organized by Danckwerts in the 1950s (Danckwerts, 1953; Fogler, 2005). Danckwerts described the RTD as the distribution of the time it takes for a particle of fluid to pass through a reactor (Danckwerts, 1953). The RTD is often described using two curves; the exit age distribution (E curve) and the cumulative exit age (F curve). The exit age distribution can be simply thought of as quantifying the time a particle has spent in the reactor and is defined mathematically as

$$E(t) = \frac{C(t)}{\int_0^\infty C(t)dt} \tag{2.3}$$

where: C (t) = concentration leaving reactor at time t
t = time

E (t) = exit age distribution

The cumulative exit age distribution defined by Danckwerts is the integration of the exit age distribution from 0 to t.

$$F(t) = \int_0^t E(t)\,dt \tag{2.4}$$

where: E (t) = exit age distribution
F (t) = cumulative exit age

By integrating the E (t) curve and analyzing the resulting F (t) curve, the percentage of molecules spending less than time t in the reactor can be determined. A F(t) at time 10 minutes of .25 means that 25% of the particles in the reactor spent less than 10 minutes inside the reactor before exiting (Crittenden et al., 2012; Danckwerts, 1953; Fogler, 2005). Another important factor in quantifying a reactor is the mean residence time, $\tau$, is the time needed for one full reactor volume to enter and exit the reactor based on the reactor flow (Fogler, 2005). In swimming pools, the mean residence time can be thought of as the calculated turnover time.

The variance, $\sigma^2$, is another important variable in quantifying reactors. The variance describes the amount of mixing in a reactor. An ideal CSTR has a variance of 1 (Cloteaux et al., 2011; Stamou, 2008). A variance close to 1 indicates a reactor that is close to an ideal CSTR. No mixing in a reactor gives a variance of 0 (Levenspiel, 1972; Teefy, 1996).

In order to compare reactors, it is often necessary to standardize the E (t) and F (t) functions. When normalized for time and concentration, different reactors can be compared directly to each other (Fogler, 2005). Referring to Danckwerts' work, the Greek

symbol θ is used as the parameter for normalized time. In formalizing the residence time distribution Danckwerts also lays out normalized time, θ, as the age of the particle as it leaves the reactor while the function E(θ), the exit age distribution, is the fraction of particles leaving the system at time θ (Danckwerts, 1953; Teefy, 1996).

$$\theta = \frac{t}{\tau} \tag{2.6}$$

where: θ = normalized time
t = time
τ = mean residence time

$$E(\theta) = \tau E(t) \tag{2.7}$$

where: E (θ) = normalized exit age distribution
E (t) = exit age distribution
τ = mean residence time

$$F(\theta) = \int_0^{\theta} E(\theta)\, d\theta = 1 \tag{2.8}$$

where: F (θ) = normalized cumulative exit age distribution
E (θ) = normalized exit age distribution
θ = normalized time

The normalized F(θ) cumulative exit age function approaches unity when E(θ) is integrated with respect to infinity (Teefy, 1996).

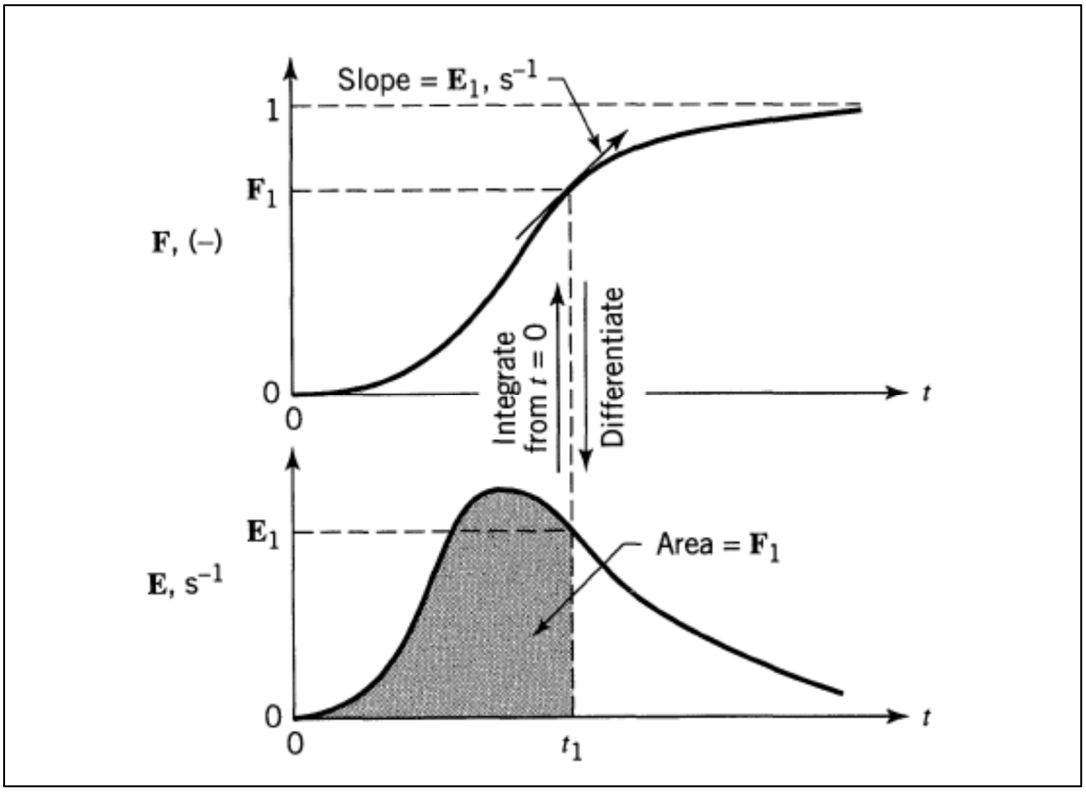


Figure 2.1: E and F curve relationship (Levenspiel, 1972)

The shapes of the curves created by the exit age distribution, the E curve, and the cumulative exit age distribution, the F curve, are useful in describing the performance of a reactor. Comparing normalized E and F curves also allows for the quantifying of non-ideal reactors. By comparing ideal and non-ideal reactor curves, conclusions can be drawn regarding mixing, bypass and dead volumes, and system efficiency (Crittenden et al., 2012; Danckwerts, 1953; Fogler, 2005; Levenspiel, 1972; Stamou, 2008; Tsai and Chen, 2013).

The RTD curves of reactors give many visual clues to problems inside non-ideal reactors. Ideal CSTR reactor RTD curves follow exponential decay models shown in Figure 2.2. The curves of reactors with dead volumes or bypass show also possess characteristic curves when viewed alongside an ideal reactor curve as shown in Figure 2.3.

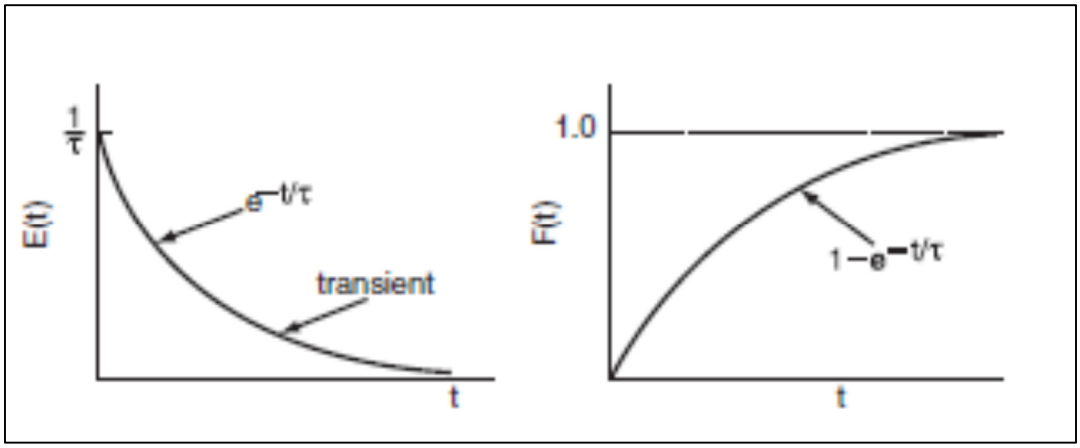


Figure 2.2: Ideal CSTR RTD curves (Fogler, 2005)

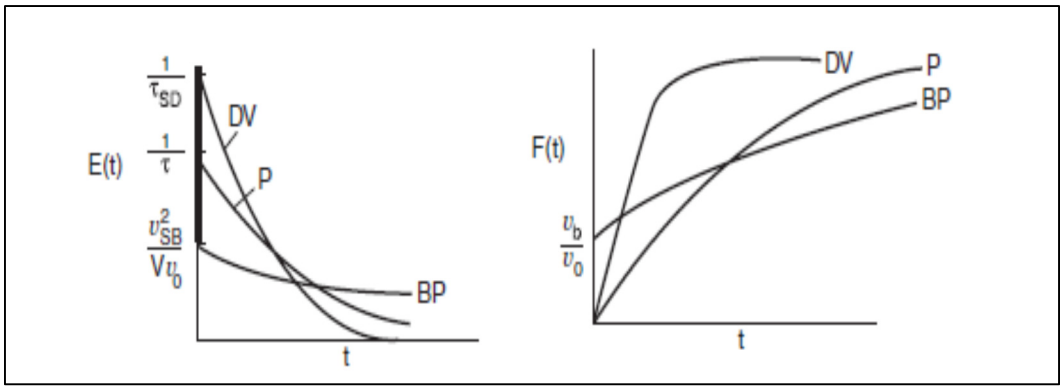


Figure 2.3: RTD curves for three reactors, dead volume = DV,
P = perfect/ideal, BP =bypass (Fogler, 2005)

Using τ, the RTD can also be described including the peak and slope of an ideal CSTR reactor. For an ideal CSTR the slope of the RTD is an exponential decay as shown in Figure 2.2. The tail, known as the transient, is also affected by the τ. A large τ will create a long and slowly decaying slope, while a short τ will give a short, quickly decaying tail. Reactors with bypassing or dead volumes give different peaks and slopes. By comparing the RTDs of the reactor, the amount of bypass or volume of dead zones can be determined.

According to Fogler, the tail of a CSTR can be approximated using an exponential decay model with very few inaccuracies due to the numerical minuteness range of measurements. Long trailing tails on RTD curves are also a sign of dead zones in the reactor as described below (Fogler, 2005)

In an ideal reactor, it is assumed that the internal flows and particle mixing is instantaneous and homogenous. However, in most reactors and non-ideal reactors the possibility of bypass and dead volumes must be accounted for when quantifying the reactor. Utilizing the RTD curves, it is possible to calculate the amount of bypass and dead zones.

In bypassing, a certain percent of the flow bypasses the reactor. In some reactors, the bypass enters the reactor but short-circuits the mixing zone and exits the reactor without properly mixing. By bypassing or short-circuiting the reactor the mean residence time is increased above the calculated mean residence time so that $\tau_b > \tau$.

$$\tau_b = \frac{V}{\nu_t - \nu_b} \tag{2.9}$$

where: $\tau_b$ = mean residence time with bypass
$V$ = reactor volume
$\nu_t$ = total volumetric flow
$\nu_b$ = volumetric flow bypassed

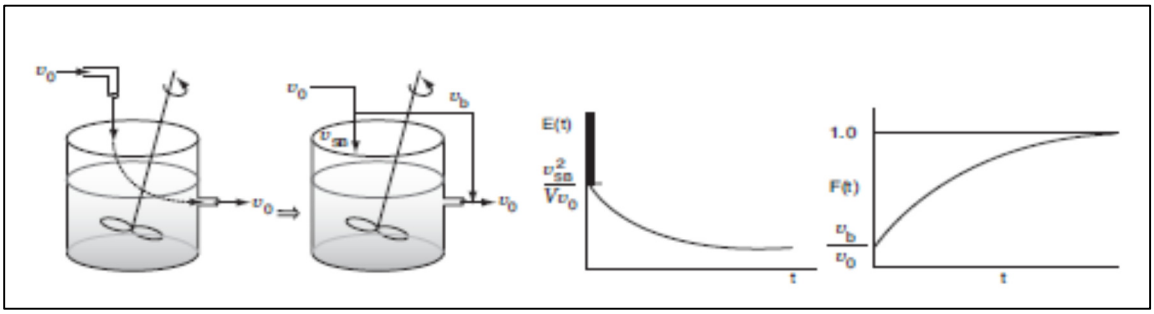


Figure 2.4: System diagram of reactor with short circuiting, and bypass (Fogler, 2005)

Another type of non-ideal reactor involves a reactor with dead zones. In a reactor with a dead zone, the active volume is less than the total volume, and thus less volume participates in mixing.

$$V = V_a + V_d \tag{2.10}$$

where: V = total volume
Va = active volume
Vd = dead volume

The dead volume also affects the mean residence time where $\tau_d < \tau$ dead volumes are often quantified as fractions of the total volume so that if $V_d = .25V$ then $V_a = .75V$. The reduction in active volume produces a reduced mean residence time for the reactor with dead zones. The reduction of the mean residence time creates long trailing tails on the exit age distribution curve (Fogler, 2005).

$$\tau_d = \frac{.75V}{\nu} = .75\tau \tag{2.11}$$

where: $\tau_d$= mean residence time with 25% dead zone
$\tau$ = mean residence time
V = Volume
$\nu$ = volumetric flow

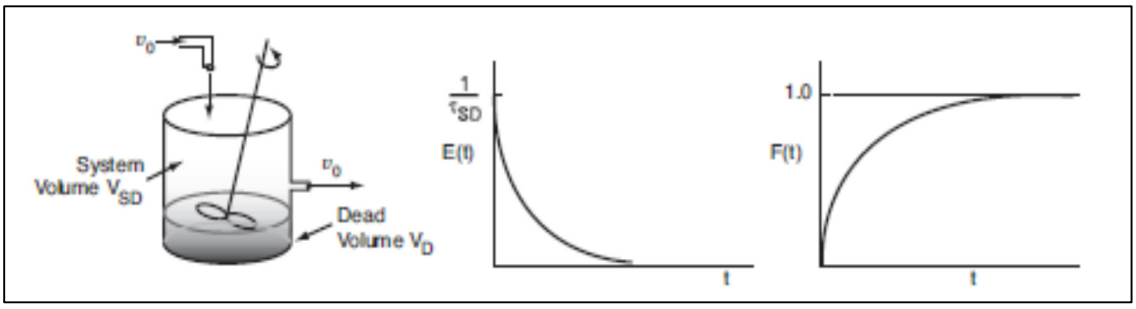


Figure 2.5: System diagram of reactor with dead volume (Fogler, 2005)

## 2.3 Application of RTD to Swimming Pools

Very little has been done using the residence time distribution to describe swimming pools, their hydraulics, or improving upon current designs. Prior to MacMullin and Weber's description of the exit age distribution curve of an ideal reactor, Gage and Bidwell predicted the results but no examples of their work on the topic survive. They accurately predicted the efficiency at which a pool would remove an initial concentration of dirty water. While it is unknown how they reached their conclusions, their numbers match an exponential decay model of an ideal CSTR. In their calculations, an ideal filter was in place so that any water that reached the filter would have 100% of contaminants removed. However, current treatment systems do not match ideal filter performance. Sand filtration treatment systems remove up to 25% of pathogens (Amburgey et al., 2012). Other treatment systems are typically used in drinking water systems and must be rated to removal rates of 99.9%. This has led to the adoption of drinking water removal rates (99.9%) becoming a common swimming pool disinfection standard. Furthermore, Gage and Bidwell predicted that at one turnover 63% of the containments would be removed, at two turnovers 86% removal and so forth, shown in Table 2.2 (Gage et al., 1926). These results compare favorably with an exponential decay model also shown in Table 2.2. It is obvious Gage and Bidwell made the assumption that swimming pools perform as an ideal CSTR with regards to mixing, hydraulics and efficiency.

Table 2.2: Removal per turnover

| Turnovers | 1 | 2 | 3 | 4 | 5 | 6 | 10 |
|---|---|---|---|---|---|---|---|
| Gage and Bidwell (1926) | 63 | 86 | 95 | 98 | 99.3 | 99.7 | 99.99 |
| Exponential Decay | 63.21 | 86.47 | 95.03 | 98.17 | 99.33 | 99.76 | 99.9998 |

The application of the residence time distribution curves allows swimming pools to be quantified in a more accurate manner, taking into account that mixing and hydraulics are likely to be non-ideal. Many factors impact the mixing and hydraulics of a swimming pool: flow rate and turnover period, inlet and outlet configuration and geometry (Cloteaux et al., 2011; Cloteaux et al., 2013; Stamou, 2008).

Pools with a 50/50 drain to overflow ratio were investigated to quantify effluent flow characteristics and produce RTD curves. Cloteaux (2011) investigated a wide variety of inlet and outlet configurations as well as a mix of flow patterns. A yttrium and nitric acid solution was used as a tracer and injected into the inlet stream. Samples were taken from specified location around the pools at 5 and 10 minute intervals. The yttrium was analyzed using Inductively Coupled Plasma-Atomic Emission Spectrometry (ICP-AES). Results showed an initial mixing and peak within $0.3\theta$. A convergence and stabilization of all sample sites occurred by $0.5\theta$.

Utilizing tracer studies with computational fluid dynamics (CFD), modeling short-circuiting in some of the experiments did not significantly affect the RTD or mean residence time of the systems. Based on their results, the conclusion can be drawn that the number and position of inlets and outlets has little effect on the RTD. A final conclusion indicated that the pools behavior closely followed an ideal CSTR (Cloteaux et al., 2013) similar to Gage and Bidwell's 1926 conclusion.

Important work was done by Stamou (2008) in describing the characteristics of disinfection tanks. His methods and conclusions are directly applicable to swimming pools, both in terms of geometry, flows, and mixing. Utilizing CFD flow fields, Stamou created RTD curves for nine disinfection tanks of varying geometry and flow patterns. The

resulting RTD curves were compared to assess short-circuiting, mixing and efficiency parameters. The normalized RTD curves were characterized using the parameters and indicators in Table 2.3. By comparing the indicators to ideal CSTR and plug flow reactors, a tank can be described with precision. High values for $\theta_0$ and $\theta_{10}$ indicated short-circuiting. Uniform and complete mixing was defined as variance ($\sigma^2$) value of 1 (Stamou, 2009).

Table 2.3: Characteristics and indicators (Stamou, 2008)

| Characteristic | Indicator | CSTR |
|---|---|---|
| Short-circuiting | $\theta_0$ | 0.000 |
| | $\theta_{10}$ | 0.105 |
| Mixing | variance ($\sigma^2$) | 1.000 |

Liu's (Liu, 2011) study on continuous stirred tank reactors (CSTR) is also applicable to swimming pools as reactors. Tanks with impellers were studied, including baffle walls, and two separate inlet/outlet configurations. When adding a tracer, Liu found two distinct stages. The initial stage begins with the tracer input increased until it became homogenous. This spike in the initial stage is location dependent, as not all areas of the reactor will have become mixed during this stage. In stirred reactors, the initial spike of tracer lasted the approximate length of the equivalent time it would take to uniformly and completely mix a CSTR during initial startup.

Practically, the exit age distribution can be used in two ways. The initial rising phase of the curve calculates the time needed to distribute a solution into the system. The slope and peak of this section of the curve predicts the rate of chlorine distribution in to a pool system. The decay of the curve from the peak can also be fitted to an exponential

decay model to allow comparisons of different pool systems. The second curve, the cumulative exit age, plots the removal of the tracer from the system against time. Practically this curve calculates the hydraulic efficiency of a pool system to return water to the treatment system.

In short, three characteristics can be used to describe a pool system accurately. The time to peak of the exit age distribution being used to describe chlorine distribution. Exit age distribution decay and cumulative exit age are used to predict and describe the time to recirculate all or part of the volume of the pool.

# CHAPTER 3: METHODS AND PROCEDURES

## 3.1 Scale Pool Design

### 3.1.1 1:25 Scale Junior Olympic Pool

The first pool built was a 1:25 bench-scale Junior Olympic swimming pool modeled on the UNC Charlotte campus pool. The scale pool was constructed to replicate both the dimensions, flow patterns and piping layout. Like the campus pool, this pool feature a shallow end, a transitional zone and a deep end (Figure 3.1). The scale pool was constructed using clear 0.6 cm thick acrylic and is 91 cm wide by 103 cm long with a the total volume of 87 Liters. The shallow end was 5 cm deep while the deepest portion was 15.5 cm deep. The pool has three bottom drains, eight skimmer outlets, and 7 jet inlets per side. The skimmers were located at the surface of the water while the inlets were submerged by 30 mm. Three drains were located at regular intervals in the deepest section of the pool. Figure 3.1 and Figure 3.2 show the dimensions of the scale pool and the locations of the inlets and outlets. Froude numbers and Camp and Stein velocity gradient ($\bar{G}$) values were calculated and compared for both bench-scale and full-scale pools to ensure proper scaling. For calculations and mixing values refer to APPENDIX C.

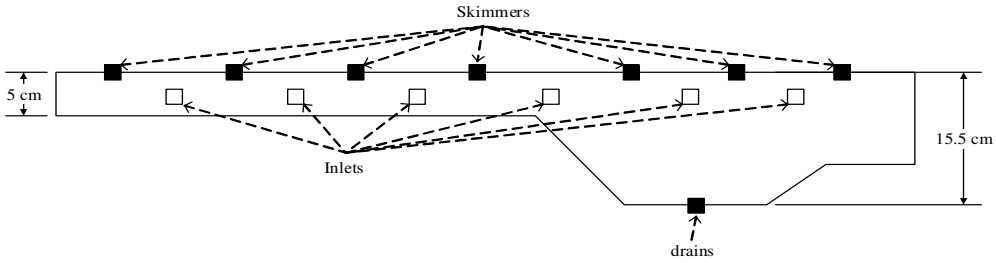


Figure 3.1: Cross section of 1:25 Junior Olympic pool

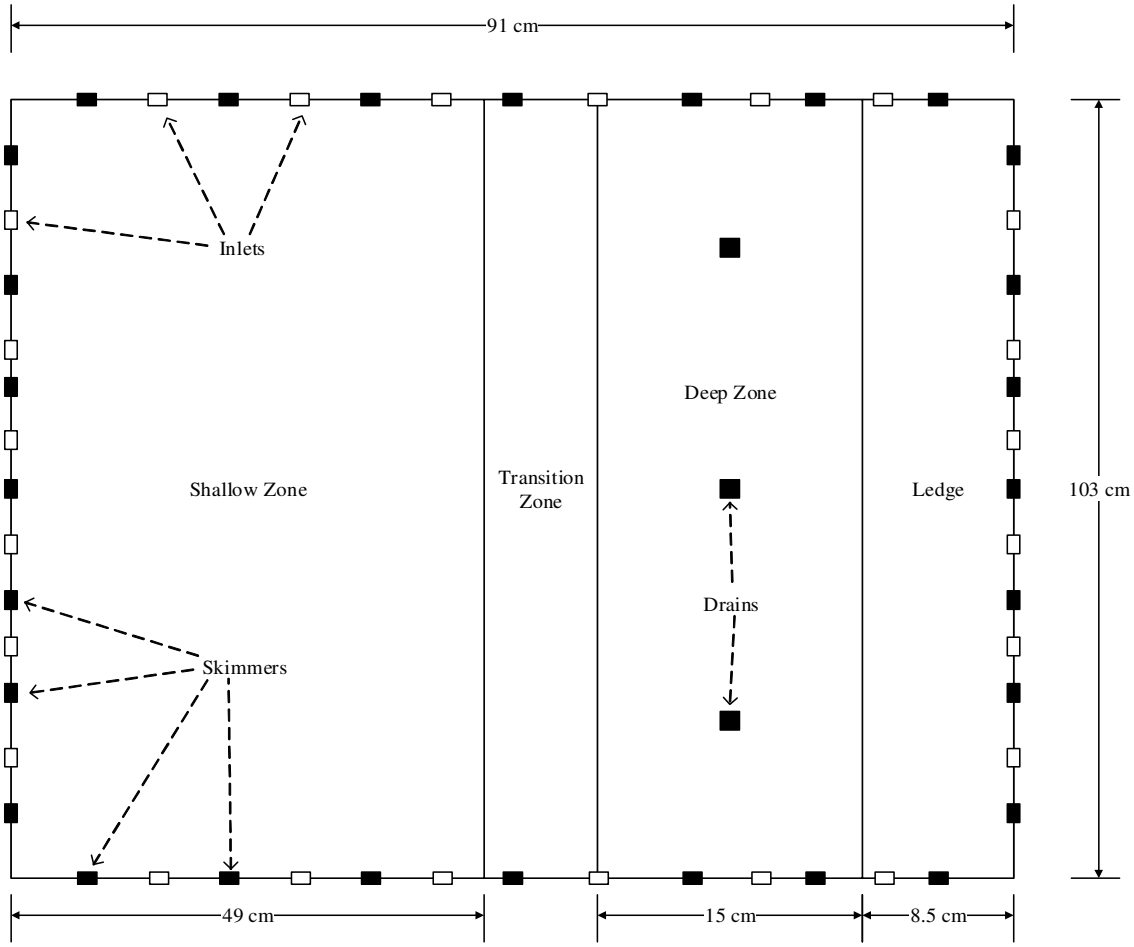


Figure 3.2: Plan view of 1:25 Junior Olympic pool

### 3.1.2 1:25 Scale Upflow Pool with Bottom Inlets

The second scale pool built was a 1:25 scale model of a pool with bottom mounted inlets and perimeter overflow. The pool feature a shallow zone and a deep zone with a uniformly sloped pool bottom (Figure 3.3). This pool was also constructed using clear 0.6cm thick acrylic and is 51 cm wide by 101 cm long with a the total volume of 46.5 Liters. The shallow end was 5 cm deep while the deep end was 7.8 cm deep. The pool has 21 bottom mounted inlets. The overflow flows over the edge of the pool into a trough

along the edge of the pool. Figure 3.3 and Figure 3.4 show the dimensions of the scale pool and the locations of the inlets and overflow outlet.

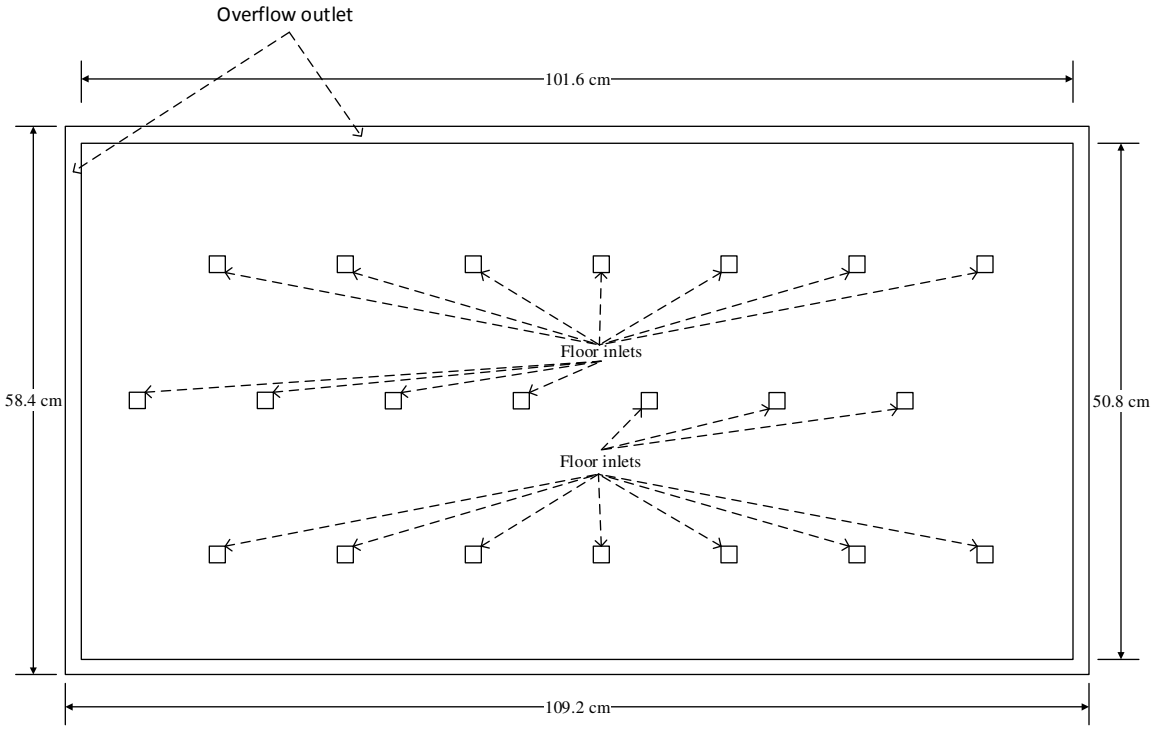


Figure 3.3: Plan view of 1:25 upflow pool

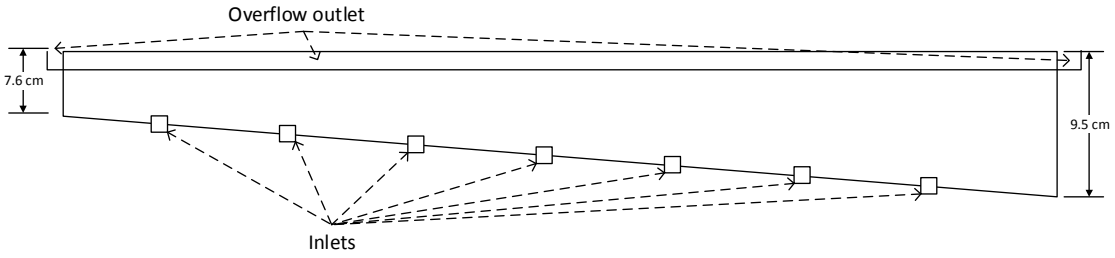


Figure 3.4: Cross section of 1:25 upflow pool

The inlets, skimmers and drains for the 1:25 Junior Olympic pool were fabricated by joining a 1/16$^{th}$ inch polypropylene nozzle into a ¼ inch threaded polypropylene fitting (Figure 3.5). These fittings, with single barb ends, were connected with flexible tubing.

The inlets and skimmers were separately plumed in series with flexible silicone tubing and controlled by their respective pumps.

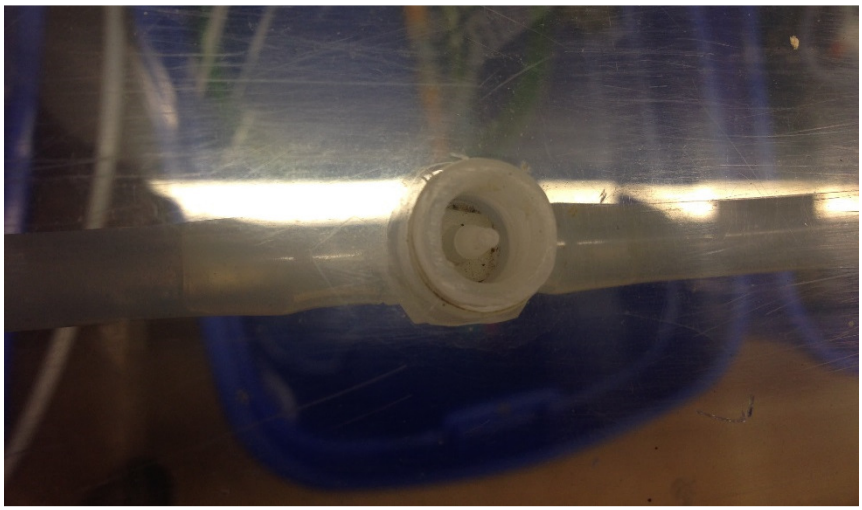

Figure 3.5: Inlet and skimmer detail

The inlets, skimmers and drains for the 1:25 upflow pool were fabricated by joining a 1/16$^{th}$ inch polypropylene nozzle into a ¼ inch threaded polypropylene fitting (Figure 3.6). A stainless steel rod and plastic cover was fabricated to direct the flow laterally. This spread flow evenly across the pool floor and prevented jets in the pool surface.

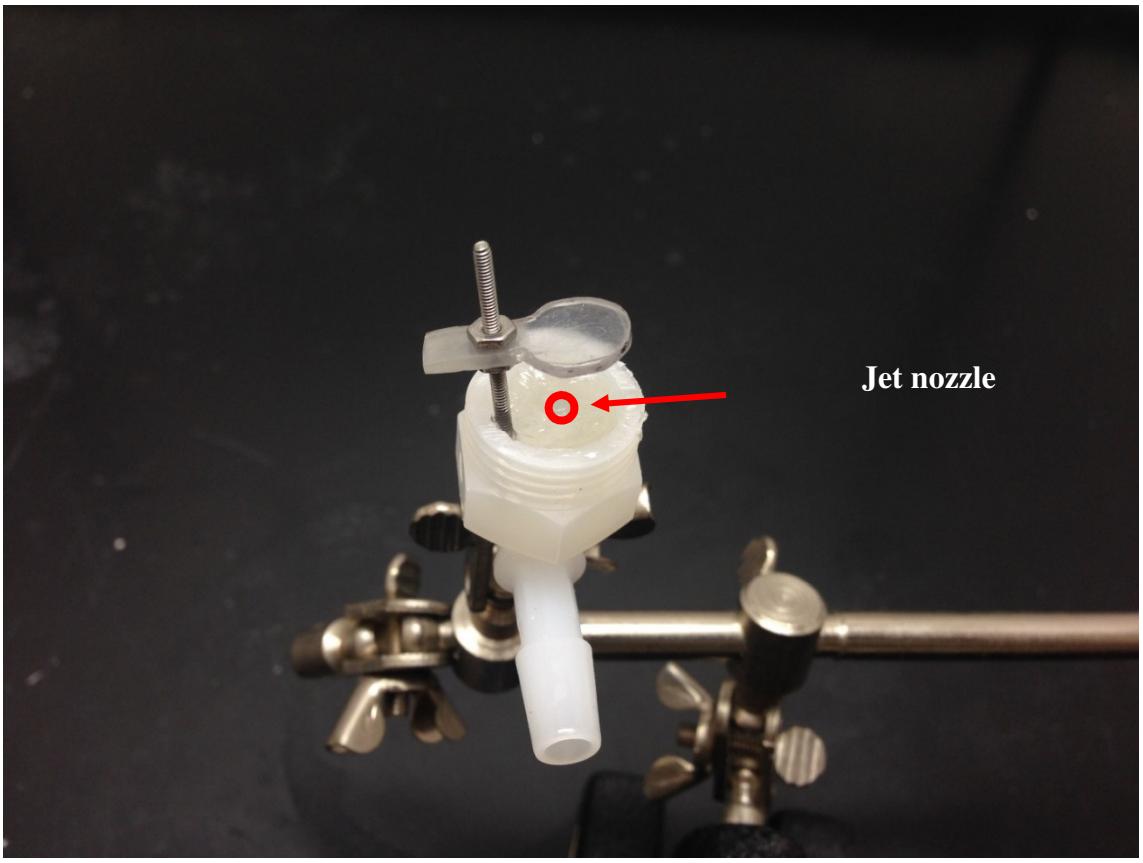


Figure 3.6: Bottom mounted jet with screw and flange detail

## 3.2 Scale Pool System Setup

The scale pool setup was designed to allow for easy modifications to flow patterns and to quickly transition from a non-recirculating system to a system with recirculation. Flexible tubing was used wherever possible to allow for the easy addition or removal of pumps, flowmeters and pulse dampeners. A diagram of the system is shown in Figure 3.7. Deionized water (DI) with an average conductivity less than 1 µS/cm was continuously supplied to the system via the DI tap in the research lab. System flow was controlled by a digital peristaltic pump (Thermo Scientific, Masterflex P/S) with two pump heads (Cole-Parmer, 7518-10) using thick-walled, ¼" internal diameter, L/S 18 tubing . The main flow

was split after the pump to supply the left shallow corner and right deep corner of the pool, respectively. These lines were further split to supply the left side/shallow end and right side/deep end inlets. The influent plumbing is shown in Figure 3.8. Flexible tubing (Cole-Palmer, L/S 15) was used throughout the system except for the DI water supply and effluent lines which used a ¼ inch and ½ inch rigid LDPE tubing, respectively. Influent flowrate was measured using a Coriolis flowmeter (Endress-Hauser, Promass 83A04) upstream of the influent supply pump. The flowmeter measured flow in mL/min and the flow was recorded in 10 second intervals.

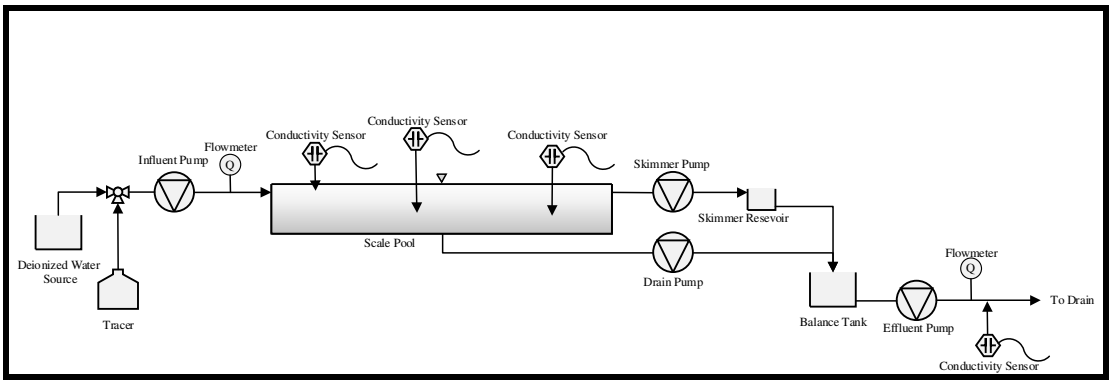


Figure 3.7: System without recirculation

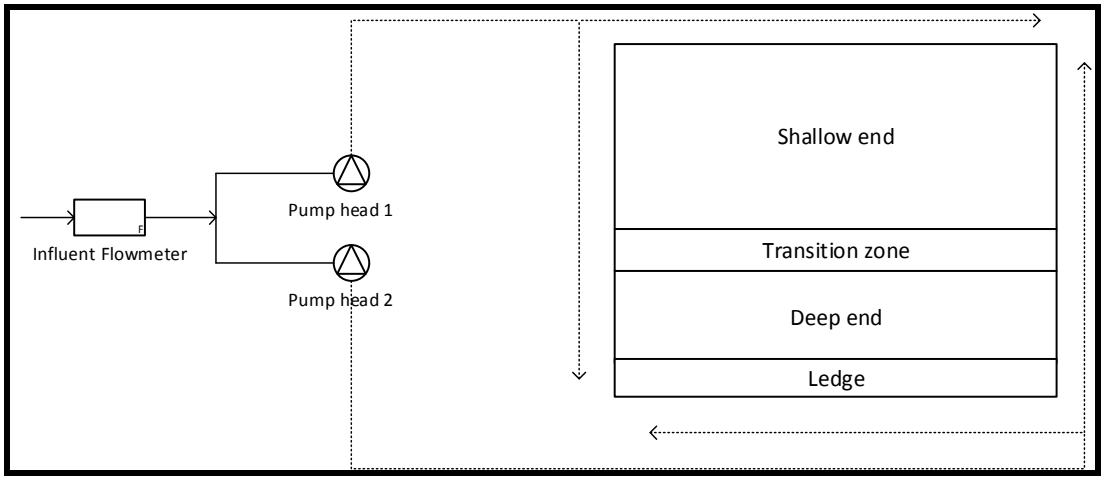


Figure 3.8: Influent flow diagram

The effluent was broken in two systems, skimmers and drains, shown in Figure 3.9. Both skimmers and drains used 1/16$^{th}$ inch openings described below. The skimmers were plumbed in series using flexible tubing (Cole-Palmer, L/S 15). Skimmer effluent was pumped by a digital peristaltic pump (Cole-Parmer, Masterflex) with two pump heads (Cole-Parmer, 77200-62) using L/S 24 tubing. Water from the skimmers was pumped the skimmer reservoir where it drained into the 2L balance tank. Three floor mounted drains were located in the deep region of the pool. These drains were controlled by a digital peristaltic pump (Cole-Parmer, Masterflex) with pump head (Cole-Parmer, 7518-02) using L/S 24 tubing. The drains were pumped directly into the balance tank. Water from the balance tank was pumped using a digital peristaltic pump (Thermo Scientific, Masterflex P/S) with pump head (Thermo Scientific, 956-000) using L/S 24 tubing to through a flowmeter (Krohne, Optimass 7050C) and to waste. The flowmeter measured flow in mL/min and measurements were recorded at 10 second intervals.

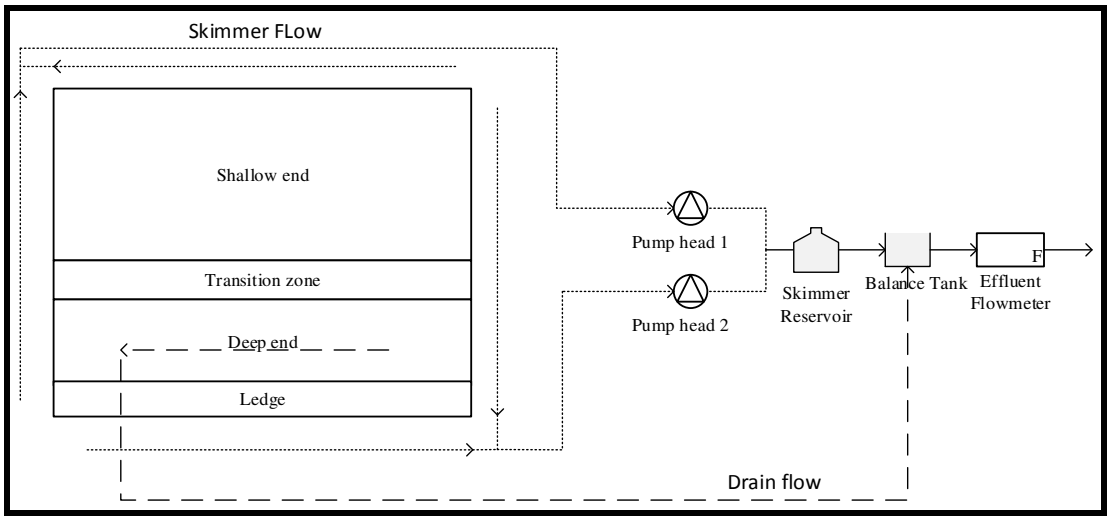


Figure 3.9: Skimmer and drain flow diagram

An analog to digital data acquisition device (Measurement Computing, 1208LS) was used to connect the flow meters, leak warning systems and conductivity sensors to the computer. The computer ran LabVIEW 8.0 (National Instruments). The LabVIEW program recorded output from flowmeters, leak detectors and conductivity sensors at 10 second intervals.

### 3.2.1 Setup with Recirculation

In order to simulate a recirculating pool system, changes were made to recirculate the pool water. The recirculation system is shown in

Figure 3.10, in these cases the flow schematic differed from the non-recirculating system. The supply line was removed from the continuous DI source and directly connected to the balance tank. No changes were made to the influent flow diagram shown in Figure 3.8. The effluent flow diagram shown in Figure 3.9 also remained unchanged except for the removal of the effluent flowmeter.

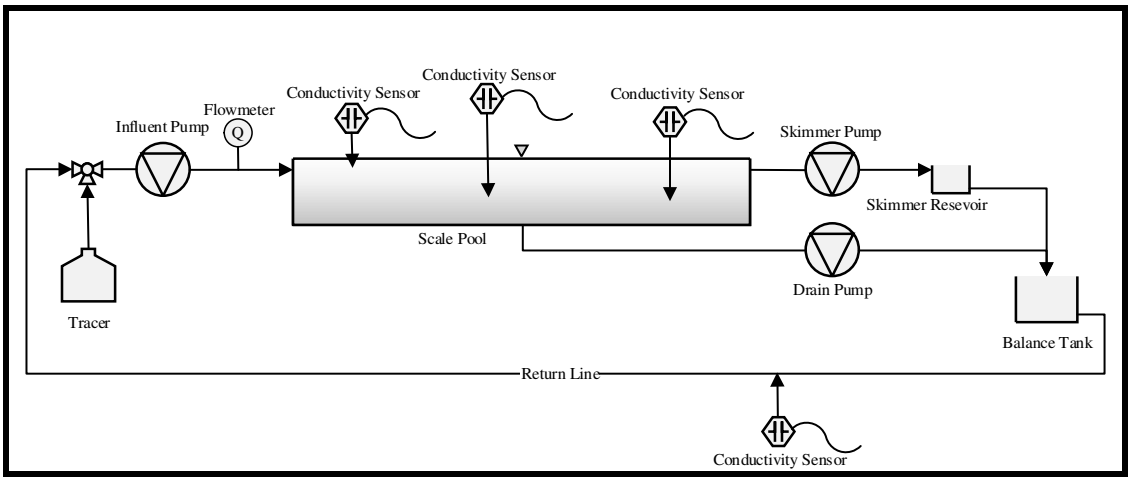


Figure 3.10: System with recirculation

### 3.2.2 Balance Tank Setup

In a full-scale swimming pool, a balance tank provides volume to accommodate water displaced by swimmers in the pool. A 2 liter beaker was used to model the balance tank in the scaled pools. The skimmers were pumped into a small reservoir that drained into the balance tank to remove air from the skimmer lines before it flowed over the conductivity probe mounted in the base of the reservoir. A small notch was formed to allow the water to flow out of the reservoir and into the balance tank. The notch was situated high enough on the wall to ensure the sensor was continuously covered as the water passed through the reservoir as shown in Figure 3.11. The drains were pumped directly into the balance tank. The balance tank was then pumped to the effluent conductivity sensor, and then to waste. The balance tank also provided overflow volume to ensure a proper water mass balance. Figure 3.12 shows the balance tank and skimmer reservoir.

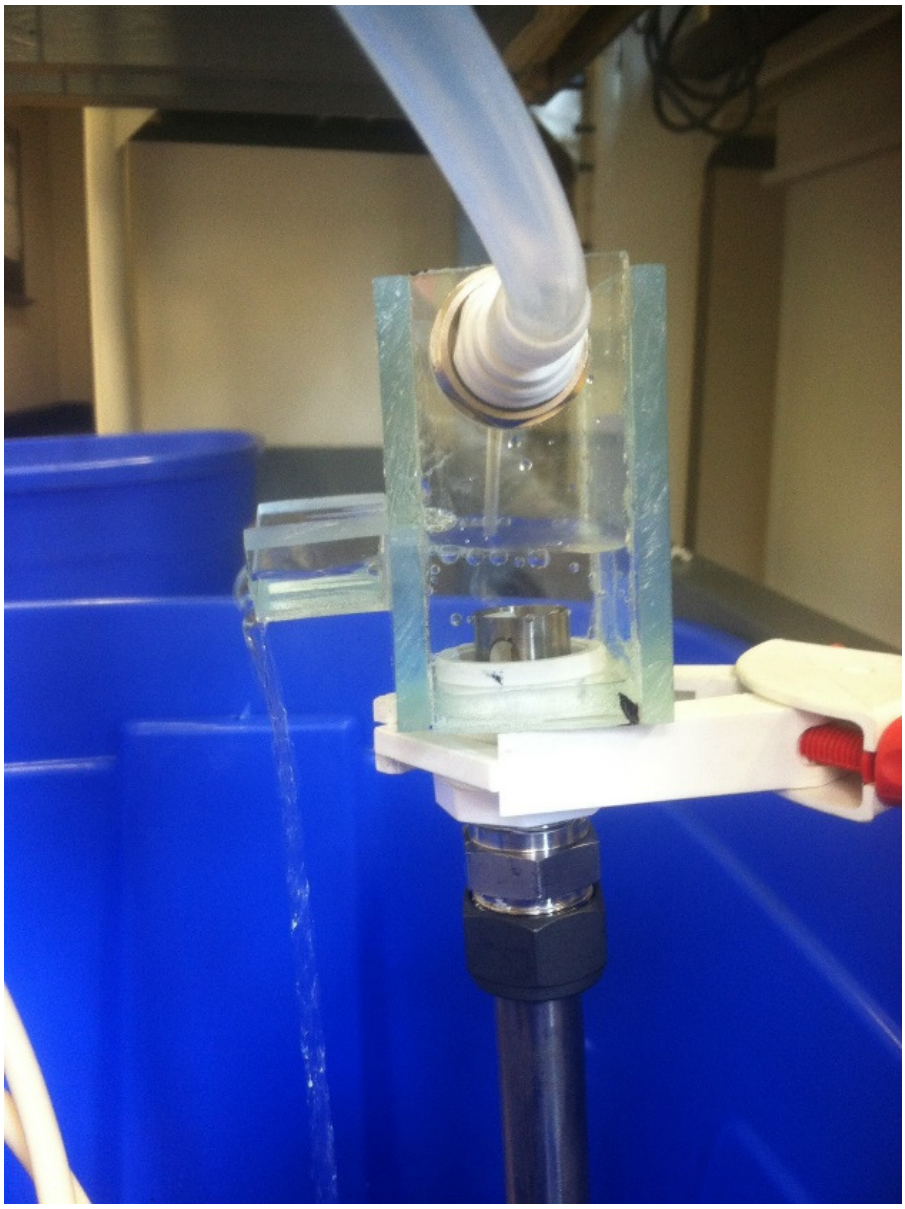

Figure 3.11: Skimmer reservoir with bottom mounted conductivity sensor

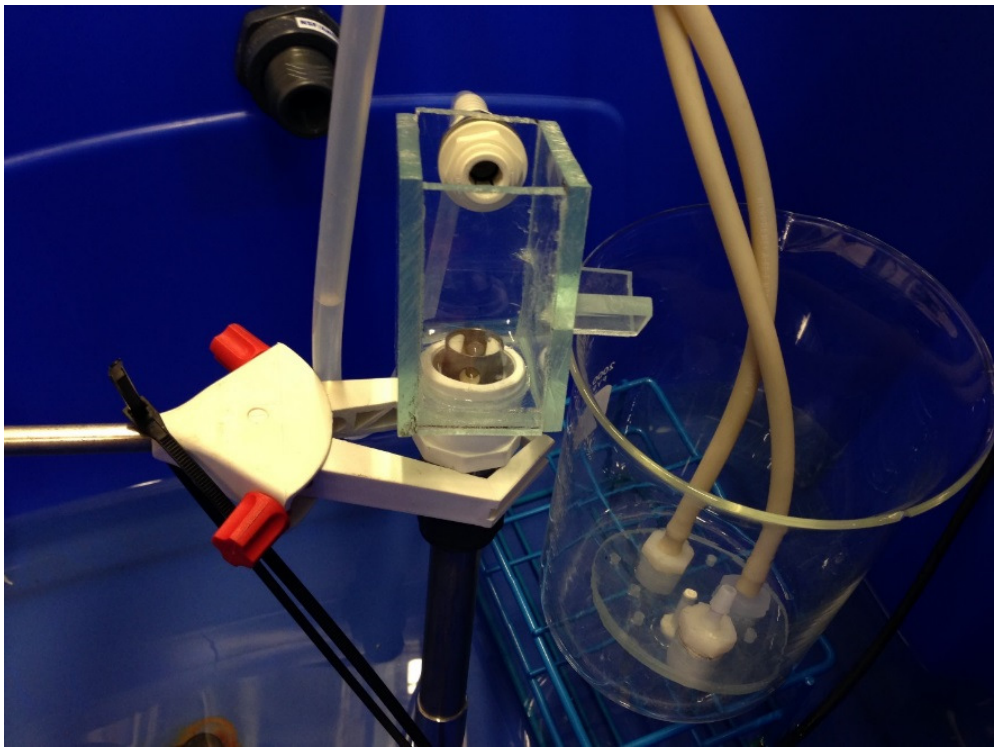

Figure 3.12: Balance tank with skimmer sensor in the foreground

## 3.3 Scale Pool Experimental Procedures

### 3.3.1 Determining the Turnover Period

To begin a scale pool experiment, a turnover period was selected. A turnover indicates that the entire volume of the pool has circulated past the filtration system, or turned over, while a turnover period describes the number of hours it takes to accomplish a single turnover. The turnover period is calculated using the pool volume and flow rate using the following equation:

$$\theta = \frac{V_p}{Q} \tag{3.1}$$

where: $\theta$ = turnover period (hr)
$V_p$ = total pool volume (L)
Q = flowrate (L/hr)

Table 3.1: Pool turnover and flowrate

| Pool | Volume (L) | Turnover Period (hr) | Flowrate (mL/min) |
|---|---|---|---|
| Junior Olympic Bench-scale Pool | 87 | 6 | 241.7 |
| | 87 | 8 | 181.3 |
| | 87 | 12 | 120.9 |
| Upflow Scale Bench-scale Pool | 46 | 6 | 127.8 |
| | 46 | 8 | 95.9 |
| | 46 | 12 | 63.9 |

### 3.3.2 Calculating Exit Age Distribution and Cumulative Exit Age

The experimental tracer data collected from the effluent conductivity probe was used to calculate create curves to describe the reactor. The exit age distribution plots the distribution of particles in the reactor as a function of time. This distribution describes the amount of time a particle resides inside the reactor.

## 3.4 Dye Test Procedure

Dye tests were used to visually observe flow patterns. During a dye test, a solution of crystal violet (Fisher Scientific, S93213) was prepared by adding 2.5g to 500 mL of DI water. The system was dosed using a feed line teed into the influent line. The feed line flow was valve controlled. Dye Studies were used for purely qualitative purposes. A high dye concentration was used to increase visibility. Dye concentrations were much larger than the concentrations used in salt tracer studies and became visually saturated in a much shorter period of time to highlight flow patterns while pools dosed with salt tracer recorded actual chemical distribution rates. Dye times cannot be compared to salt tracer distribution times do to the difference in measuring technique and variability in visual measurements.

## 3.5 Salt Tracer Procedure

For test using a salt tracer, a potassium chloride (Fisher Scientific, P217-3) solution was used. A solution volume of 870 mL was used in dosing the system. The solution volume was 1% of the total system volume. The solution volume was held constant during all experiments and this allowed for consistent dosing over changing flowrates and turnover periods. The solution of potassium chloride was prepared by dissolving 1.297grams of KCl in 870 mL of DI water to achieve a 0.02 M KCl solution. The system was dosed by a feed line connected by valve to the influent line. The feed line would be inserted into the solution, and the valve was opened to siphon out the solution.

## 3.6 Calculating Density of Salt Tracer Solution

During early salt tracer experiments, noticeable density currents formed after dosing. Visible salt currents, shown in Figure 3.13 , flowed from the inlets and pooled in the deep regions of the pool. The effects of the density differences became more pronounced as the turnover period increased. Although enough salt must be added to measure the change in conductivity, large doses of salt may create density currents that can affect tracer studies (Teefy, 1996). To eliminate the effects of the density currents, the salt solution was reduced to a density of within 1% of the pool water density. However, at a density difference of 1% density currents were still visible while the salt tracer was dosed. Thus, a density difference of no more than 0.1% was found to be optimal to eliminate the effects of salt density currents. Both the tracer solution and water densities are compared in three concentrations and shown in Table 3.2 and Table 3.3 for 25ºC and 20ºC, respectively.

Figure 3.13: Visible density current in initial dosing

Table 3.2: Tracer density at 25°C

| Water Density kg/m$^3$ | KCl Solution Density kg/m$^3$ | KCl Concentration (M) | Percent Difference |
|---|---|---|---|
| 997.04 | 998 | 0.02 | 0.10% |
| 997.04 | 1,007 | 0.2 | 0.94% |
| 997.04 | 1,043 | 1.0 | 4.41% |

Table 3.3: Tracer density at 20°C

| Water Density kg/m3 | KCl Solution Density kg/m3 | KCl Concentration (M) | Percent Difference |
|---|---|---|---|
| 998.22 | 999.18 | 0.02 | 0.10% |
| 998.22 | 1,007.71 | 0.2 | 0.94% |
| 998.22 | 1,044.38 | 1.0 | 4.42% |

### 3.6.1 Calculate Volume and Molarity of Solution

To achieve a 0.02M solution the mass of KCl must be calculated for the solution volume. The volume of tracer solution, 870 mL, equaled 1% of the total pool volume. 1.297g of KCl was dissolved in 870 mL of DI water.

$$M = \frac{\text{moles of solute}}{\text{solution}}$$

Where: M= molarity
moles of solute = moles present in solute (mol)
solution = volume of solution (L)

Table 3.4: Tracer solution specifications

| Scale Pool | Solution Concentration (M) | Solution Volume (L) | KCl mass (g) |
|---|---|---|---|
| Junior Olympic | 0.02 | 0.87 | 1.297 |
| Upflow | 0.02 | 0.47 | 0.701 |

### 3.6.2 Calculate Conductivity of Solution

The conductivity of the solution must be calculated to predict the pool conductivity and to ensure the conductivity is within range of the instruments. Conductivity that is too low will not be detected, while high conductivity will exceed the detection limits of the sensors.

Table 3.5: Calculated conductivity of solutions

| Conc. (M) | Conductivity at 20 °C (µS/cm) | Conductivity at 25 °C (µS/cm) |
|---|---|---|
| 1 | 121,940.3 | 111,310.2 |
| 0.2 | 26,063.9 | 23,791.8 |
| 0.02 | 2,935.7 | 2,679.8 |
| 0.002 | 319.4 | 291.6 |
| 0.0002 | 34.1 | 31.1 |

### 3.6.3 Measurement of Salt Tracers

To measure the concentration of the salt tracer in the system a network of digital conductivity contacting sensors (HACH, 3400sc) were placed throughout the pool system. Each sensor was connected to a central controller (HACH, SC1000). In total six conductivity sensors were used to characterize the flow pattern and concentration of the salt. To describe the internal hydraulic patterns of the pool three sensors were placed in the main pool body. The conductivity sensors were placed just below surface level, diagonally across the pool as shown in Figure 3.14. These three sensors were suspended from supports mounted to the pool (Figure 3.15). When placing the sensor, care was taken to prevent air from becoming trapped in the sensor probe. If air became trapped in the sensor end, faulty measurements would occur. Prior to each experiment the sensor ends were flushed with DI water using a 5ml syringe to ensure there was no air present.

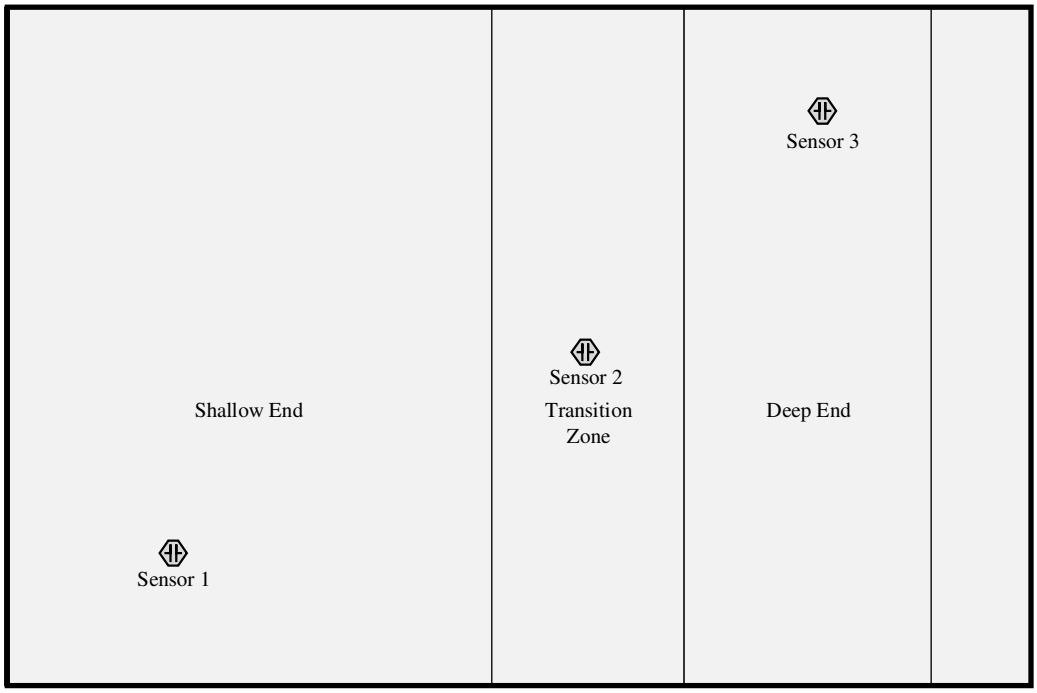


Figure 3.14: Plan view of conductivity sensor location

A fourth conductivity sensor was place on the drain line. This probe was described the fraction of effluent leaving the system from the drain line. The fifth conductivity sensor was placed in the bottom of the skimmer reservoir. This sensor recorded the conductivity from the skimmers and allow for the characterization of the fraction of the effluent leaving the system through the skimmers. Together, the drain sensor and skimmer sensor combined to provide a clear picture of the path of the tracer as it left the system. The final sensor was placed on the combined effluent line, after the effluent exited the balance tank. This sensor allowed for the calculation of the system RTD and the characterization of the system using reactor modelling. The effluent conductivity sensor was mounted in a ½ in PVC tee fitting (Figure 3.16) to allow the water to flow past the sensor. After initial test showed an air build up in the tee, resulting in faulty conductivity measurements, the tee and sensor was inverted to allow air bubbles to flow through the sensor and fitting without becoming trapped. The conductivity probes measured conductivity (µS/cm) and water temperature (°C) and recorded the data in 10 second intervals.

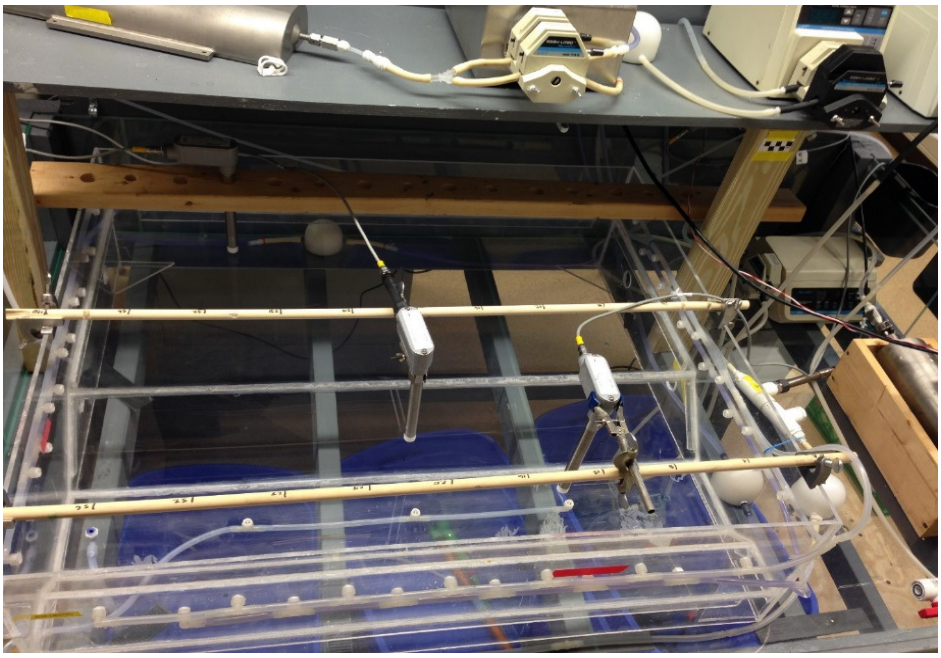

Figure 3.15: Conductivity sensors mounted in pool

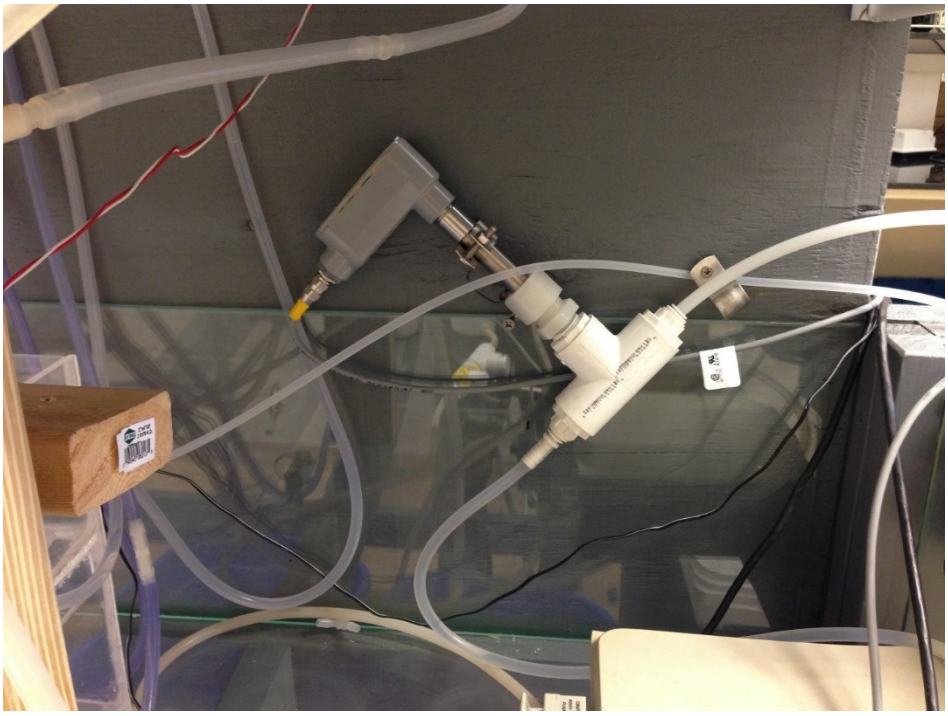

Figure 3.16: Effluent conductivity sensor placement before inversion

# CHAPTER 4: RESULTS AND DISCUSSION

## 4.1 1:25 Scale Junior Olympic Pool

Quantifying the bench-scale Junior Olympic pool comprised of four main phases; standard operation, turnover period, modified configuration, and ideal flow configuration. The system was first quantified under a standard pool operating mode. The second phase compared turnover rates and examined how the flowrate and hence turnover period (1, 6, 8, 12, and 24hr) affected efficiency. In the third phase, different inlet configuration and flow patterns were examined. Finally, the last phase tested the system under conditions in an attempt to simulate ideal plug flow and completely stirred reactor models. The pool was considered quantified if short-circuiting, mixing, circulation efficiency and exit age distribution could be described. A single parameter exponential decay model was fitted to the exit age distribution to mathematically describe the exit of salt from the system. The initial increasing slope of the exit age distribution curve was investigated. The distribution of salt through the system can be directly compared to the distribution of chlorine. This slope describes the chlorine distribution time of the pool system and can be used to determine the percent of the turnover period needed to completely distribute chlorine to the system. The cumulative exit age distributions was investigated to define the efficiency at which the salt tracer was removed from the system. The cumulative exit age can be used practically to describe the hydraulic efficiency of the pool to return water/contaminants to the treatment system.

### 4.1.1 Dye Studies

Dye studies were conducted utilizing the standard pool condition of 6 hour turnover. Crystal violet was dosed over a 2.5 minute period. The pool was visually observed for signs of short circuiting and low-flow zones. All conductivity probes were removed from the system. Dye began exiting the inlets within 30 seconds of the dye injection (Figure 4.1). The dye quickly spread throughout the pool and within 90 seconds, a large eddy, shown in Figure 4.2, was formed in the center of the pool. This eddy created a clockwise flow pattern. At this point, stagnant zones began to form in each corner of the pool (Figure 4.3). However, within 270 seconds, the dye had completely saturated both the stagnant zones and the center eddy, and the pool had reached a completely dyed condition as shown in Figure 4.4.

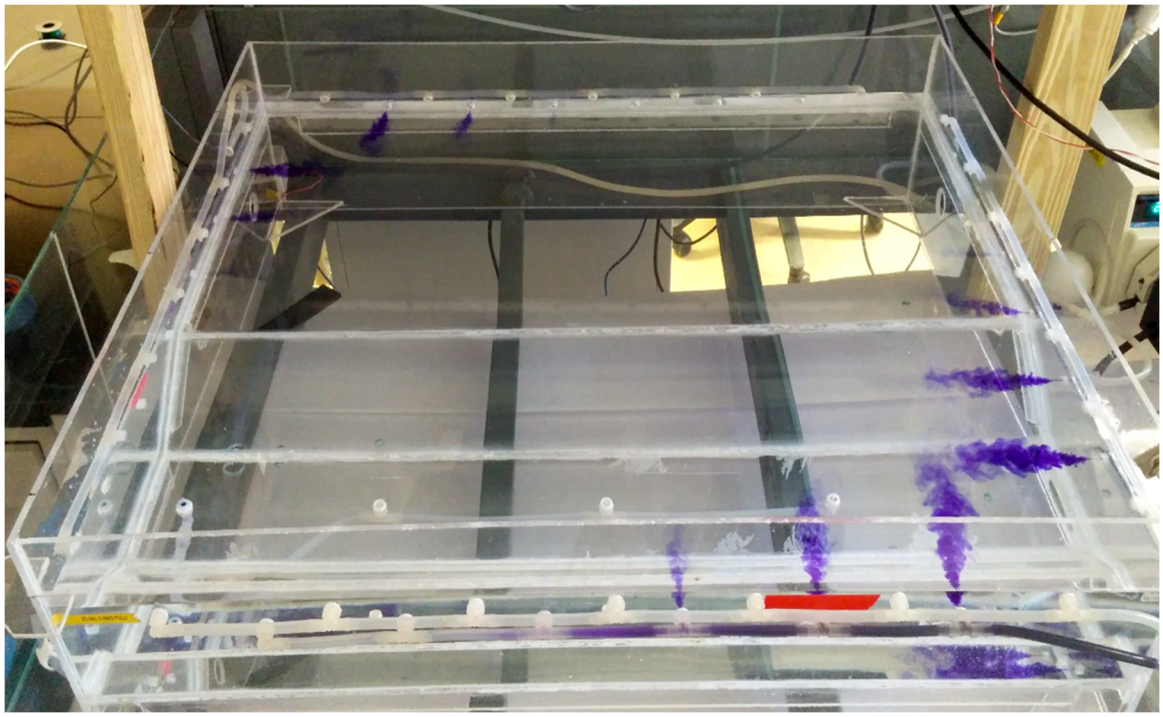

Figure 4.1: Dye exiting inlets t = 30 seconds

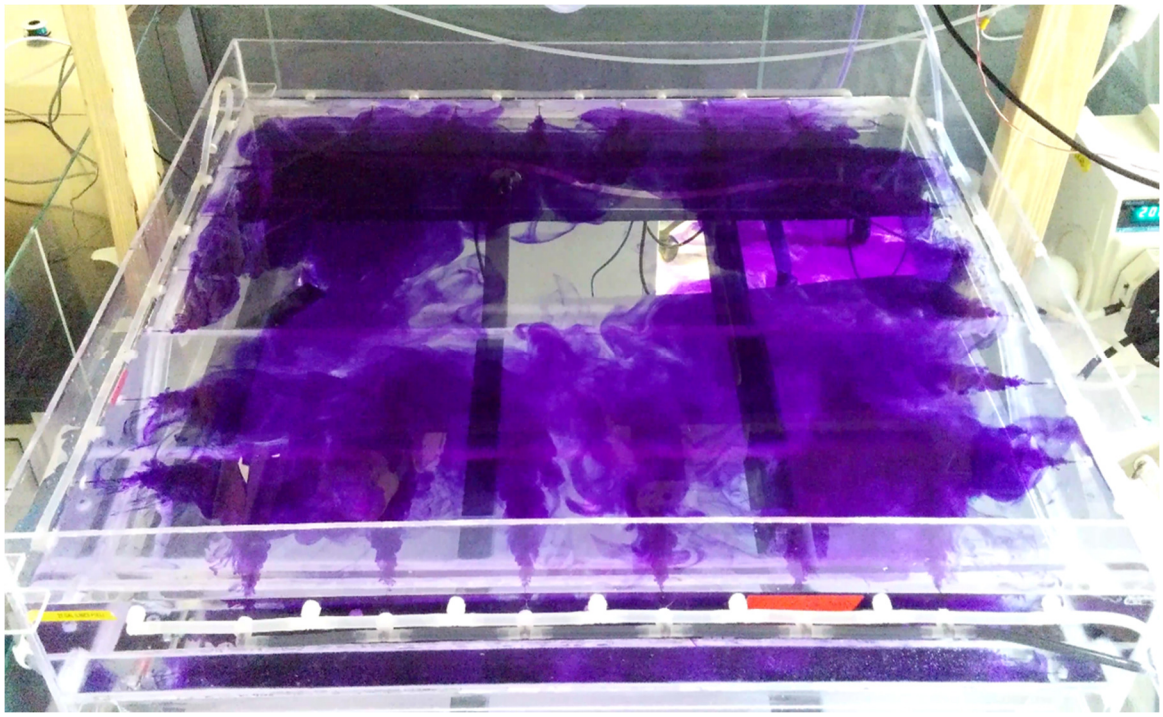

Figure 4.2: Formation of central eddy t = 90 seconds

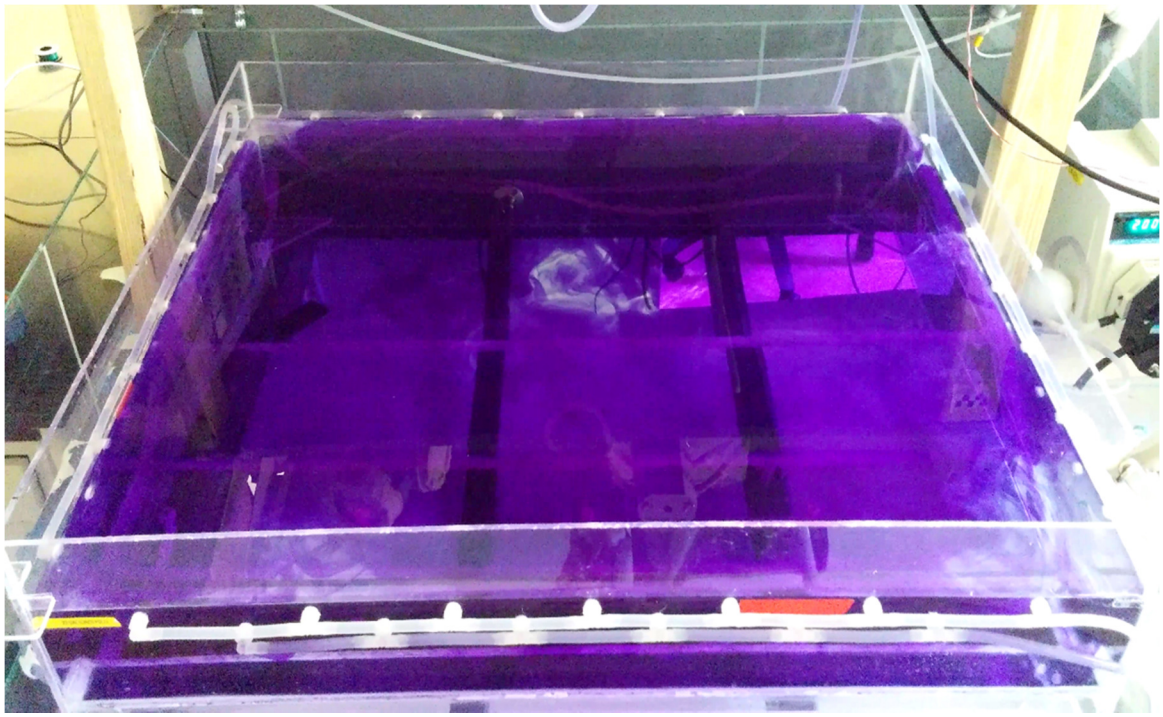

Figure 4.3: Incomplete mixing in corners and central eddy t = 180 seconds

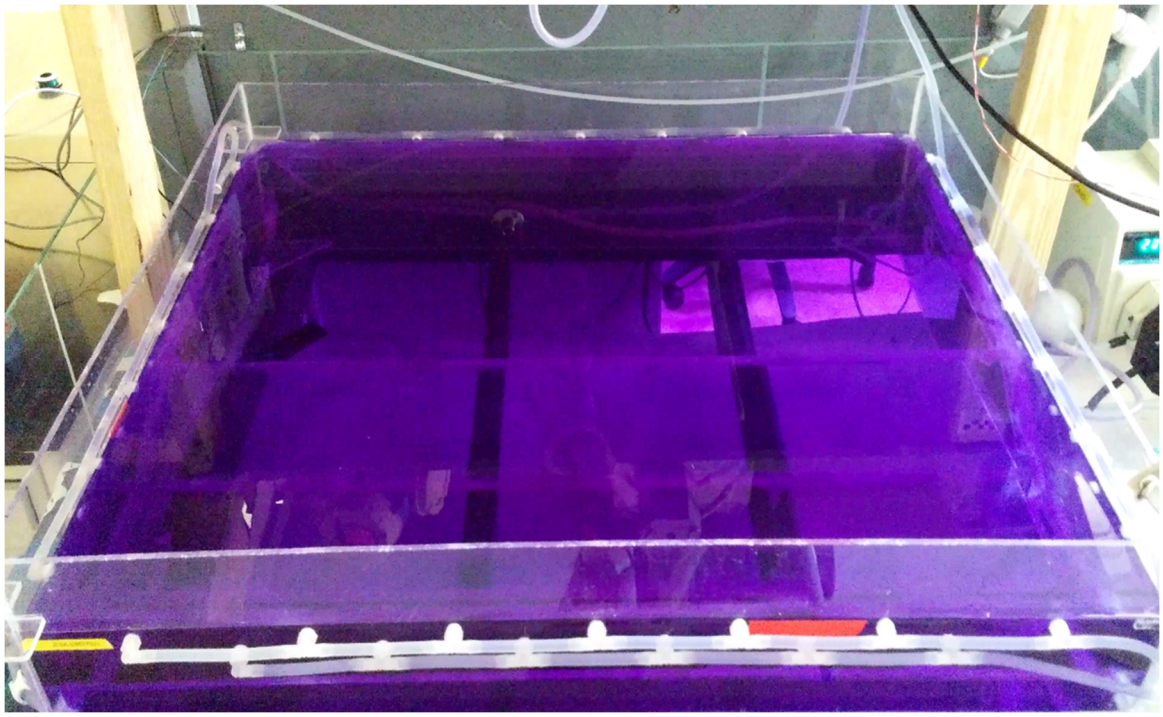

Figure 4.4: Complete mixing of dye t = 270 seconds

### 4.1.2 Standard Pool Condition Tracer without Recirculation

Three experiments were performed to establish the standard pool condition. In bench-scale experiments, the standard pool condition was defined as a 6 hour turnover period. In this mode, all inlets and outlets were operational. Skimmers contributed 75% of effluent while the floor drains contributed 25% of effluent. Influent and effluent flow rate were set at 241 mL/min. The salt tracer was injected over a 2.5 minute period.

As shown in Table 4.1, the standard pool condition exhibited minimal short-circuiting, and the value for short-circuiting indicators were extremely close to those of an ideal CSTR. The variance ($\sigma^2$) indicated the pool at 70% of an ideal CSTR.

Table 4.1: Indicator for standard pool condition

| Characteristic | Indicator | Ideal CSTR | **Standard pool condition** | Ideal PFR |
|---|---|---|---|---|
| Short-circuiting | $\theta_0$ | 0.00 | **0.00** | 1.00 |
| | $\theta_{10}$ | 0.11 | **0.15** | 1.00 |
| Mixing | variance ($\sigma^2$) | 1.00 | **0.70** | 0.00 |

Efficiency is a function of the cumulative exit age. In Figure 4.5, the efficiency of the standard pool condition is compared to an ideal CSTR and to the Gage and Bidwell results. By the end of the first turnover period 61% of the water has circulated past the effluent conductivity probe. By the second turnover 85% and by the third 97% of the water has passed as effluent. As the tracer enters the system, the initial slope is described in Figure 4.6. The exit age distribution of each experiment increased at 0.02θ (or 7.5 minutes) after the experiment started. From 0.02θ, the slope increased to its peak of 0.97 and begins to decrease by 0.10θ (36 minutes). The initial slope of the exit age distribution curve is practically important for understanding the distribution of chlorine to the swimming pool. During a standard pool operating condition, chlorine is distributed between 0.05θ to 0.10θ (or 36 minutes). For Figure 4.7, the sharp drop and rise between 1.5θ and 2.0θ of Experiment 2 and Experiment 3 was caused by a buildup of air in the sensor that quickly passed through the effluent conductivity probe. The cumulative exit age shown in Figure 4.8 follows an ideal CSTR curve. At 1 turnover (θ), 61% of the pool volume had exited the system. Practically applied, Figure 4.8 describes the hydraulic efficiency of the system in returning the pool volume to the treatment system.

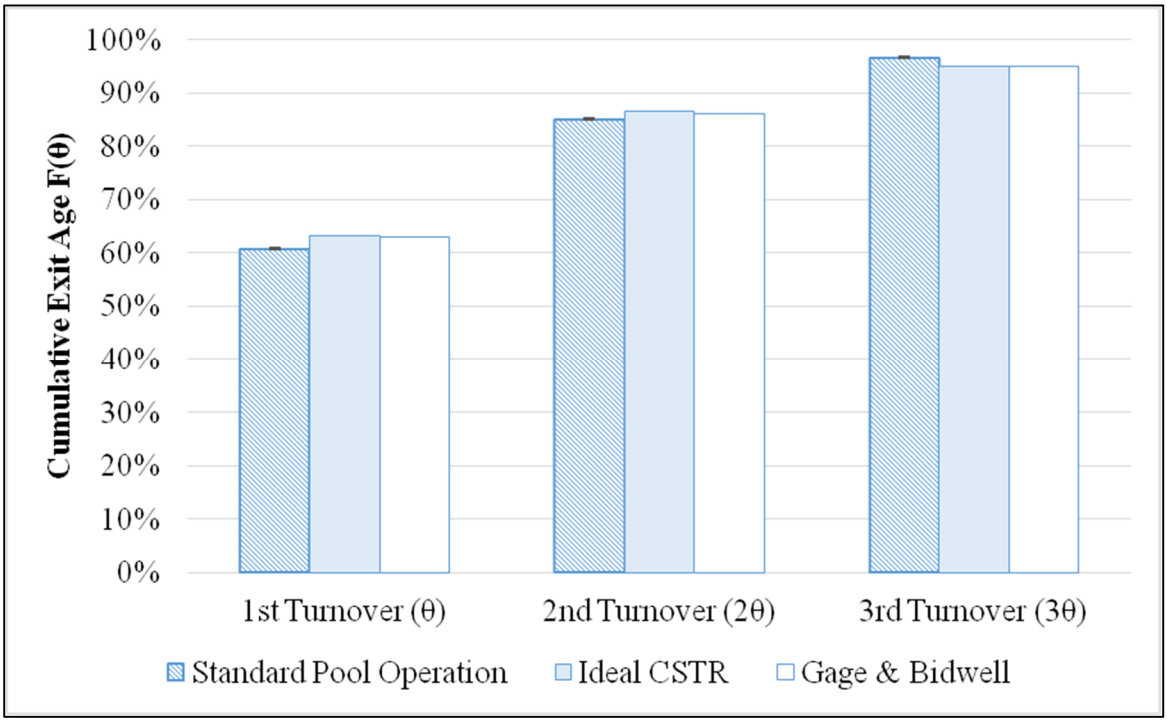


Figure 4.5: Efficiency of recirculation in standard 6 hour turnover Junior Olympic pool (n=3)

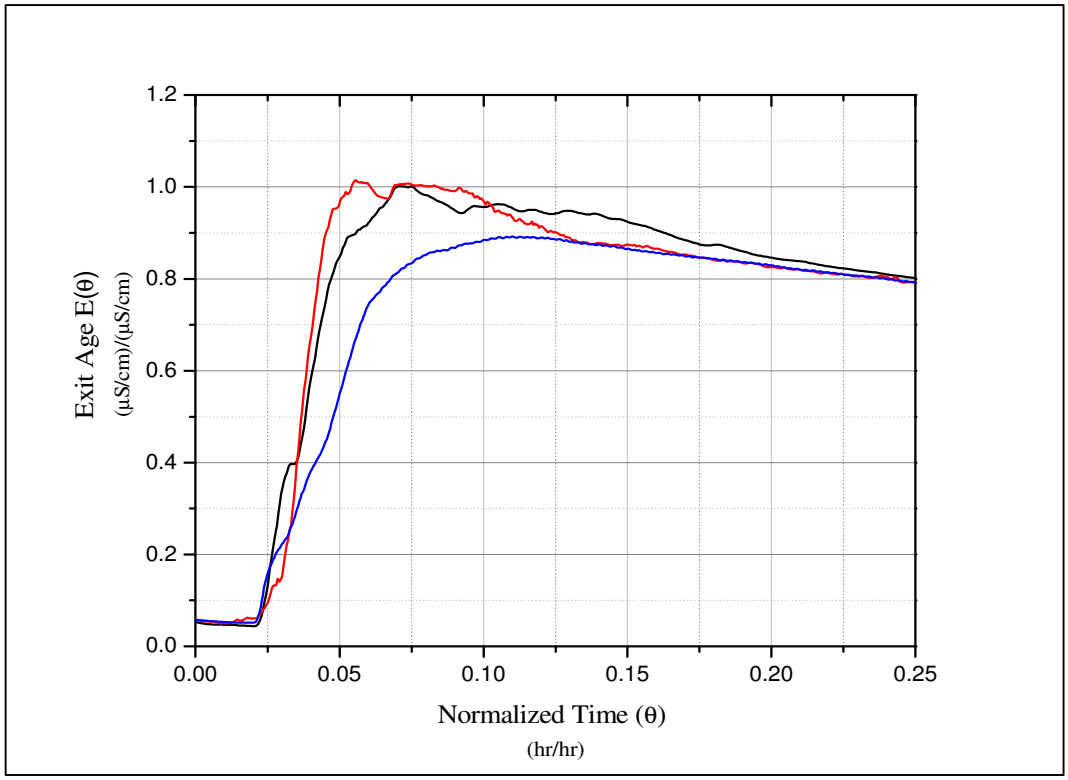


Figure 4.6: Initial slope of standard pool condition exit age distribution with 6 hour turnover period (n=3)

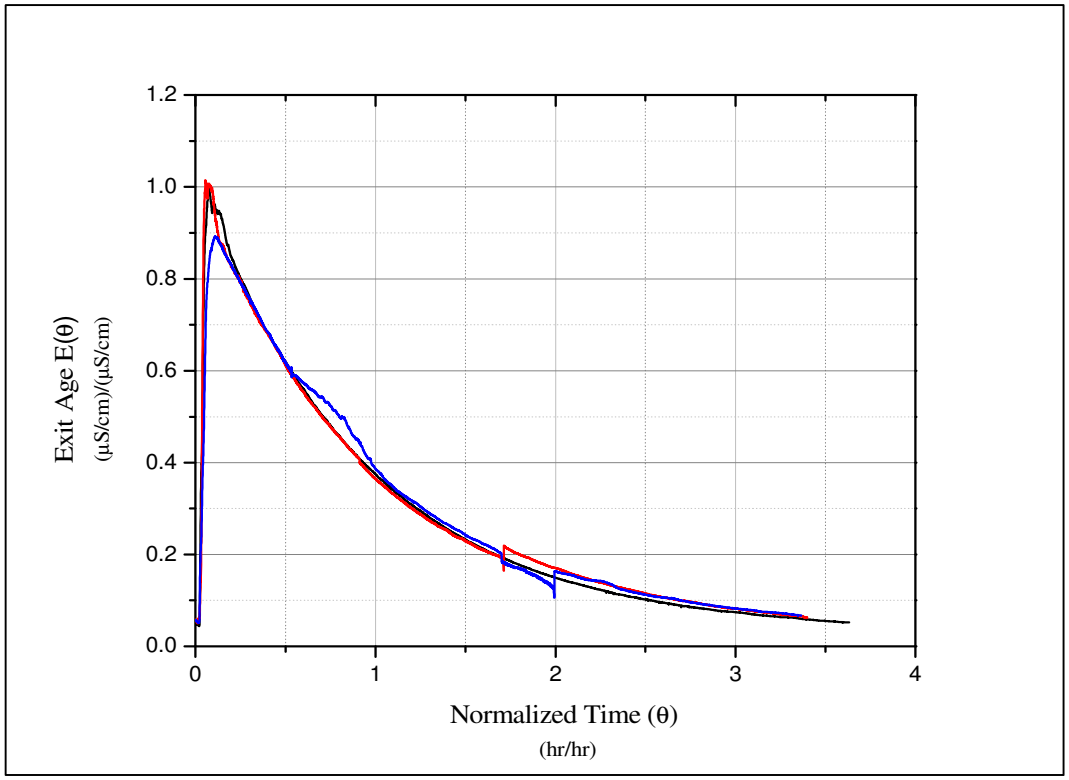


Figure 4.7: Standard pool condition exit age distribution with 6 hour turnover period (n=3)

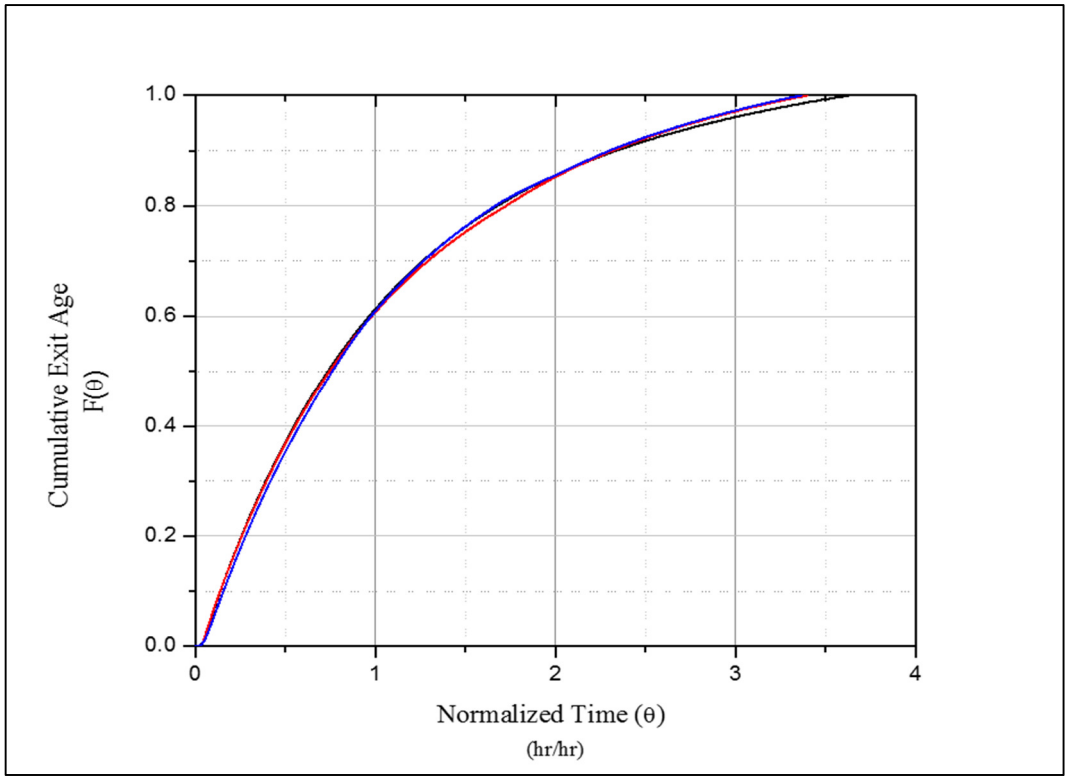


Figure 4.8: Standard pool condition cumulative exit age distribution with 6 hour turnover period (n=3)

### 4.1.3 Modified Pool Operating Conditions

#### 4.1.3.1 Turnover Period

Turnover periods of 1 hour, 6 hour, 12 hour, and 24 hours were examined. Flowrates for the turnover times are shown in Table 4.2 . Skimmers contributed 75% of effluent while drains contributed 25% of effluent. The salt tracer was injected over a 2.5 minute period. The characteristics of the modified turnover periods were tightly grouped and consistent with an ideal CSTR (Table 4.3).

Table 4.2: Turnover period flowrates for bench-scale Junior Olympic pool

| Turnover Period (hr) | Influent Flowrate (mL/min) | Skimmer Flowrate (mL/min) | Drain Flowrate (mL/min) |
|---|---|---|---|
| 1 | 1450 | 1087.5 | 362.5 |
| 6 | 241.7 | 181.3 | 60.4 |
| 12 | 120.9 | 90.5 | 30.2 |
| 24 | 60.4 | 45.3 | 15.1 |

Table 4.3: Comparison of characteristics of turnover times

| Characteristic | Indicator | Ideal CSTR | **1 hour** | **6 hour** | **12 hour** | **24 hour** | Ideal PFR |
|---|---|---|---|---|---|---|---|
| Short circuiting | $\theta_0$ | 0.00 | **0.00** | **0.00** | **0.00** | **0.00** | 1 |
| | $\theta_{10}$ | 0.11 | **0.14** | **0.14** | **0.14** | **0.09** | 1 |
| Mixing | variance ($\sigma^2$) | 1.00 | **0.79** | **0.70** | **0.75** | **1.00** | 0.00 |

The salt tracer removal efficiency per turnover period results are shown in Figure 4.9. While all turnover period experiments performed similarly. The initial slope of the exit age distribution, Figure 4.10, shows a clear difference between 24 hour turnover period and the other results. The 24 hour turnover period created a sharp rise in the exit age

distribution immediately after dosing (Figure 4.11). The sharp spike indicates a bypass in the system. This bypassing can be explained by the low flowrate of a 24 hour turnover period being unable to initially mix the tracer solution efficiently into the pool volume. This is supported by Teefy's (1996) assertion that as flowrates decrease the effect of tracer densities become more pronounced. In the cumulative exit age curve shown in Figure 4.12, the distortion of the 24 hour curve is also visible. The other three turnover period experiments (1-24 hour) performed in a manner consistent with previous experiments and in line with an ideal CSTR.

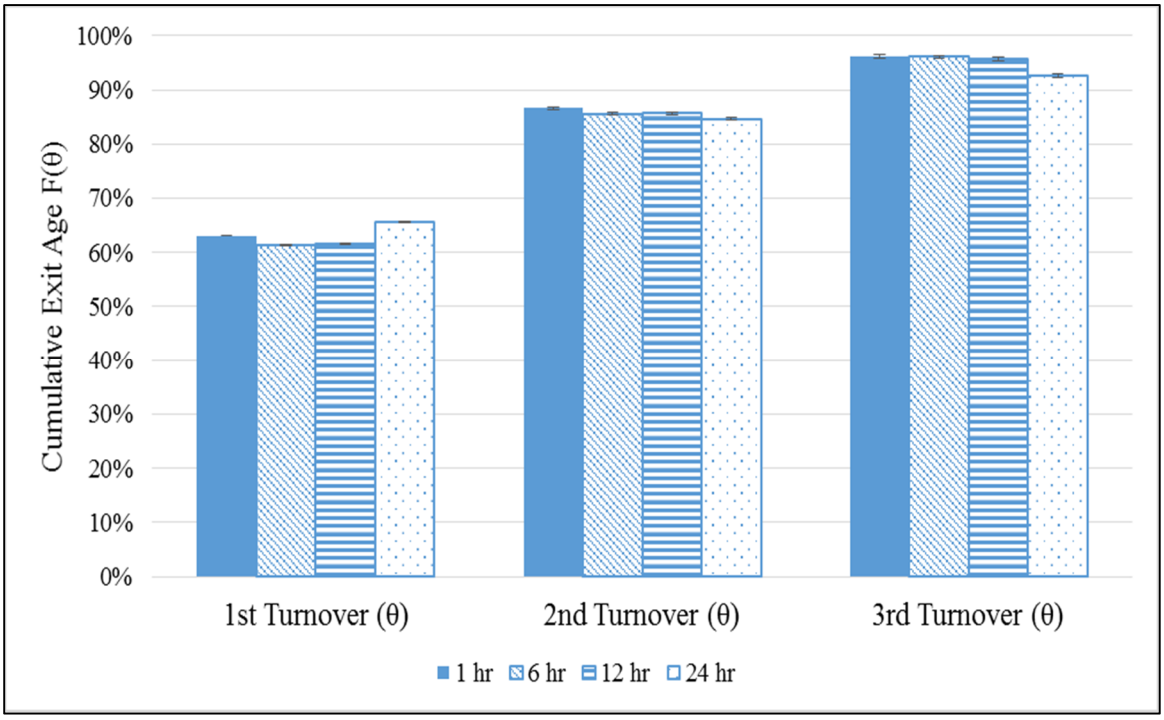


Figure 4.9: Cumulative exit age efficiency for 1, 6, 12 and 24 hour turnover period

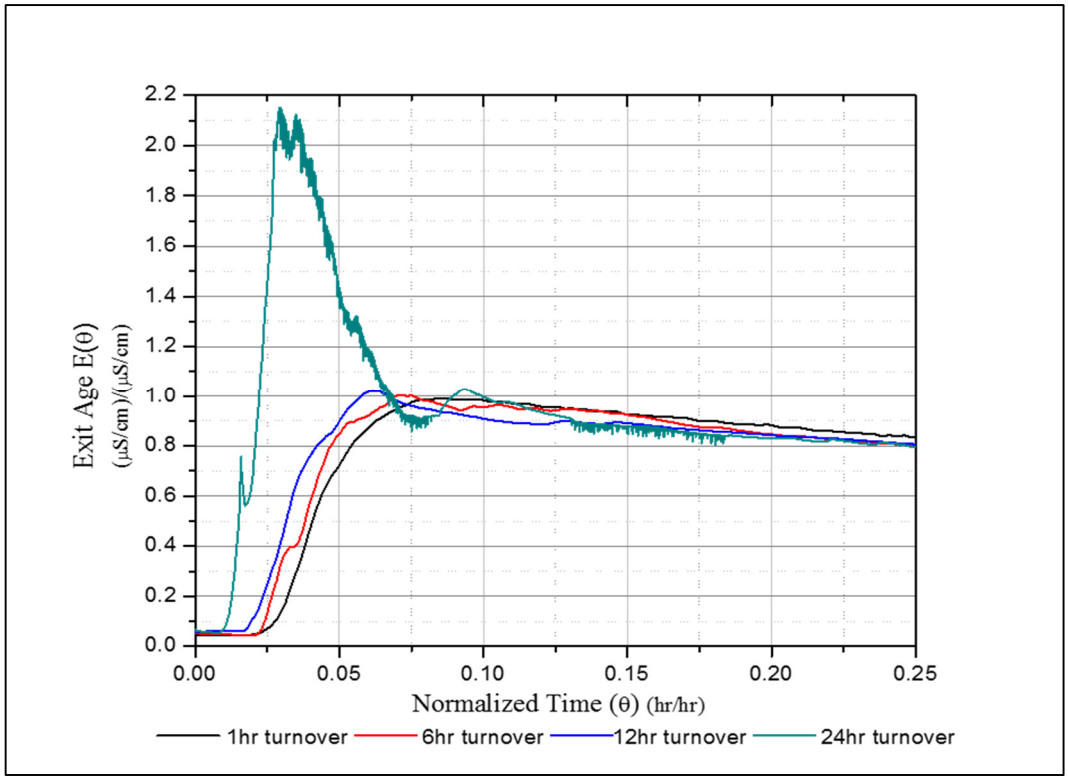


Figure 4.10: Initial slope of exit age distribution for pool with varied turnover period

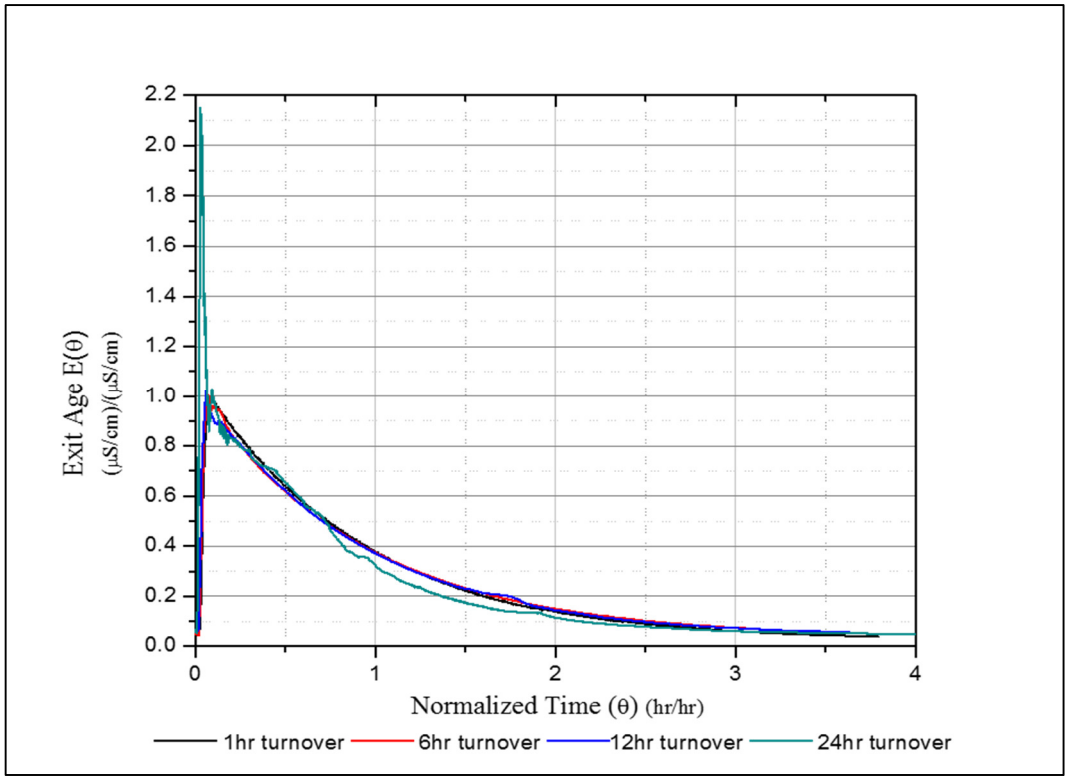


Figure 4.11: Exit age distribution for pool with varied turnover period

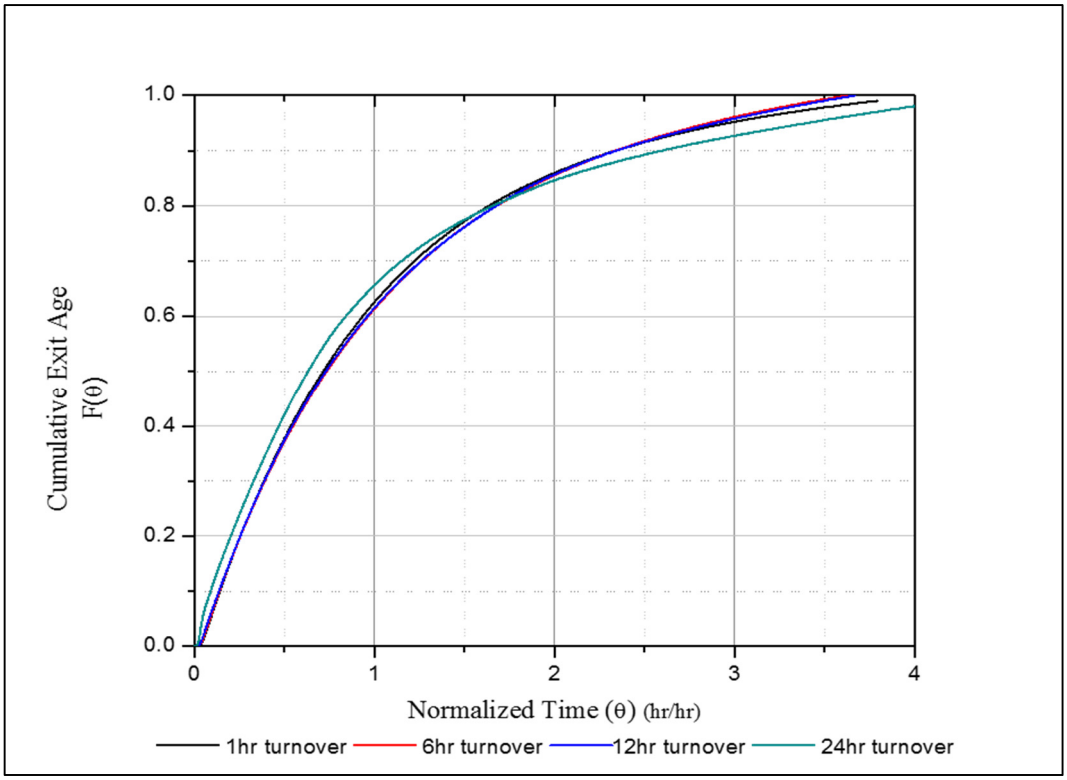


Figure 4.12: Cumulative exit age distribution for pool with varied turnover period

4.1.3.2 Modified Inlet Configuration

To assess the impact of different flow patterns, the inlet and outlet configurations were changed. The results of changes to the system's efficiency were investigated. Experiments were performed using a 6 hour turnover period. Influent and effluent flow rate were set at 241 mL/min. The salt tracer was injected over a 2.5 minute period.

The first pattern was designed to create a diagonal flow pattern, with input on only two sides, output on two sides and a 3:1 skimmer to drain ration, as shown in Figure 4.13. A second reconfiguration pattern, designated 50/50, was based on the ratio of drain to skimmer flow, standard inlet patterns were retained. The drain flow rate was increased from 25% to 50% of total effluent flow. The skimmer was reduced from 75% to 50% of effluent flow. The efficiency of the reconfigured flow patterns are shown in Table 4.4. The efficiency of the salt tracer leaving the system with altered effluent flow pattern was consistent with the standard pool operating condition. Indicators, Table 4.5, did not show short-circuiting.

The initial slope of the exit age distribution (Figure 4.14) reached peak between $0.05\theta$ and $0.10\theta$. The peaks for the reconfigured flow patterns are noticeably higher than the peak for the standard pool condition, Figure 4.15. This can be explained by an increased inlet velocity. By reducing the number of inlets, while maintaining the same turnover period, inlet velocity was doubled. This created a higher variance and thus more intense mixing as shown in Table 4.5.

Table 4.4: Turnover efficiency for reconfigured flow patterns

| Configuration | 1 θ | 2 θ | 3 θ |
|---|---|---|---|
| Diagonal | .668 | .860 | .937 |
| 50/50 | .662 | .861 | .938 |
| Standard | .608 | .852 | .938 |

Table 4.5: Indicators for reconfigured flow patterns

| Characteristic | Indicator | **Diagonal** | **50/50** | Ideal CSTR | Ideal PFR |
|---|---|---|---|---|---|
| Short-circuiting | $\theta_0$ | **0.00** | **0.00** | 0.00 | 1 |
| | $\theta_{10}$ | **0.11** | **0.10** | 0.11 | 1 |
| Mixing | variance ($\sigma^2$) | **1.17** | **1.17** | 1.00 | 0 |

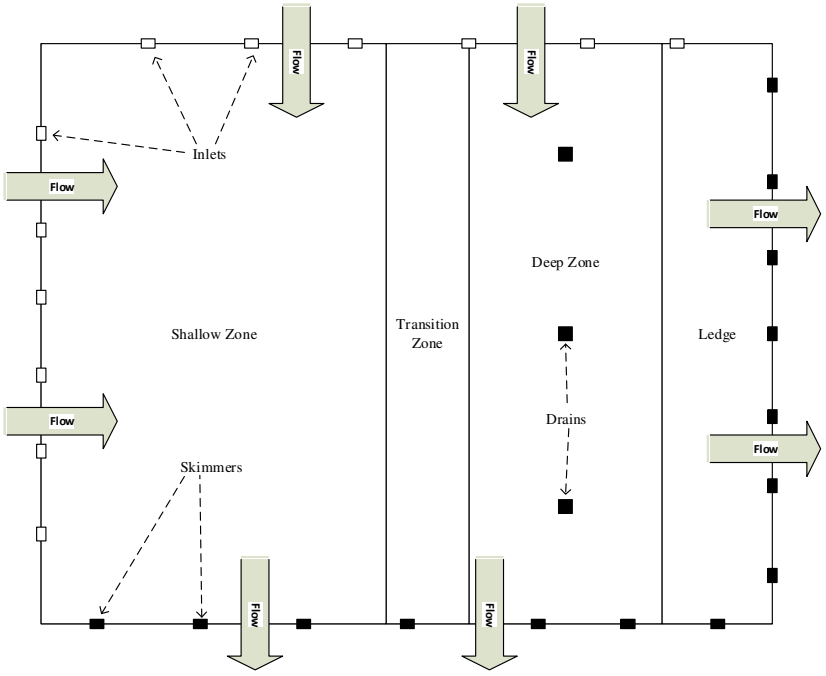


Figure 4.13: Diagonal flow diagram

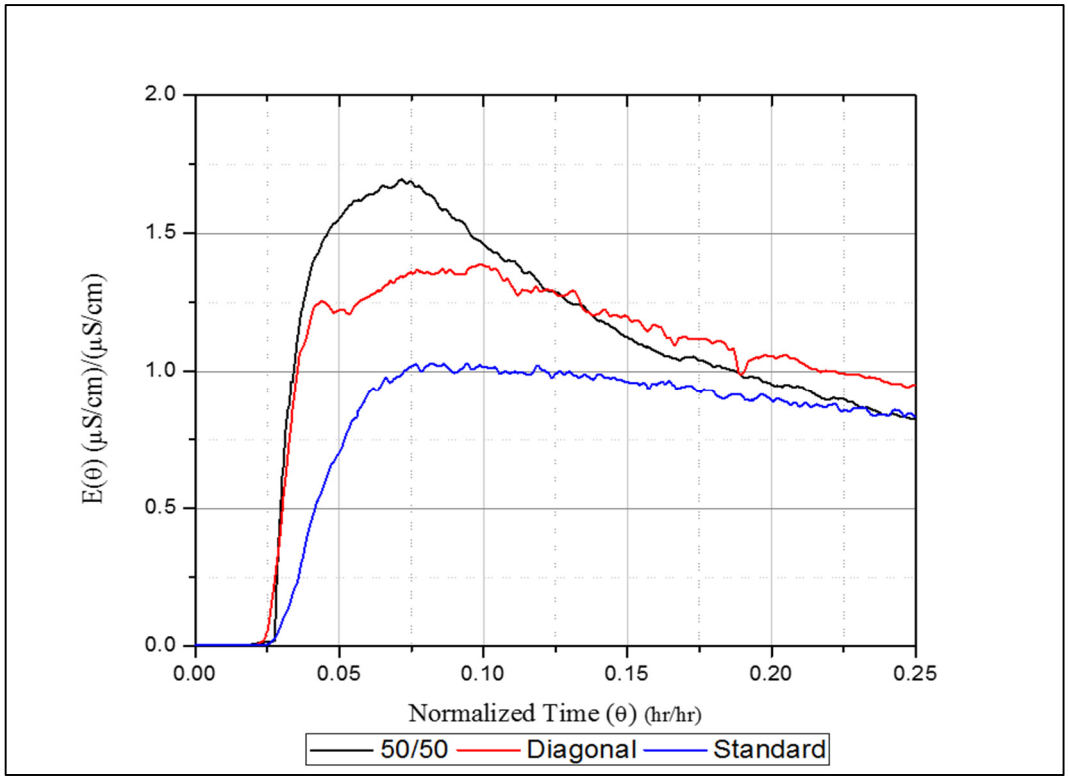


Figure 4.14: Initial slope of exit age distribution for reconfigured flows with 6 hour turnover period

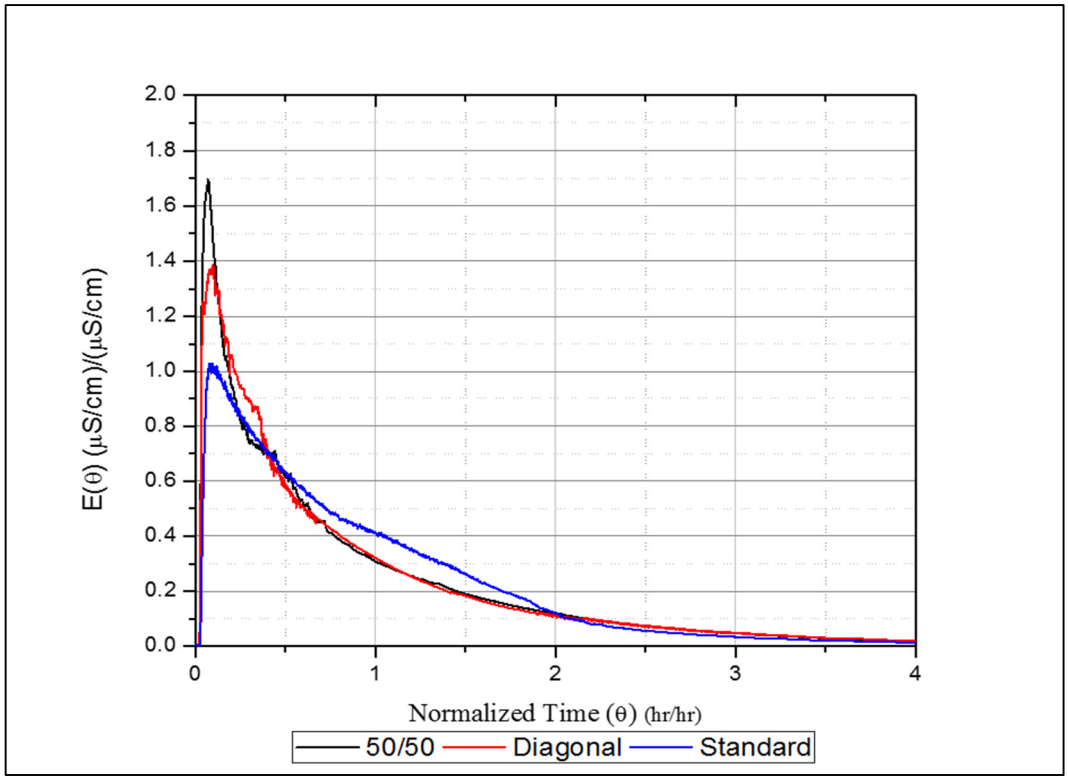


Figure 4.15: Exit age distribution of reconfigured flows with 6 hour turnover periods

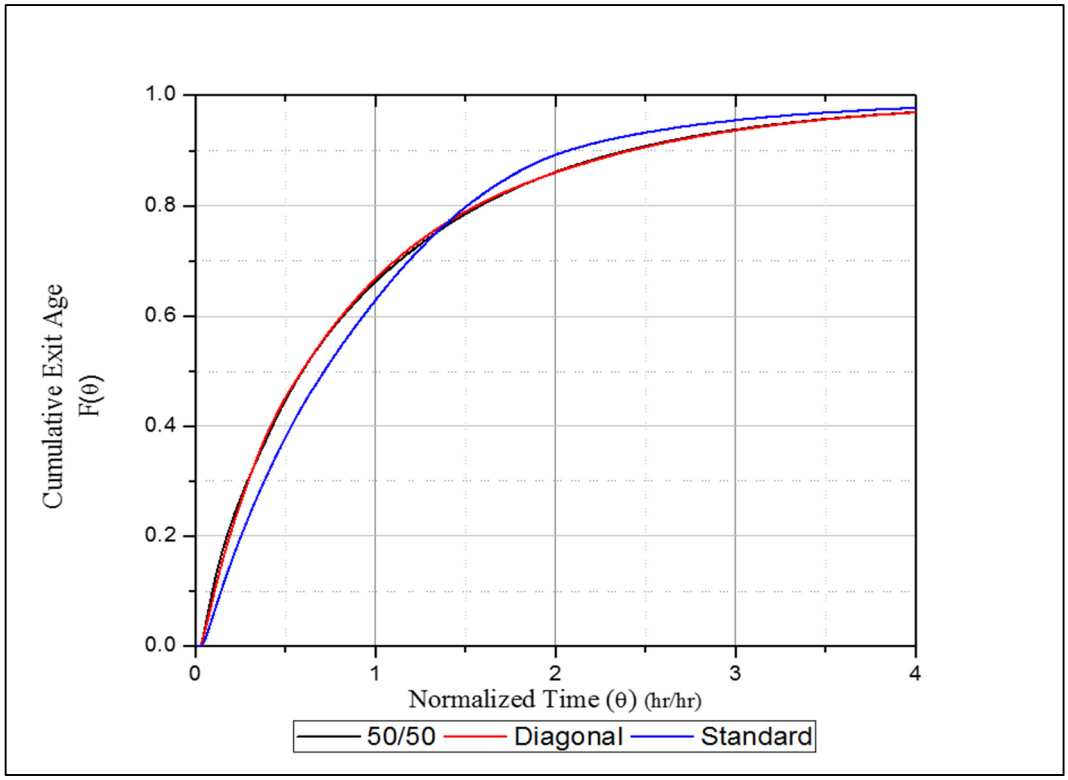


Figure 4.16: Cumulative exit age distributions of reconfigured flows with 6 hour turnover periods

4.1.3.3 Single Direction Flow

Single direction flow was examined to create internal flow patterns closer to those of a plug flow reactor. The inlets and outlets were configured as shown in Figure 4.17 and Figure 4.18. Experiments were performed using a 6 hour turnover period. Influent and effluent flow rate were set at 241mL/min. No skimmers were used in single direction flow. Instead, three bottom drains with a flowrate of 241mL/min were used for all effluent. The salt tracer was injected over a 2.5 minute period. In experiment 1, the balance tank was bypassed, with the drain pumped directly to the effluent conductivity probe. By bypassing the balance tank, a short circuit was produced. For experiment 2 and 3 the drain was pumped into the balance tank and then to the effluent conductivity probe. The short circuit was evident as a spike in the exit age distribution of experiment 1 shown in Figure 4.19. The initial spike created by the bypass lasted less than 0.10 θ. As shown in Figure 4.20, by the time the three experiments have reached 1 θ, they have converged and behave similarly for the remainder of the experiments. The spike caused by the short-circuiting was shown to have very little impact on the cumulative exit age results (Figure 4.21).

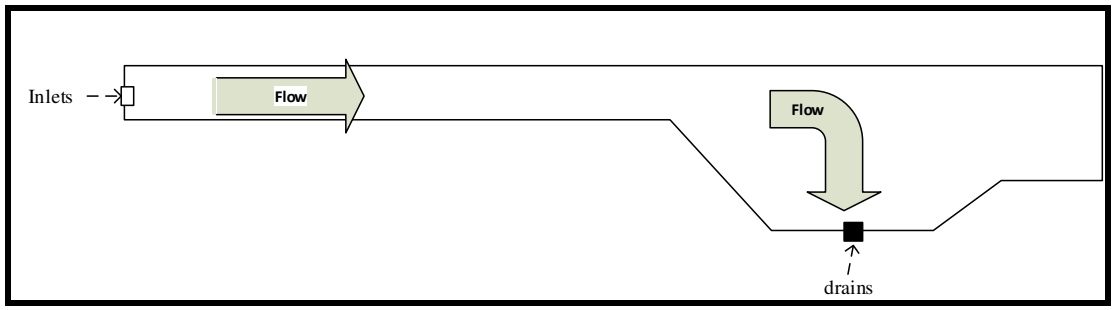


Figure 4.17: Single direction flow plan view diagram

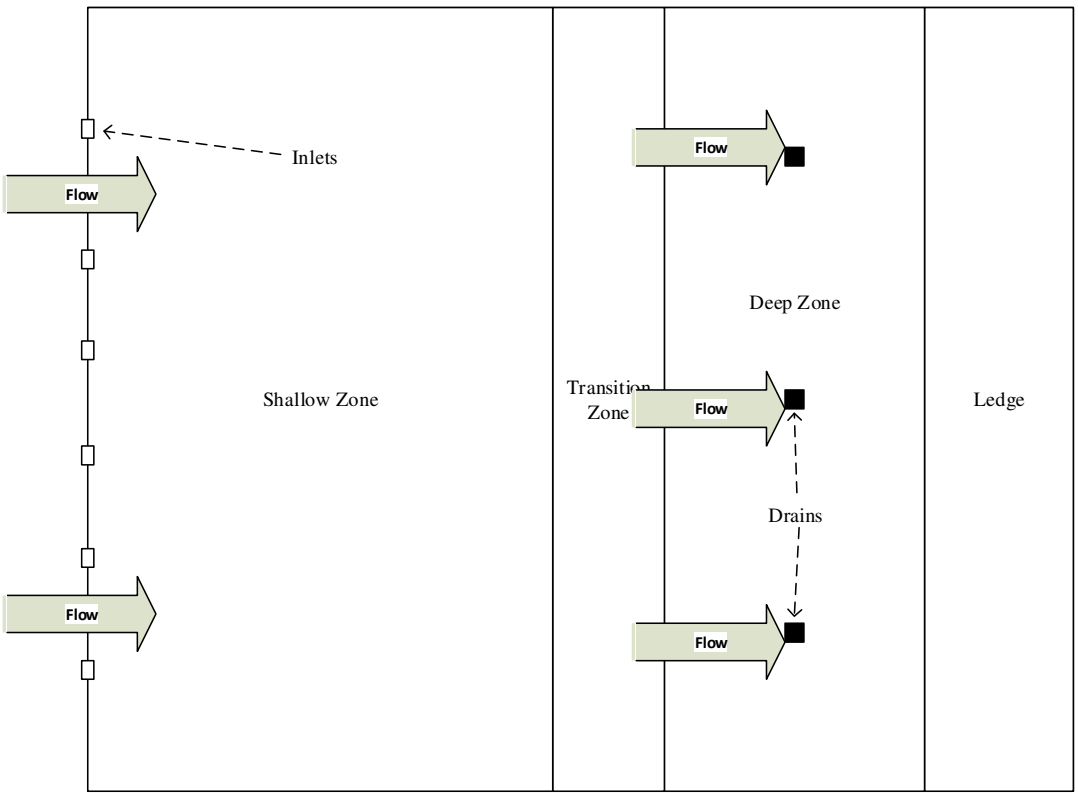


Figure 4.18: Single direction flow diagram

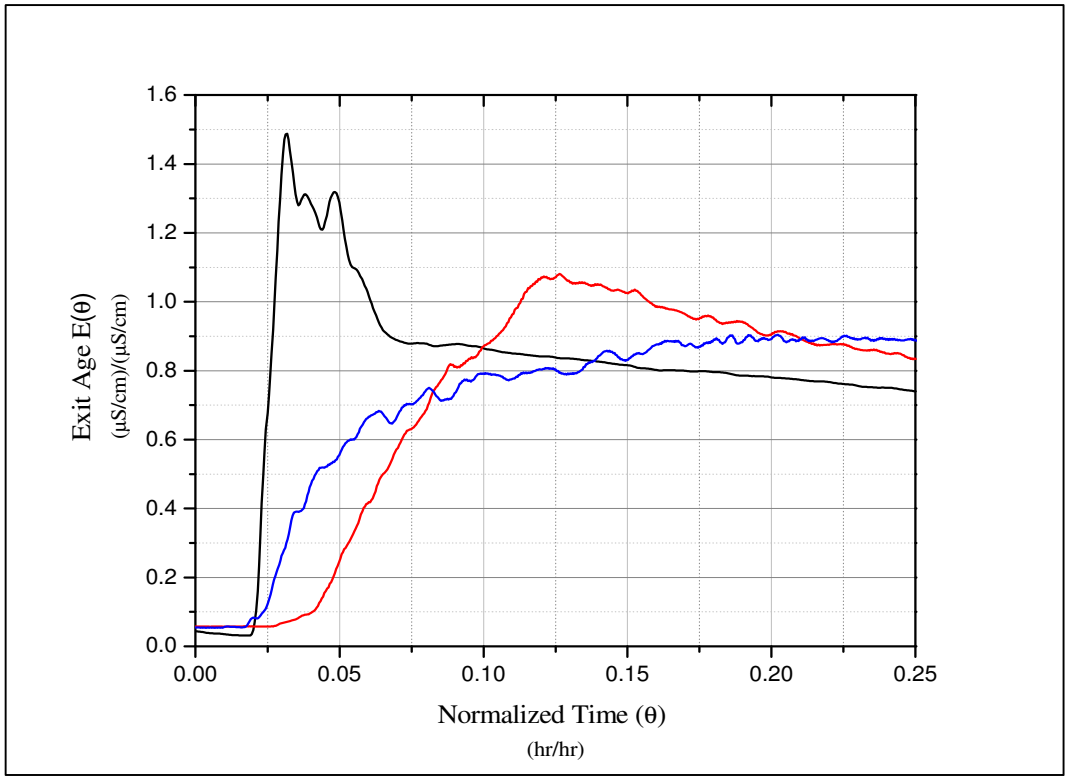


Figure 4.19: Initial slope of the exit age distribution of 6 hour turnover period experiments with single direction flow pattern

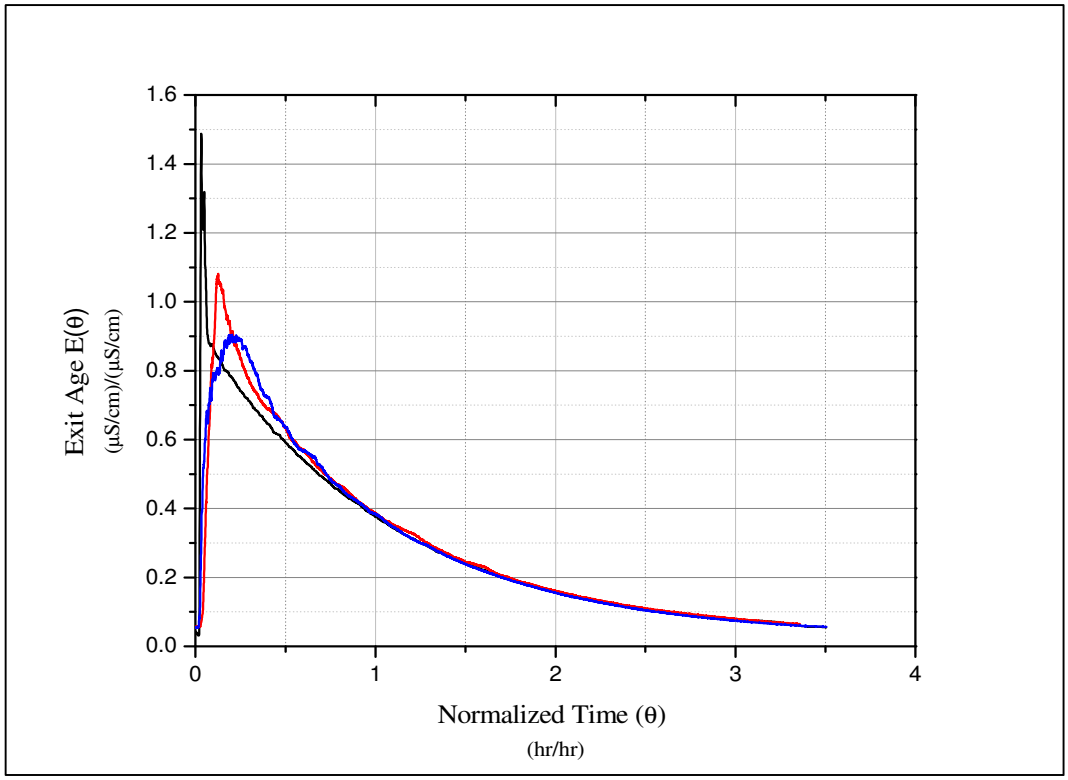


Figure 4.20: Exit age distribution of 6 hour turnover period experiments with single direction flow pattern

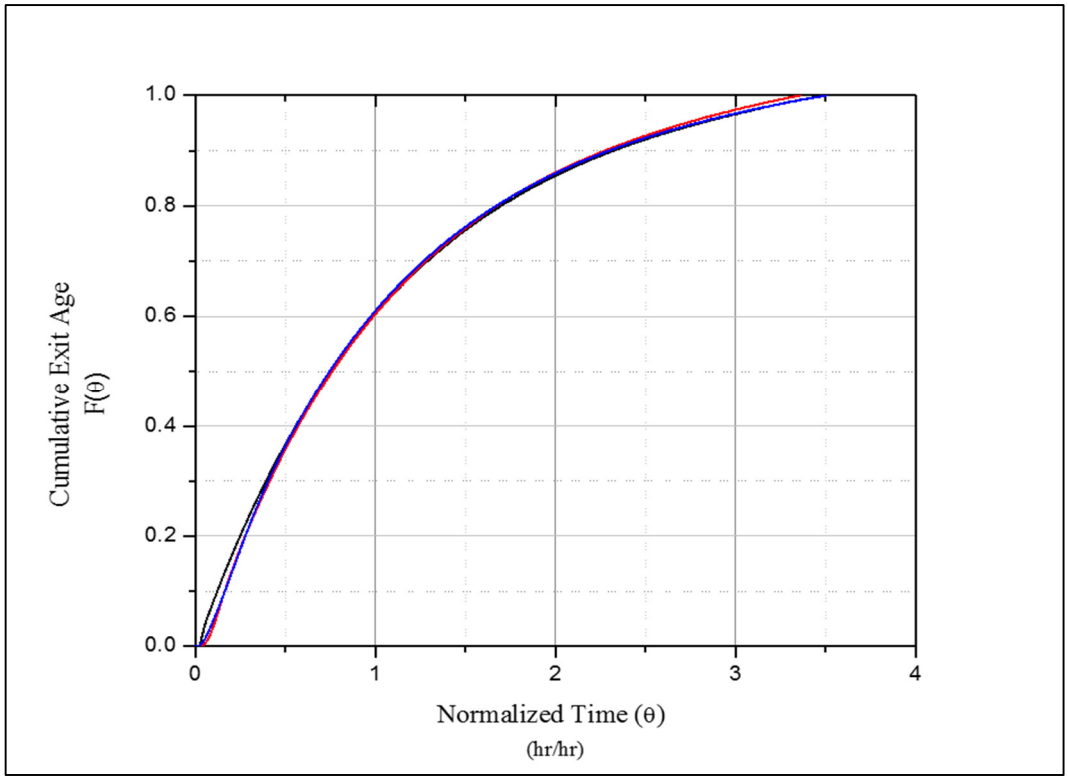


Figure 4.21: Cumulative exit age distribution of 6 hour turnover period experiments with single direction flow pattern

4.1.3.4 Standard Pool Condition with Mixer

To simulate a continuous flow stirred-tank reactor (or a pool with heavy bather load) an overhead stirrer (Eurostar PWR CVS1, IKA) was installed in the center of the pool as shown in Figure 4.22. The mixer was fitted with a 4.3 inch diameter, 3 bladed, hydrofoil impeller. During experiments, the mixer ran at 300rpm for the entirety of the experiment. At a rate of 300 rpms, the impeller did not create a vortex, as shown in Figure 4.23. Experiments were performed using a 6 hour turnover period. Influent and effluent flow rate were set at 241mL/min and the normal 3:1 skimmer to drain flowrate was observed. The salt tracer was injected over a 2.5 minute period. The initial exit age distribution, shown in Figure 4.24, reaches a peak between 0.05θ and 0.10θ. The curve then smoothly transitions to an exponential decay curve as shown in the complete exit age distribution curve shown in Figure 4.25. The cumulative exit age, Figure 4.26, behaves similarly to an ideal CSTR.

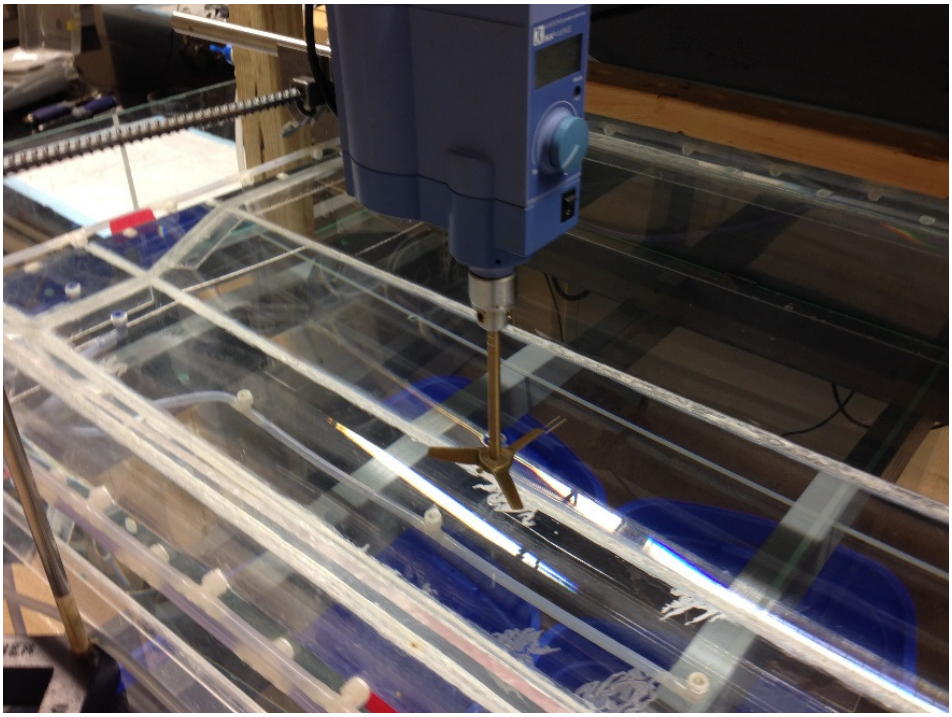

Figure 4.22: Mounted mixer for CMFR experiments

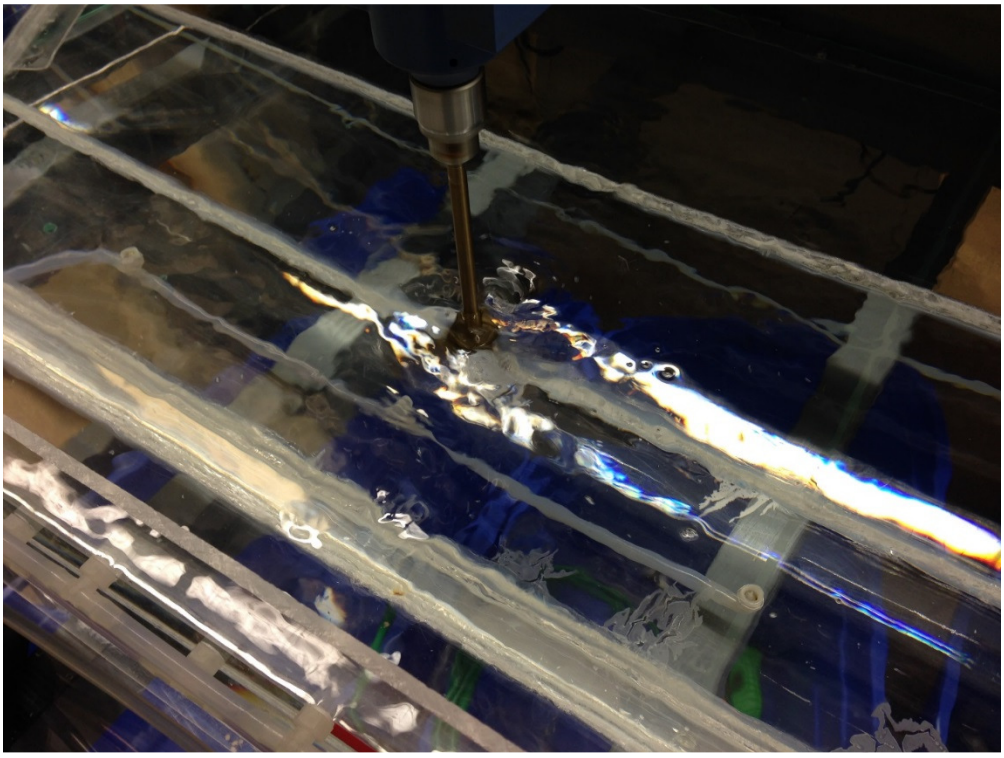

Figure 4.23: Mixing the pool

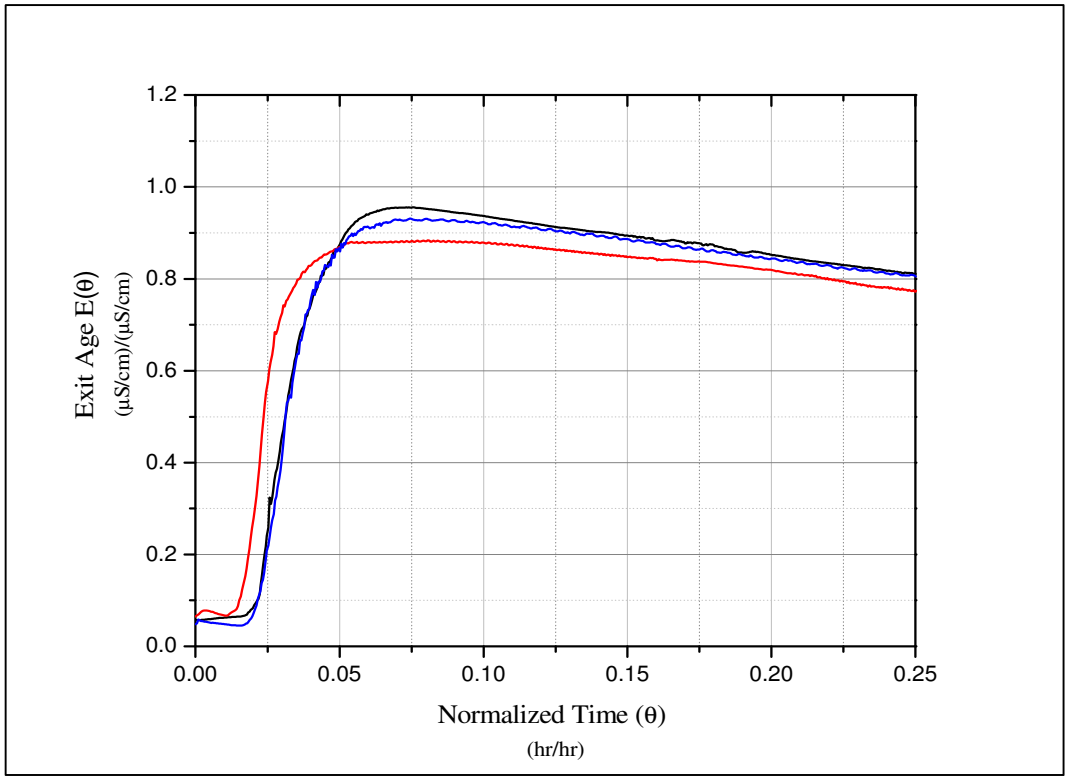


Figure 4.24: Initial slope of the exit age distribution of 6 hour turnover period experiments with completely mixed flow pattern

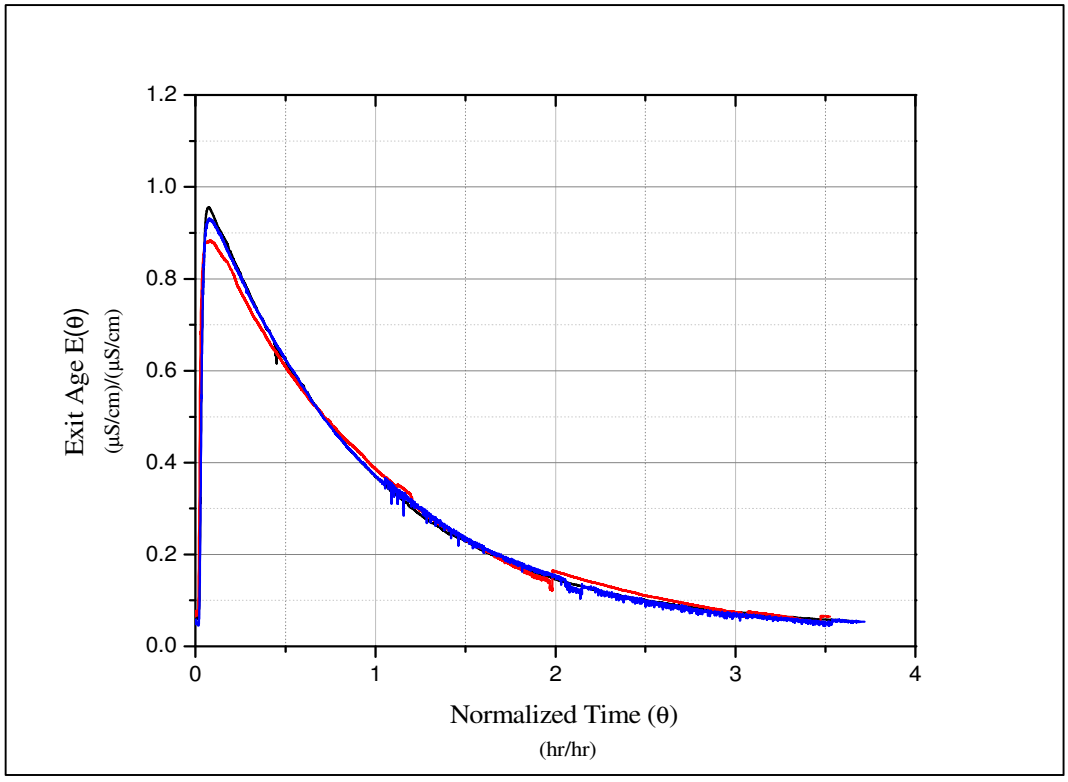


Figure 4.25: Exit age distribution of 6 hour turnover period experiments with completely mixed flow pattern

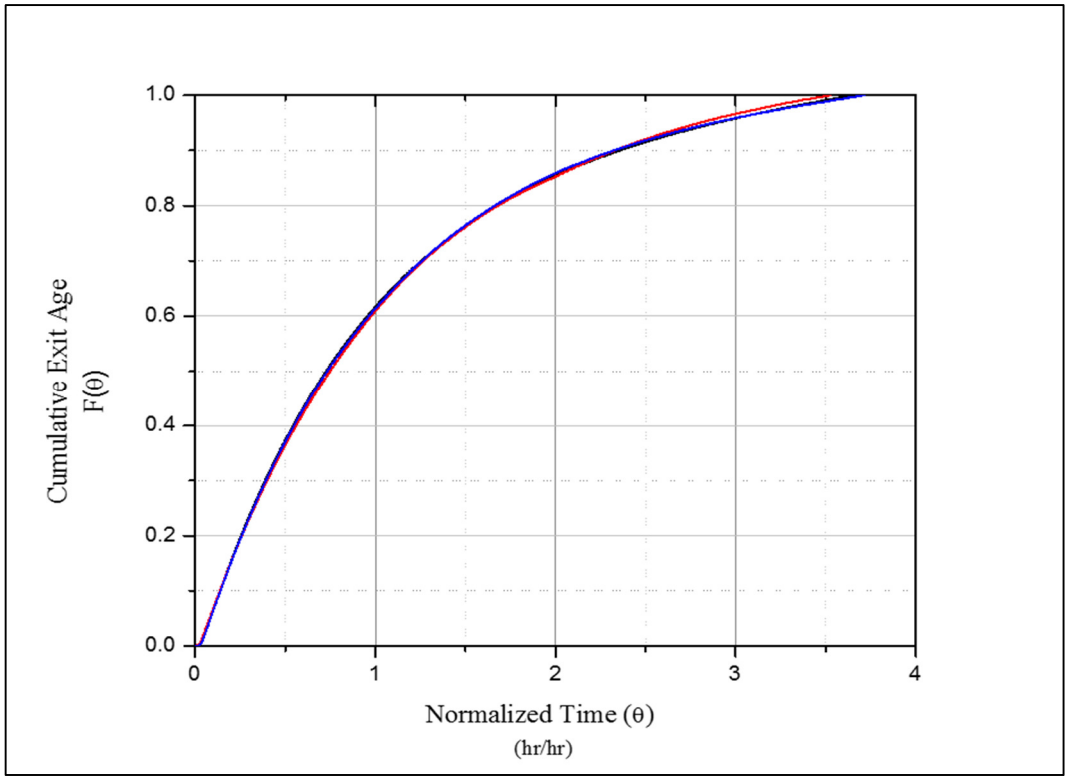


Figure 4.26: Cumulative exit age distribution of 6 hour turnover period experiments with completely mixed flow pattern

4.1.3.5 Flow Configuration Comparison

The completely mixed, single direction flow, and standard pool condition flow systems were compared. A comparison of the indicators, shown in Table 4.6 of short-circuiting and mixing shows very little difference. Indicators of short-circuiting, $\theta_0$ and $\theta_{10}$ are nearly ideal CSTR. Mixing indicators showed a range of value. Indicators $\theta_{75}$-$\theta_{25}$ and $\theta_{90}$-$\theta_{10}$ were 97% ideal CSTR. The efficiency of all three operating conditions did not change significantly from the standard pool condition efficiency as shown in Figure 4.27. During initial mixing, by the time 0.25 turnover period, ($\theta$), has passed, each condition has peaked and begun its decline. The complete RTD curve, Figure 4.28 results show that once the test reaches its peak, the RTD curve behaves as an exponential decay model. The results of the cumulative exit age distribution, Figure 4.29, show that each experiment follows an ideal reactor model. There was no significant difference between the standard condition, the pool with mixer, or the single direction flow.

Table 4.6: Characteristics for bench-scale Junior Olympic pool

| Characteristic | Indicator | Ideal CSTR | **Exp. Standard Condition** | **Exp. w/ Mixer** | **Exp. Single Direction** | Ideal PFR |
|---|---|---|---|---|---|---|
| Short-circuiting | $\theta_0$ | 0.00 | **0.00** | **0.00** | **0.00** | 1.00 |
| | $\theta_{10}$ | 0.11 | **0.15** | **0.14** | **0.15** | 1.00 |
| Mixing | $\theta_{75}$-$\theta_{25}$ | 1.10 | **1.13** | **1.12** | **1.13** | 0.00 |
| | $\theta_{90}$-$\theta_{10}$ | 2.20 | **2.17** | **2.20** | **2.15** | 0.00 |

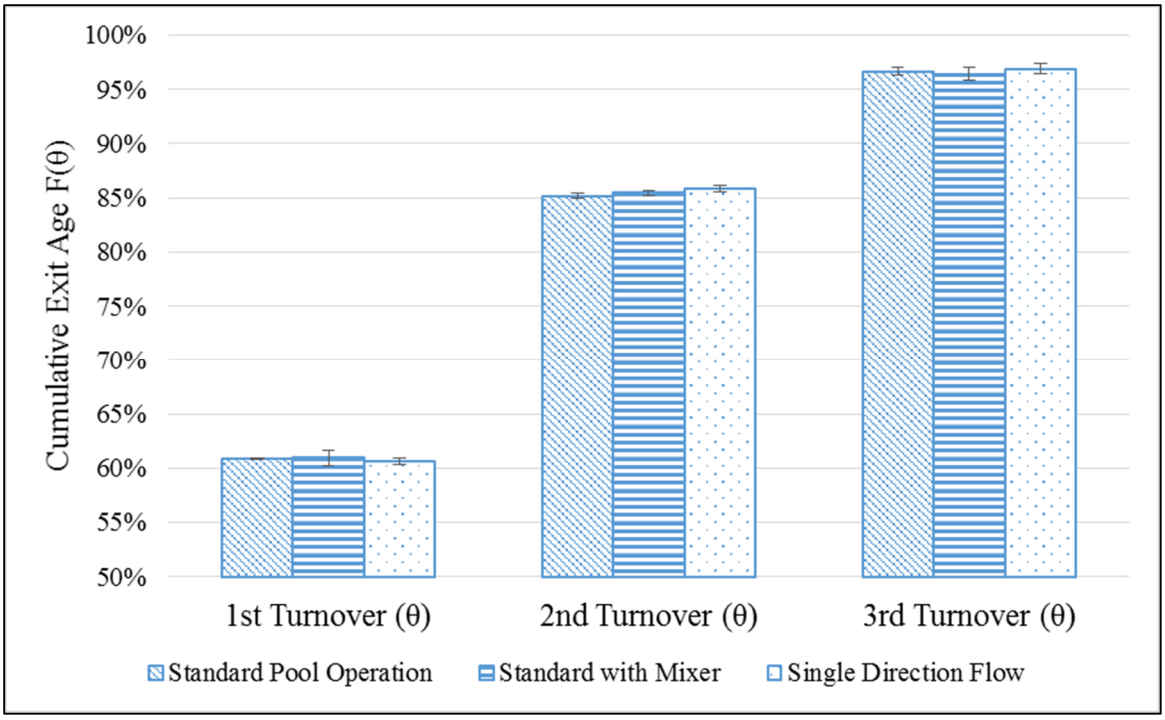


Figure 4.27: Efficiency of exit age comparison

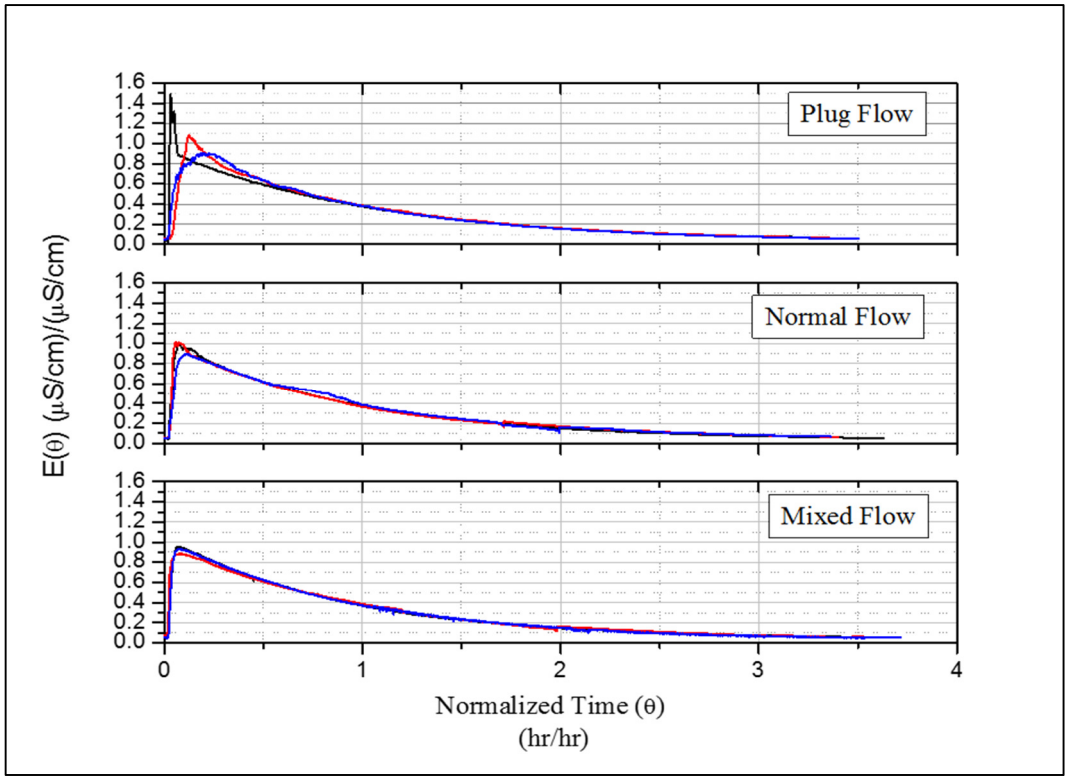


Figure 4.28: Exit age distribution for three operating modes (n=3)

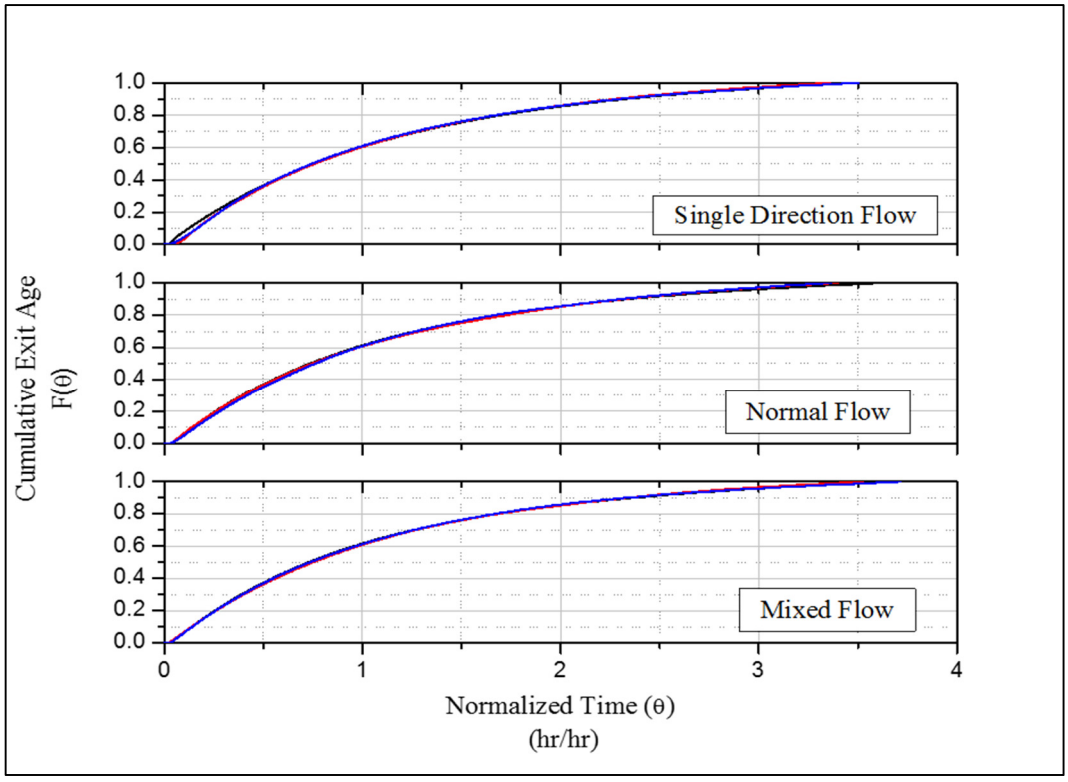


Figure 4.29: Cumulative exit age distribution

### 4.1.4 Recirculation

During the second phase of quantifying, the bench-scale Junior Olympic pool the system was operated in recirculating mode. The recirculation allowed the tracer to reach a steady state. The results of the recirculation phase helped define the initial mixing and lend understanding to the timescales on which pool mixing occurs. With no tracer exiting the system, an exit age distribution is not possible. However, the conductivity over time provides an adequate description of the initial mixing. In Figure 4.30, the conductivity began to increase after 7.5 minutes of the tracer being injected into the system. The conductivity increased at a steady rate until a peak steady state was reached at 30 minutes. Conductivity after peak was extrapolated in an even line to accentuate steady state in Figure 4.30.

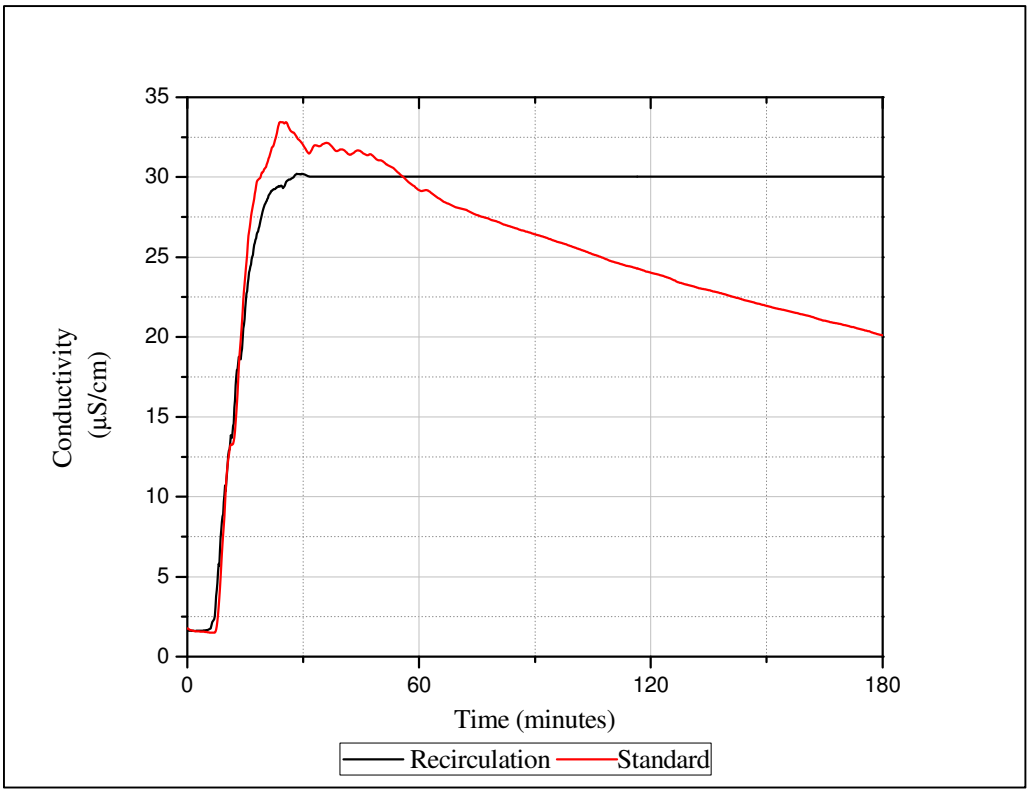


Figure 4.30: Averaged initial slope of conductivity for standard pool condition (n=3)

## 4.2 1:25 Bench-Scale Upflow Swimming Pool with Bottom Inlets

To quantify the efficiency of the bench-scale upflow swimming pool with bottom inlets with upflow to circulate water to the treatment system experiments were performed. Experiments comprised of three main phases; standard operation, varying turnover period, and flow with weirs. The system was first quantified under standard pool operating modes, and then a variety of turnover periods were investigated. Second phase experiments compared turnover rates and examined how the flowrate and turnover period effected hydraulic efficiency. In the third phase, experiments were performed with weirs in place. Weirs simulated a pool skimmer system allowing for 1-5% of the pool perimeter to permit flow.

### 4.2.1 Dye Studies

Triplicate dye studies were performed using crystal violet. The system was set to the standard pool condition with a 6 hour turnover. All conductivity probes were removed from the system. Bottom inlets dispersed the dye laterally along the bottom of the pool within 17 seconds of dye injection as shown in Figure 4.31. After 90 seconds, stagnant zones began to appear in the corners of the pool (Figure 4.32). Flow path lines became apparent with the corners becoming low flow zones as shown in Figure 4.33. As shown in Figure 4.34, after 280 seconds, the dye had diffused throughout the dead zone and the pool had reached a steady state.

The upflow scale pool responded to the dye injection at the same time scale as the Junior Olympic bench-scale pool. In both pools, dye began exiting the inlets in between 17 to 30 seconds. The dye progressed rapidly through the pool. In the upflow scale pool, no central eddy was created. This can be explained by the inlet locations. The grid of

upflow mounted inlets prevented the formation of a central eddy. However, the upflow scale pool did form larger low-flow corner areas than the scale junior Olympic pool. Both pools became completely dyed in between 270 seconds and 280 seconds, or 0.13θ.

Figure 4.31: Dye exiting bottom mounted inlet t = 17 seconds

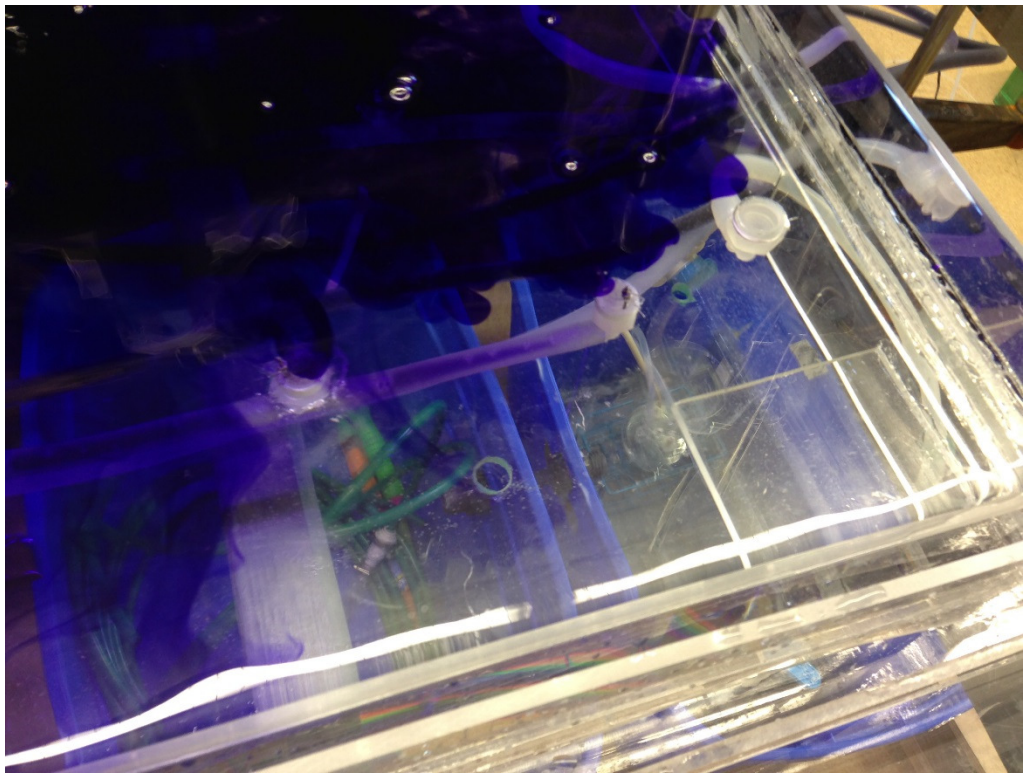

Figure 4.32: Dead zone in pool corner t = 90seconds

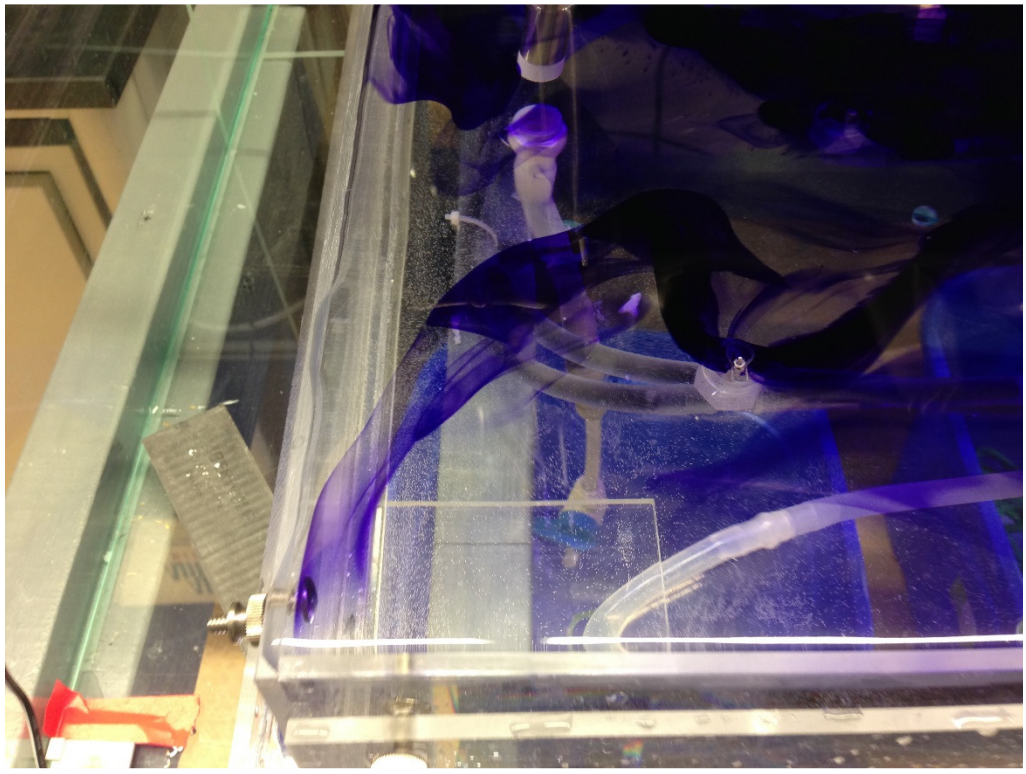

Figure 4.33: Flow path line through the corner area t = 100 seconds

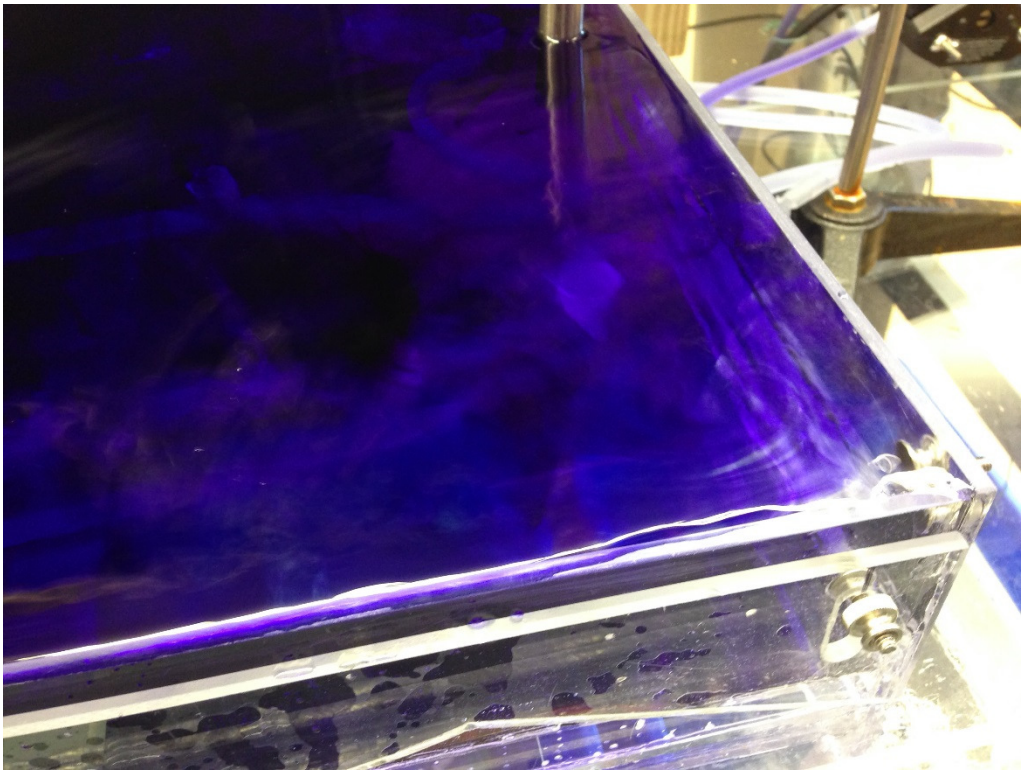

Figure 4.34: Completely dyed in corner area t = 280 seconds

### 4.2.2 Standard Pool Condition Tracer without Recirculation

For bench-scale experiments, the standard pool condition was defined as a 6 hour turnover period, with 100% of the perimeter open as overflow. Indicators for mixing and short-circuiting were quantified for standard pool condition. The exit age distribution of the standard pool condition experiments were compared to the exponential decay curve and the standard operation of the Junior Olympic scale pool. The cumulative exit age distributions were also investigated to understand the efficiency at which the salt tracer was removed from the system.

To characterize the system under standard pool condition conditions, three experiments were performed using a 6 hour turnover period. Influent and effluent flow rate were set at 128 mL/min. Under standard pool condition conditions, the skimmers were

removed and 100% of the perimeter was available for overflow. The salt tracer was injected over a 2.5 minute period. As shown in Table 4.7, the standard pool condition exhibited minimal short-circuiting and the values for short-circuiting were comparable to those of an ideal CSTR.

Both the upflow and Junior Olympic bench-scale pools preformed similarly when comparing efficiency as shown in Figure 4.35. In the initial growth phase of the exit age distribution, Figure 4.36, the upflow pool took longer to reach peak. While the Junior Olympic pool reached peak concentration within 0.1θ, the upflow pool reached peak concentration at 0.25θ. This resulted in the peak coming 1 hour later in the upflow pool than in the junior Olympic pool. The shift in peak resulted in the entire exit age distribution being shifted to the right until the curves converged at 1.5θ as shown in Figure 4.37. While this shift is visible as the beginning of the cumulative exit age, Figure 4.38, the two curves intersect at 1.0θ at an efficiency of 61%.

Table 4.7: Comparison of characteristics for standard conditions

| Characteristic | Indicator | Ideal CSTR | **Upflow Standard** | **Junior Olympic Standard** | Ideal PFR |
|---|---|---|---|---|---|
| Short circuiting | $\theta_0$ | 0.00 | **0.00** | **0.00** | 1.00 |
| | $\theta_{10}$ | 0.11 | **0.21** | **0.15** | 1.00 |
| Mixing | variance ($\sigma^2$) | 1.00 | **0.60** | **0.70** | 0.00 |

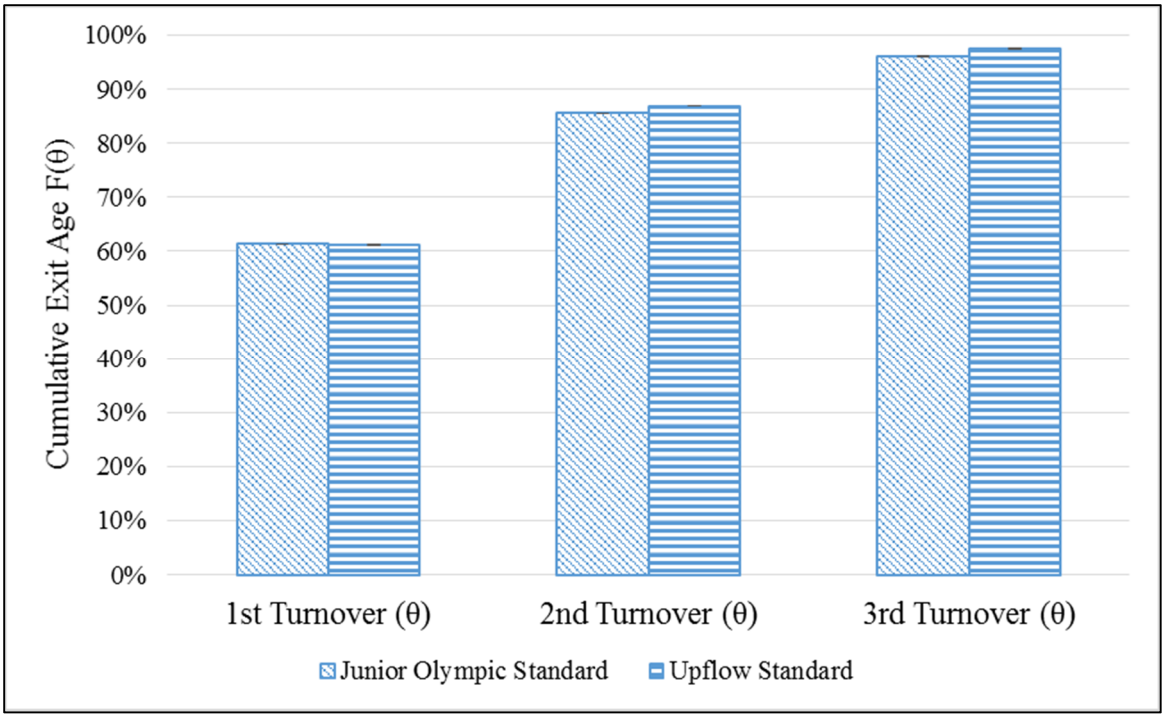


Figure 4.35: Comparison of cumulative exit age efficiency

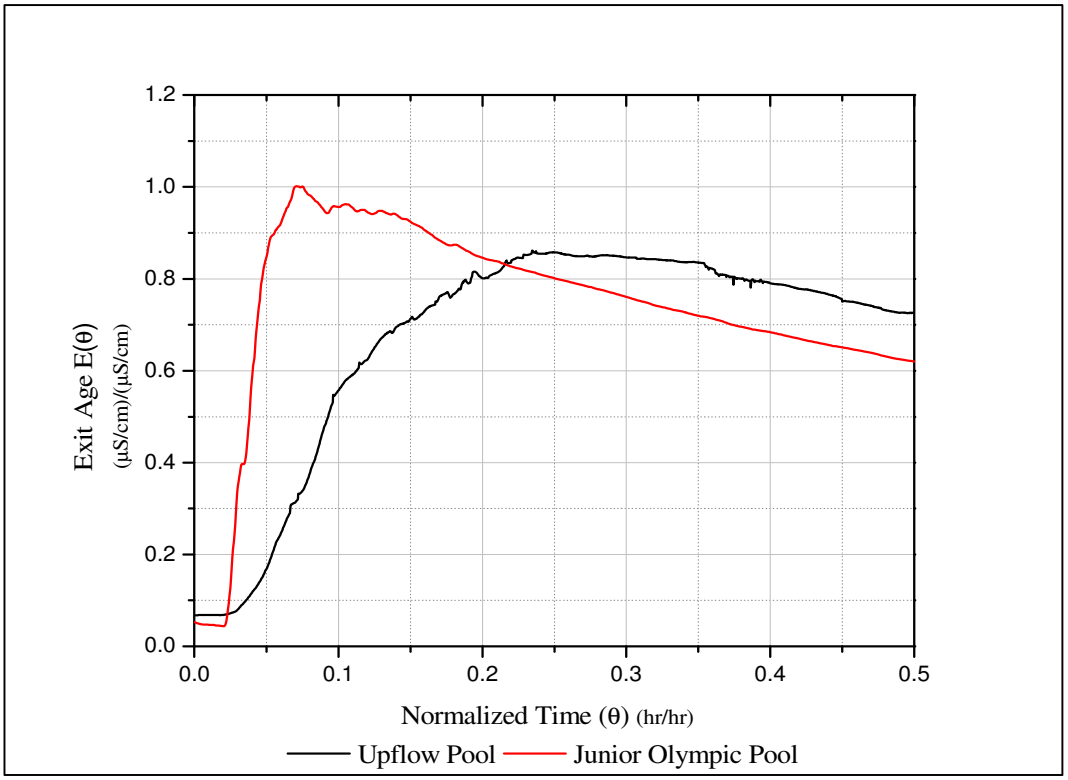


Figure 4.36: Initial exit age distribution comparison of standard pool conditions

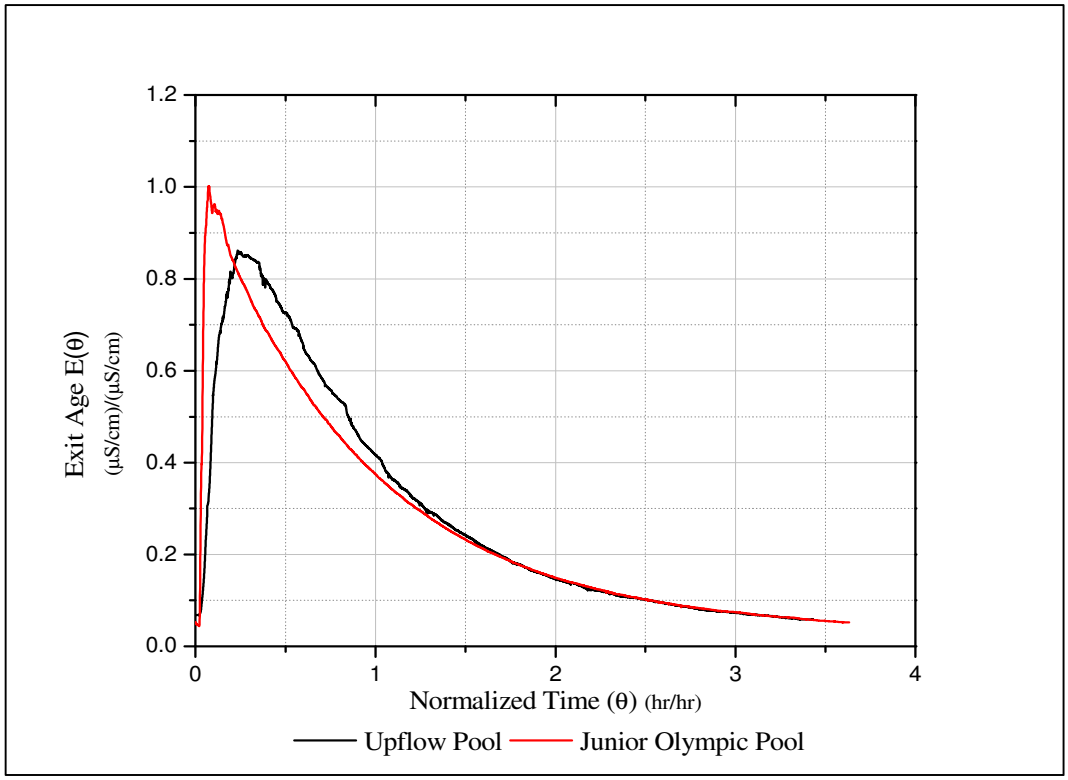


Figure 4.37: Exit age distribution comparison for standard pool conditions

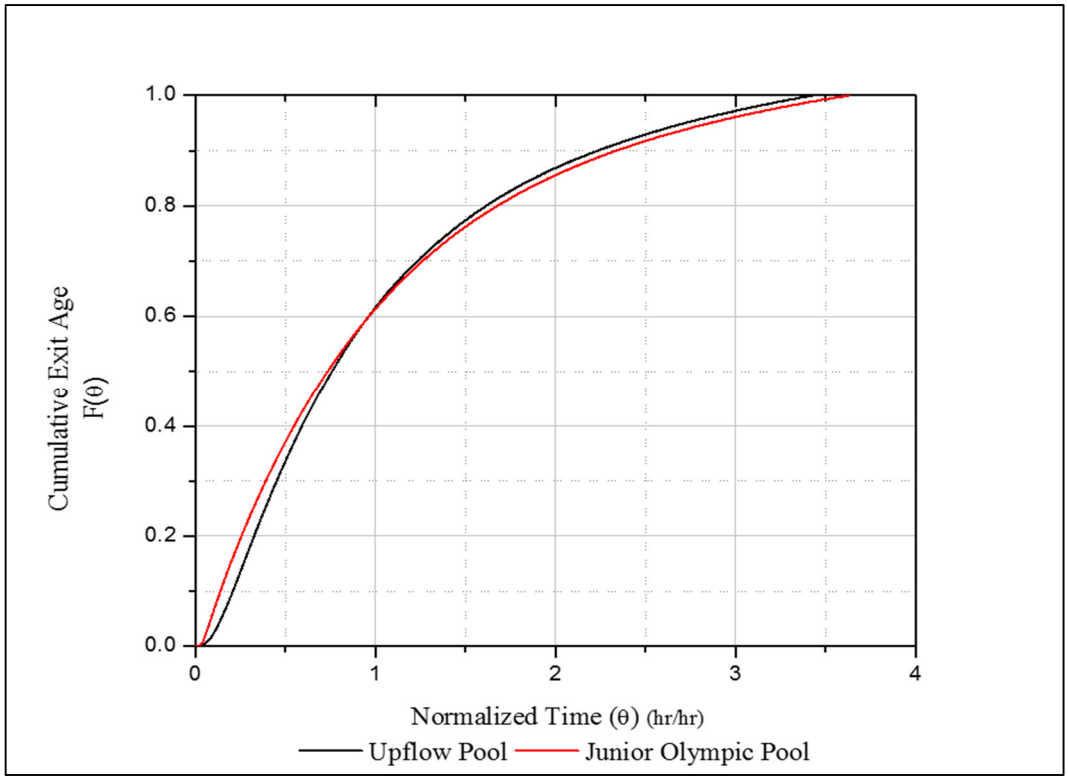


Figure 4.38: Cumulative exit age distribution comparison of standard pool conditions

### 4.2.3 Turnover Time with Continuous Overflow

Three turnover periods were investigated to determine the effects of flowrate and turnover time on the upflow bench-scale pool. Turnover periods of 1 hour, 6 hour, and 12 hour were examined. Flowrates for the turnover times are shown in Table 4.8. The salt tracer was injected over a 2.5 minute period.

Table 4.8: Turnover period flowrates for bench-scale upflow pool

| Turnover Period (hr) | Influent flowrate (mL/min) |
|---|---|
| 1 | 766.8 |
| 6 | 127.8 |
| 12 | 63.9 |

When comparing the characteristics of the various turnovers, all indicators were closely grouped as shown in Table 4.9. No flowrate exhibited short circuiting. Mixing, while less than an ideal CSTR, was consistent between all three turnover periods.

Table 4.9: Comparison of characteristics of turnover times with continuous overflow

| Characteristic | Indicator | Ideal CSTR | **1 hour** | **6 hour** | **12 hour** | Ideal PFR |
|---|---|---|---|---|---|---|
| Short circuiting | $\theta_0$ | 0.00 | **0.00** | **0.00** | **0.00** | 1 |
| | $\theta_{10}$ | 0.11 | **0.14** | **0.14** | **0.14** | 1 |
| Mixing | variance ($\sigma^2$) | 1.00 | **0.79** | **0.70** | **0.75** | 0.00 |

All three turnover periods performed similarly. There was very little difference between the efficiency with which the solution exited the system as shown in Figure 4.39. The three turnover periods exhibited initial exit age distribution phases that peaked

between 0.10θ and 0.30θ as shown in Figure 4.40. This did not seem to be dependent on flowrate, as the increase in peak time did not correspond to a decrease in flowrate. The complete exit age distribution curves (Figure 4.41) followed the same shape, but did not converge until after the second turnover (2θ). The cumulative exit age, Figure 4.42, followed the predicted path with efficiencies between 61% and 63%.

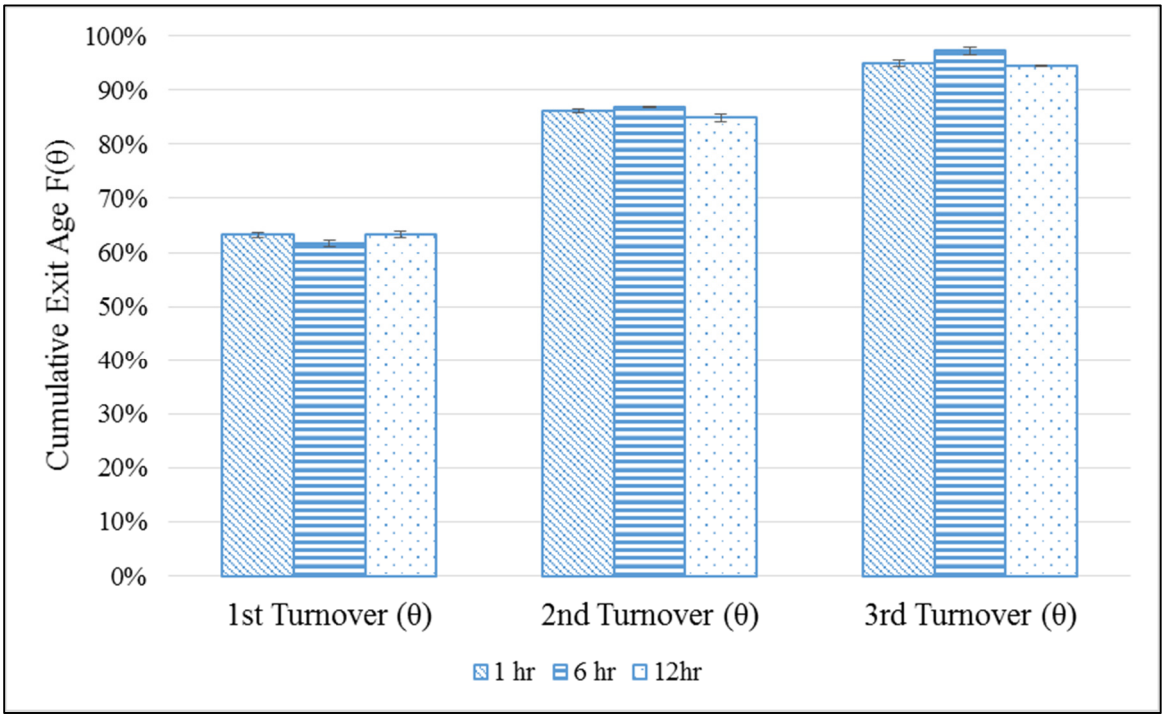


Figure 4.39: Comparison of cumulative exit age efficiency for various turnover periods with continuous overflow

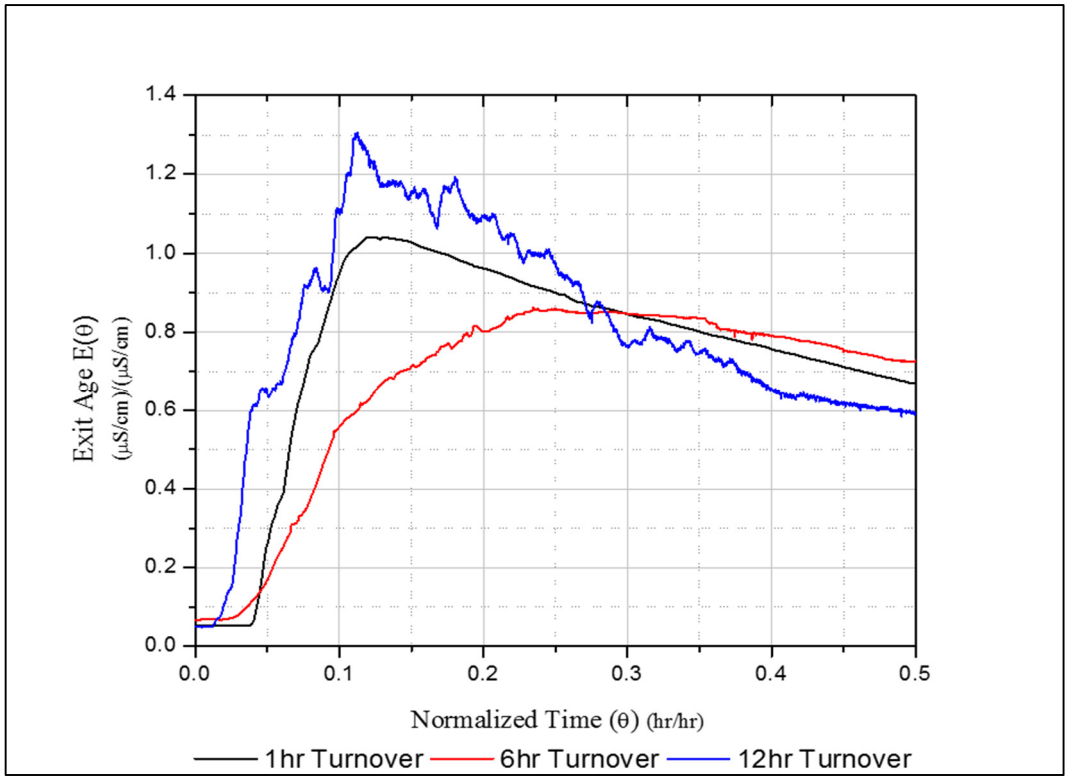


Figure 4.40: Initial slope of exit age distribution for various turnover periods with continuous overflow (n=9)

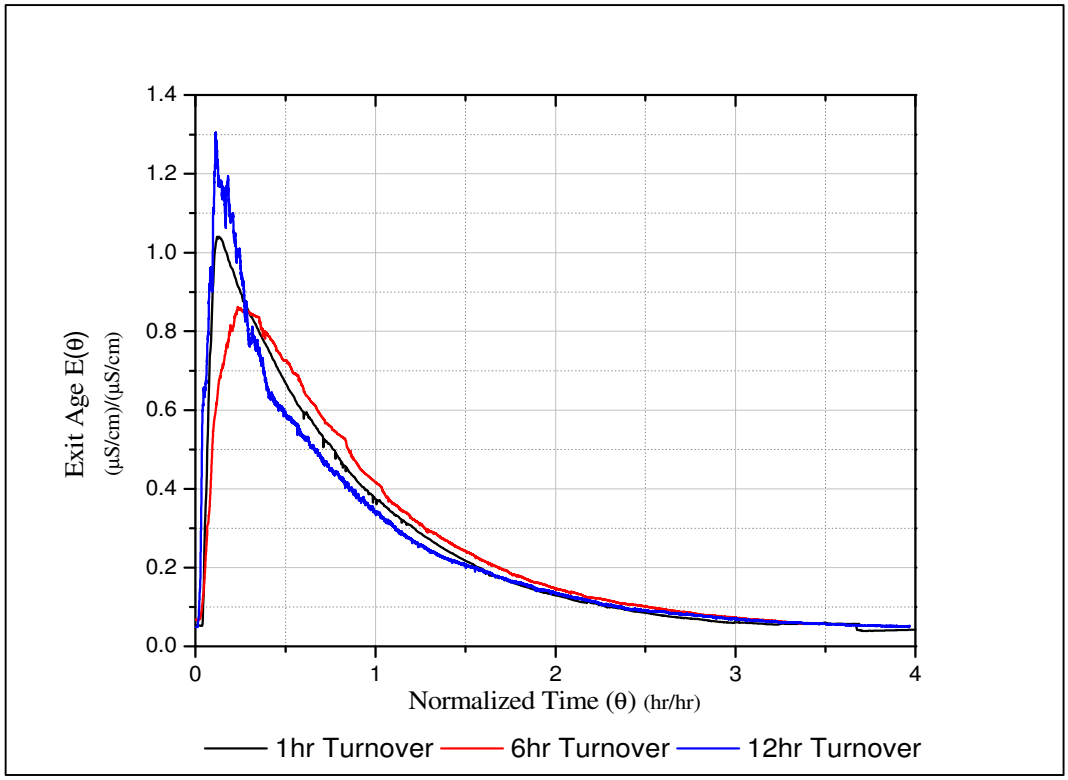


Figure 4.41: Exit age distribution for various turnover periods with continuous overflow (n=9)

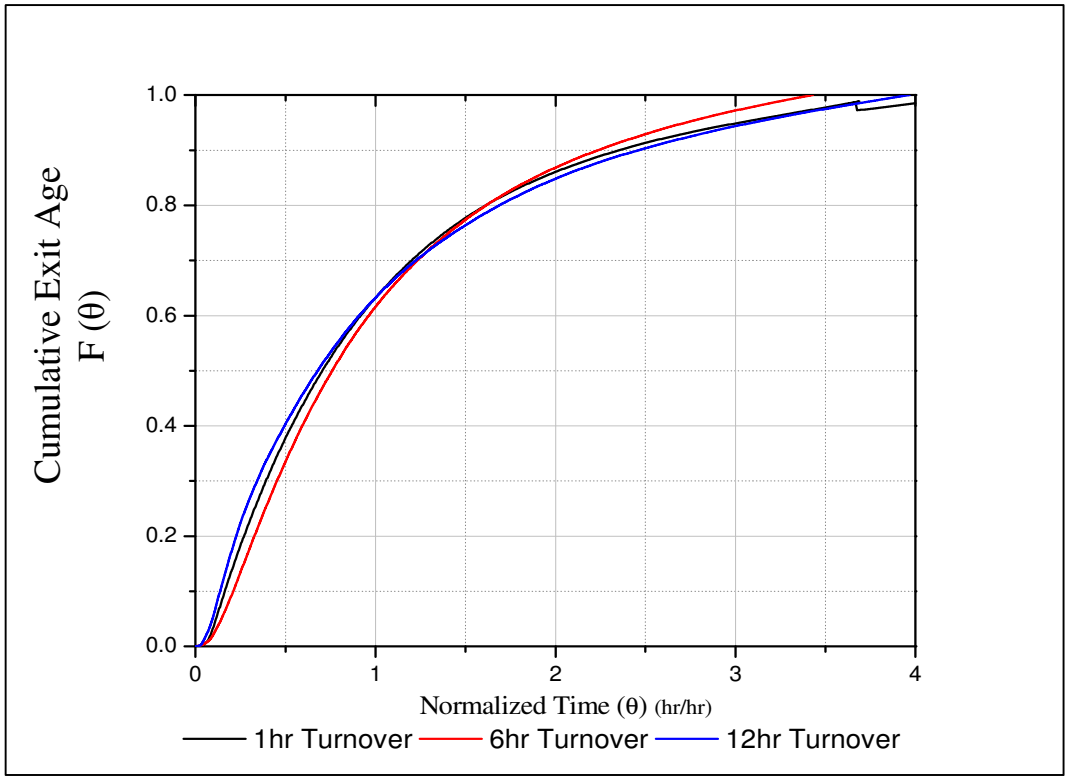


Figure 4.42: Cumulative exit age distribution for various turnover periods with continuous overflow (n=9)

### 4.2.4 Normal Turnover with Weirs

Utilizing a 6 hour turnover period, experiments were performed with weirs to compare to the normal continuous overflow. The overflow was restricted by weirs to a set percentage of the pool perimeter. A 5% overflow opening was chosen as an analog to the average skimmer setup typically used in full scale pools. Short-circuiting and mixing characteristics described in Table 4.10 indicate pools with and without weirs operated very similarly. However, the variance, or the dispersion around the mean, was much high when weirs were added to the pool. As shown in Figure 4.43, there was no difference in the standard pool operation with or without weirs. Both designs performed at the same efficiency, removing 62% of the salt tracer in the first turnover.

Table 4.10: Comparison of characteristics for 6 hour turnover period

| Characteristic | Indicator | Ideal CSTR | **Standard No Weir** | **Standard with 5% Weir** | Ideal PFR |
|---|---|---|---|---|---|
| Short circuiting | $\theta_0$ | 0.00 | **0.00** | **0.00** | 1.00 |
| | $\theta_{10}$ | 0.11 | **0.21** | **0.17** | 1.00 |
| Mixing | variance ($\sigma^2$) | 1.00 | **0.63** | **0.85** | 0.00 |

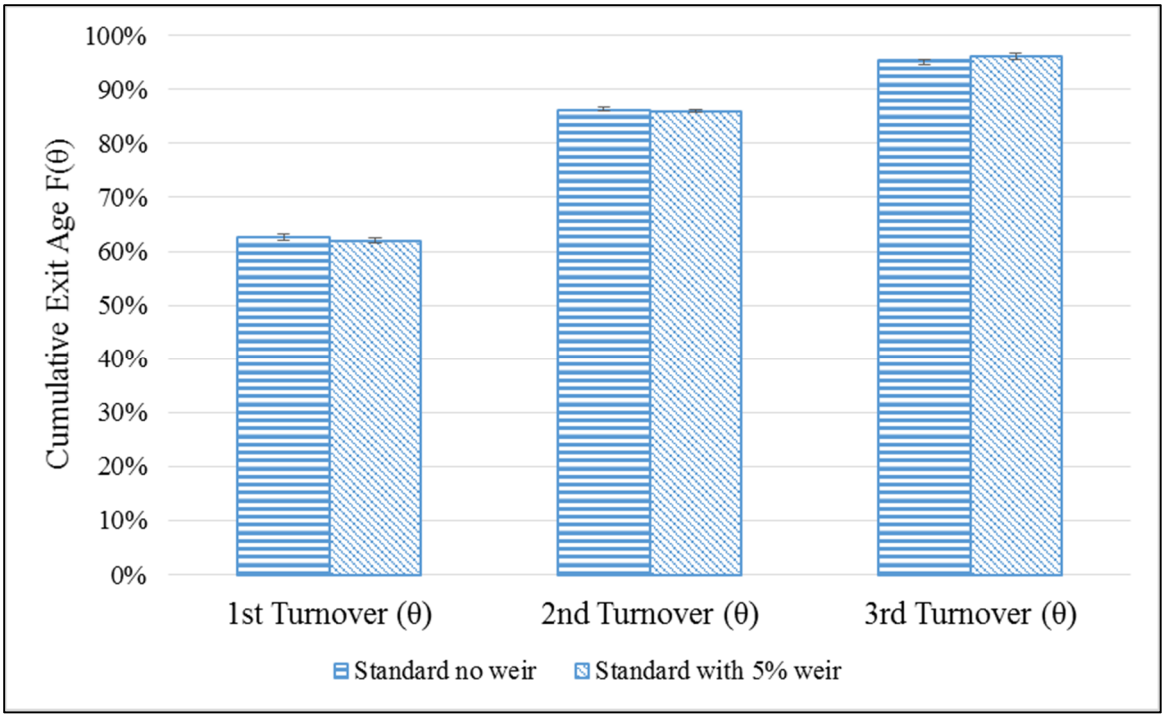


Figure 4.43: Comparison of cumulative exit age efficiency with and without weir (n=3)

### 4.2.5 Rapid Turnover with Weirs

Utilizing a 1 hour turnover period, experiments were performed both with and without weirs. In the first phase, the system was set to continuous overflow, with the entire pool perimeter allowed to overflow. In the second phase, the overflow was restricted to 1% of the pool perimeter. The 1% overflow was chosen as an analog to the minimum skimmer setup typically used. Flows and skimmer percentage are shown in Table 4.11. Short-circuiting and mixing characteristics described in  indicate pools with and without weirs operated very closely to an ideal CSTR. The initial slope of the exit age distribution, Figure 4.45, for the rapid turnover shows a peak reached between 0.10θ and 0.20θ. The complete curve, Figure 4.46, followed an exponential decay, with all slopes being closely grouped. The cumulative exit age shown in Figure 4.47, was closely grouped. The curves

began to diverge, and a small opening appears surrounding the 1θ mark. However, this is a small difference, with the range being from 62.7% and 63.0%.

Table 4.11: Flowrate and perimeter opening 1hour turnover

| | Influent Flowrate (mL/min) | Perimeter overflow | Perimeter restricted |
|---|---|---|---|
| Open flow | 766.8 | 100.0 % | 0.0 % |
| Skimmer flow | 766.8 | 5.0% | 95.0% |
| Skimmer flow | 766.8 | 1.0 % | 99.0 % |

Table 4.12: Comparison of characteristics for 1 hour turnover period

| Characteristic | Indicator | Ideal CSTR | **No Weir** | **1% Weir** | **5% Weir** | Ideal PFR |
|---|---|---|---|---|---|---|
| Short circuiting | $\theta_0$ | 0.00 | **0.00** | **0.00** | **0.00** | 1.00 |
| | $\theta_{10}$ | 0.11 | **0.17** | **0.17** | **0.17** | 1.00 |
| Mixing | variance ($\sigma^2$) | 1.00 | **0.87** | **1.16** | **0.67** | 0.00 |

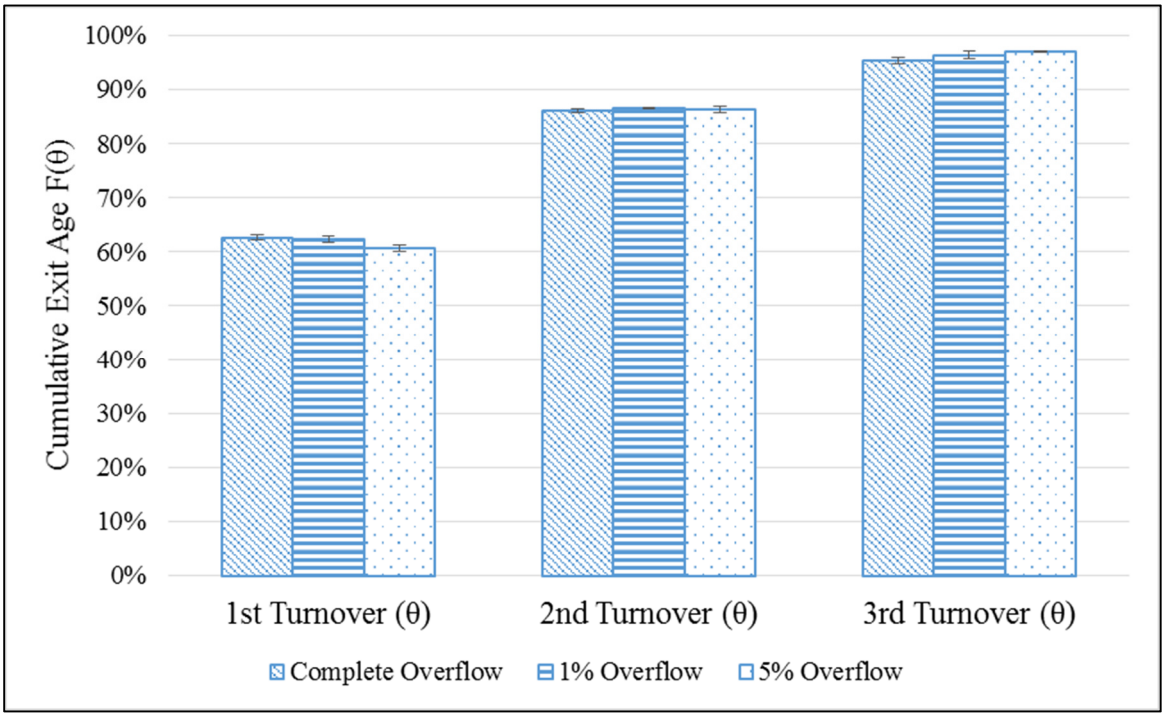


Figure 4.44: Comparison of cumulative exit age for 1 hour turnover period with various overflow percentages

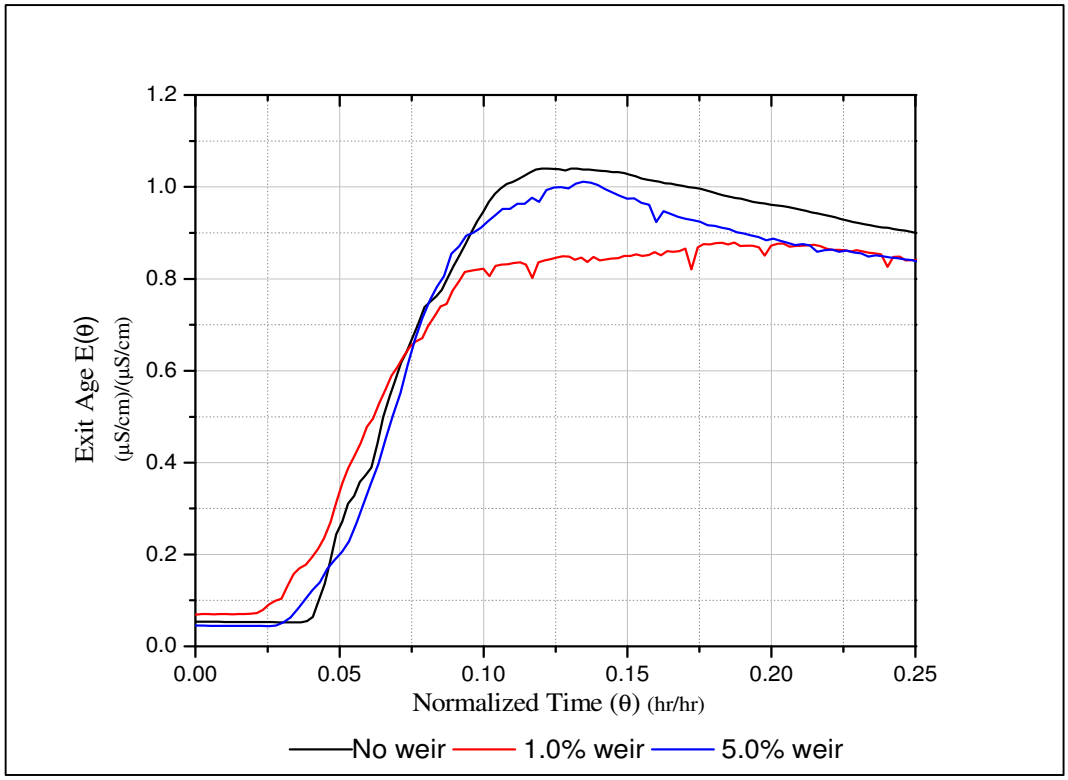


Figure 4.45: Comparison of initial slope of exit age distribution for 1 hour turnover period (n=3)

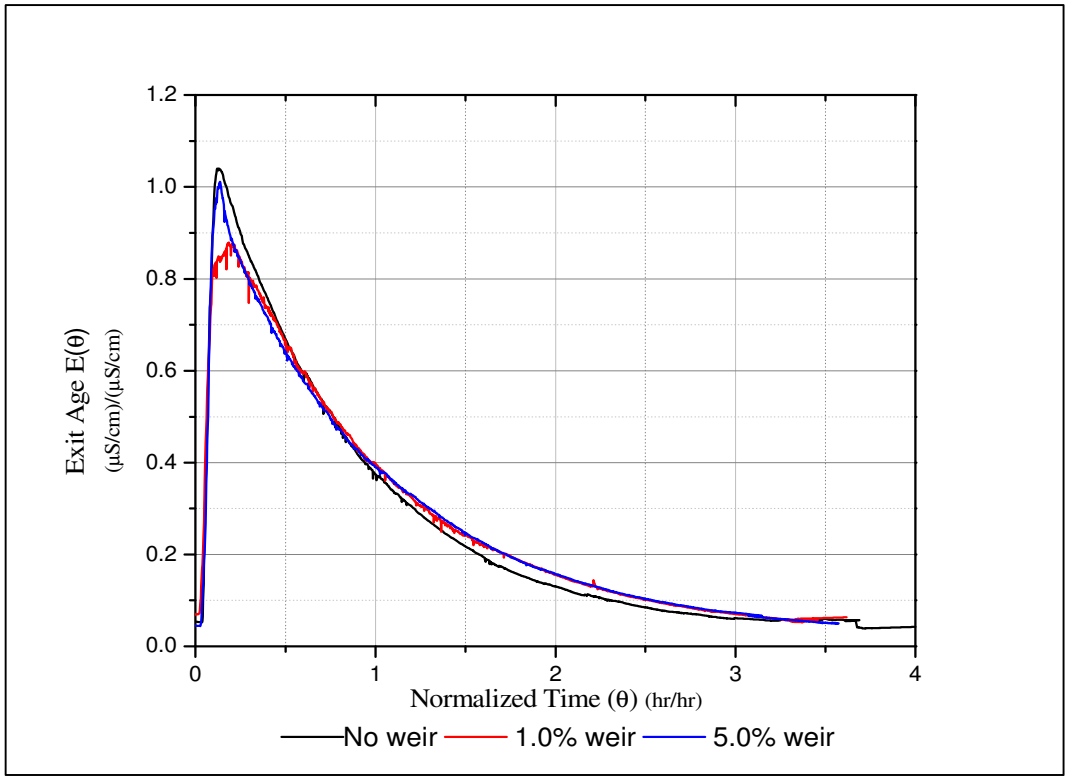


Figure 4.46: Comparison of exit age distribution for 1 hour turnover period (n=3)

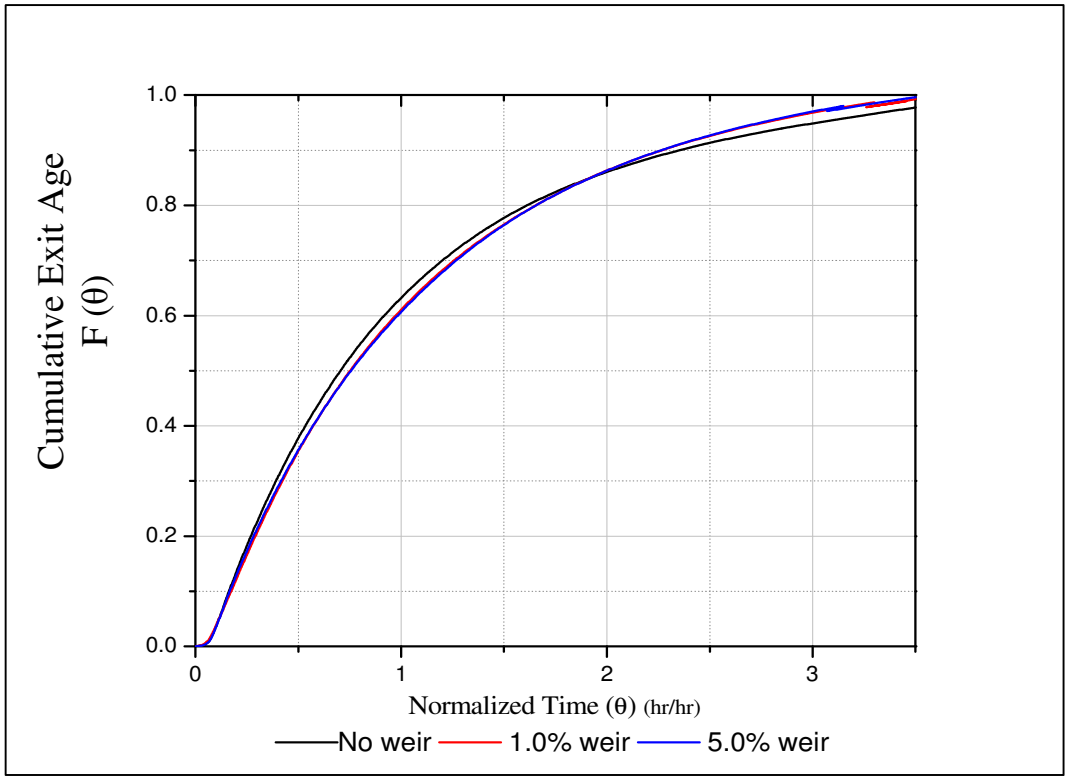


Figure 4.47: Comparison of cumulative exit age distribution for 1 hour turnover period (n=3)

### 4.2.6 1:25 Scale Upflow Pool in Recirculation Mode

The bench-scale pool was operated in recirculation mode to quantify initial mixing. The system was operated with a 6 hour turnover period. Salt tracer was injected and allowed to operate until steady state was reached. As shown in Figure 4.48, the tracer first arrived at the effluent probe after 9 minutes. The tracer concentration increased sharply for 27 minutes, accounting for 90% of the total concentration. After the initial sharp increase, concentration slowly climbed the remaining 10% until reaching a steady state at 1 hour 15 minutes. The concentration tail in Figure 4.48 has been lengthened to accentuate the steady state. The steady state conductivity is closely aligned with the standard, non-recirculating, conductivity. In both the initial increase accounts for over 90% of the total conductivity. Both recirculating and non-recirculating systems reached their peak conductivity within 0.10θ. Predicting the rate at which the system reaches steady state can provide system users with the ability to correctly predict chlorine distribution in pool systems.

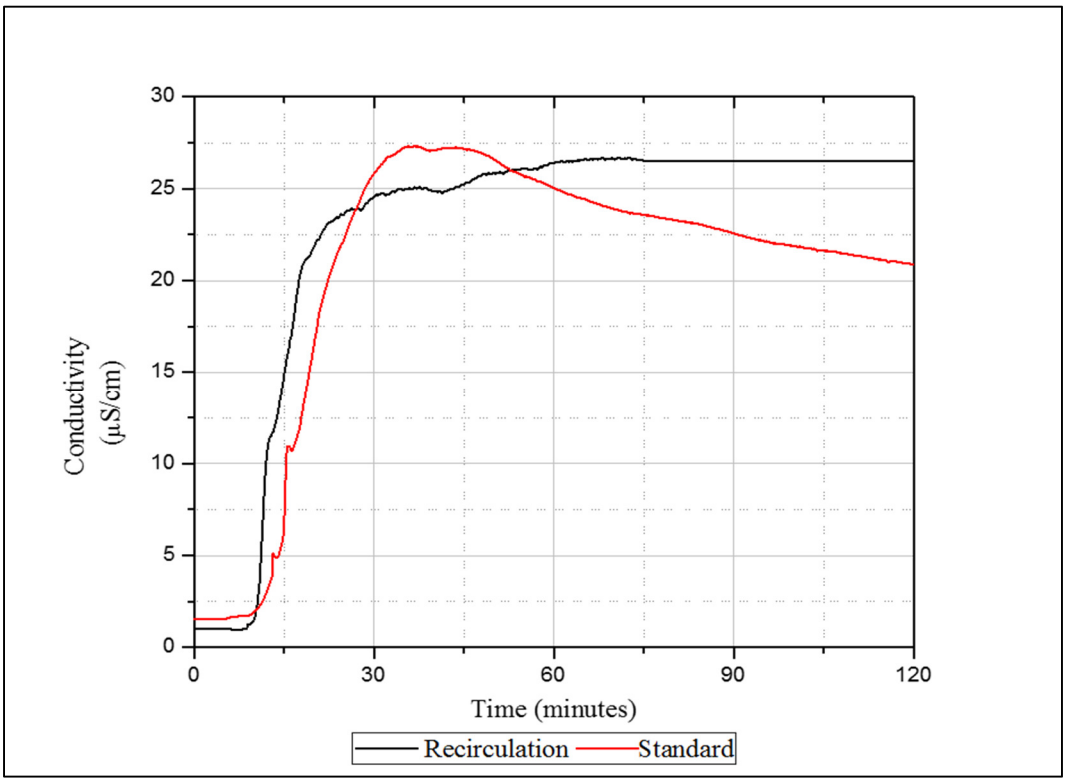


Figure 4.48: Exit age distribution for recirculation until steady state

## 4.3 Predicting System Exit Age Distribution

The recirculation efficiency of the swimming pool closely follows an exponential decay model. Models with bypass, dead volumes, and plug flow were also considered (APPENDIX D), but were did not improve predictions while adding significant complexity. To simplify calculations, it is useful to us the normalized conductivity of the tracer rather than the actual concentration. When using the normalized conductivity the y intercept becomes 1, allowing the constant to be removed from the decay equation. The x-axis can be plotted against time, rather than normalized time.

$$y = \exp\left(-\frac{Q_s}{V_t}\alpha t\right) \tag{4.1}$$

Where: y = y-intercept
$Q_S$ = flowrate of pool system (L/hr)
$V_t$ = total volume of system (L)
t = time (hr)
α = fitting parameter

Setting the x-axis as time, provides a direct correlation between the decay parameter times time, and the pool's flowrate divided by volume. The calculated Q/V for selected pool operations is compared to the fitted decay parameter in Table 4.13. Due to initial short-circuiting and non-ideal mixing, there is a small difference in the calculated flowrate divided by volume and the fitted decay parameter. However, by removing Q/V from the model, a fitting parameter can be found to fit the scale pool's exit age distribution. The fitting parameter is a single parameter that can be used in conjunction with the systems inherent characteristics of volume and flowrate to predict hydraulic efficiency. The fitting parameter's for the bench-scale swimming pools ranged from 0.94 to 1.11. The exit age distributions compared to the exponential decay model are shown in Figure Figure 4.49, Figure 4.50, Figure 4.51, and Figure 4.52.

Table 4.13: Comparison of calculated detention time and decay rates

| | Bench-scale Junior Olympic Pool | Bench-scale Junior Olympic Pool | Bench-scale Upflow Pool | Bench-scale Upflow Pool |
|---|---|---|---|---|
| Turnover Period (hour) | 1 | 6 | 1 | 6 |
| Calculate Q/V ($hr^{-1}$) | 1.00 | 0.167 | 1.00 | 0.167 |
| Modeled Decay Rate | 0.908 | 0.160 | 1.065 | 0.150 |
| $R^2$ | 0.986 | 0.978 | 0.989 | 0.962 |
| Fitting Parameter | 1.10 | 1.04 | 0.94 | 1.11 |

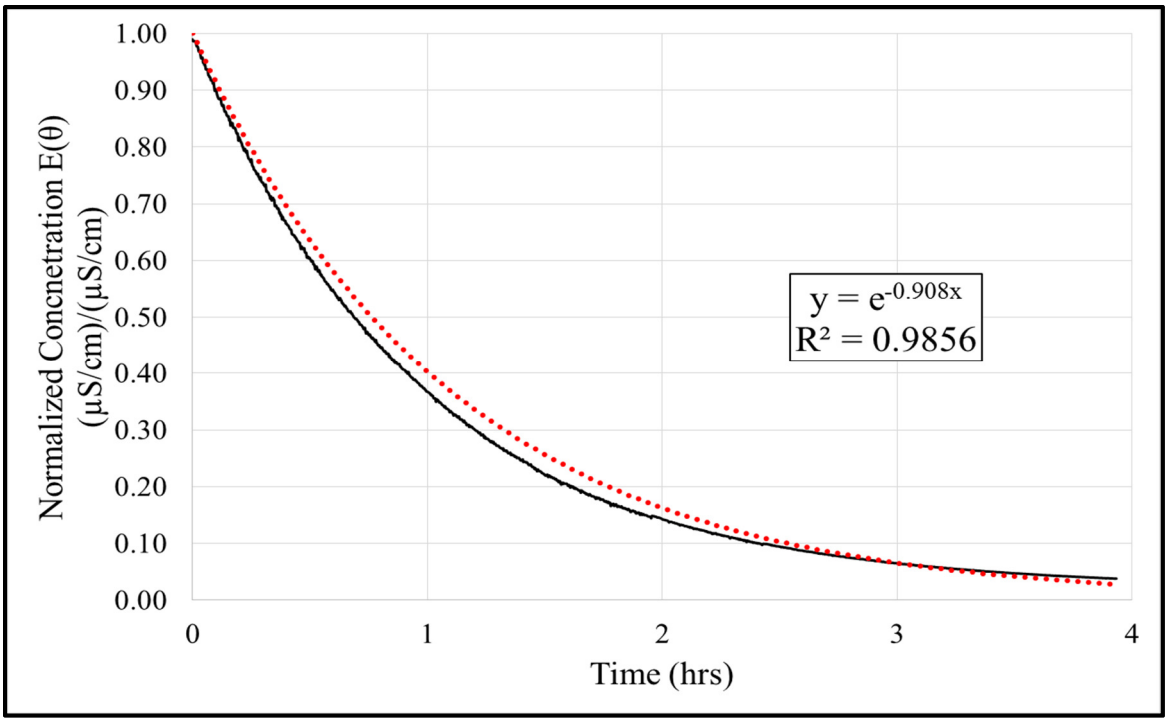


Figure 4.49: Normalized concentration distribution of 1 hour turnover period for the bench-scale Junior Olympic pool compared to exponential decay model

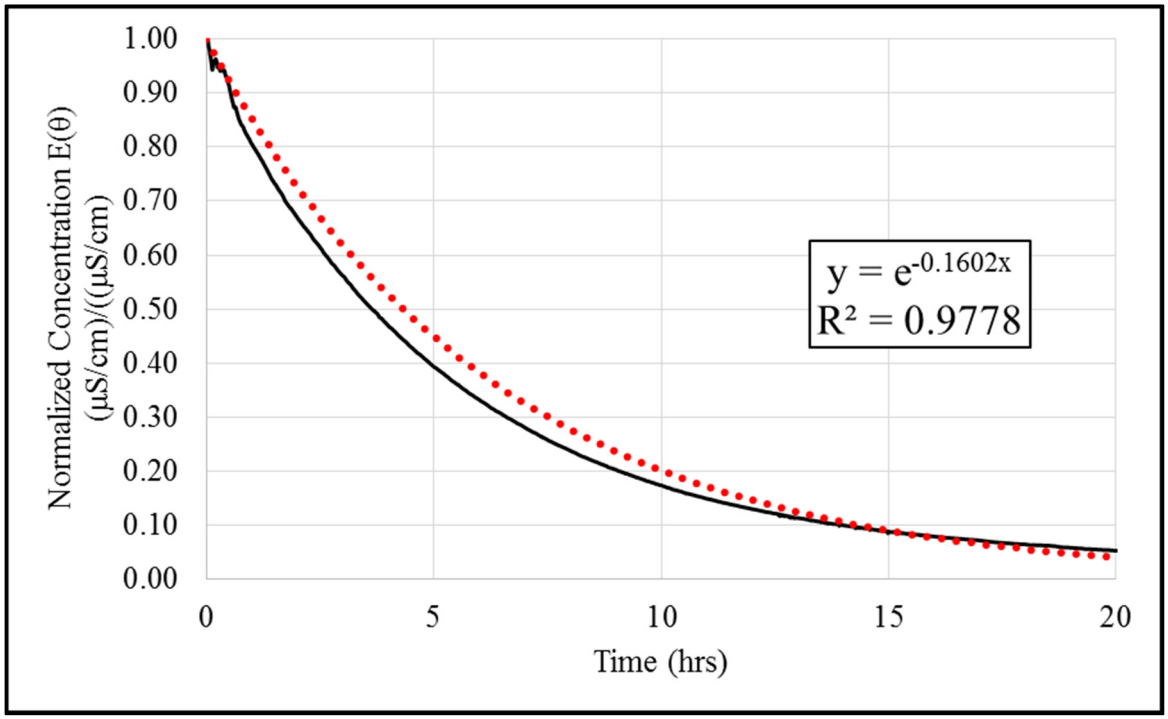


Figure 4.50: Normalized concentration distribution of 6 hour turnover period for the bench-scale Junior Olympic pool compared to exponential decay model

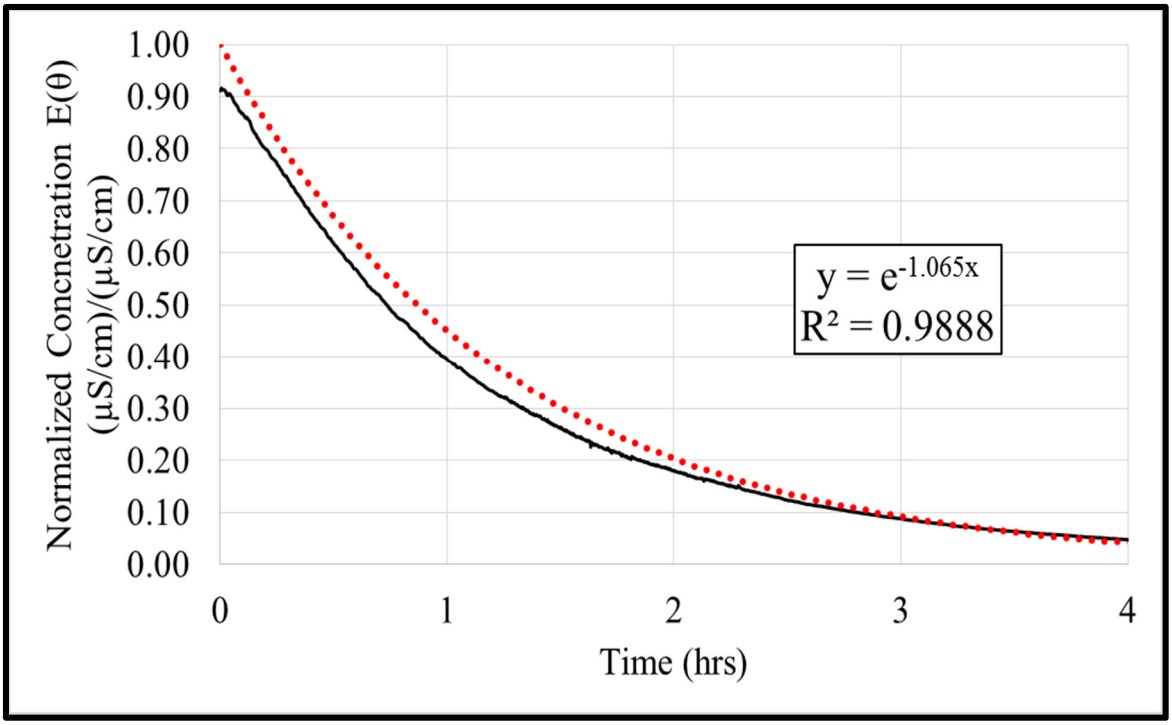


Figure 4.51: Normalized concentration distribution of 1 hour turnover period for the bench-scale upflow pool compared to exponential decay model

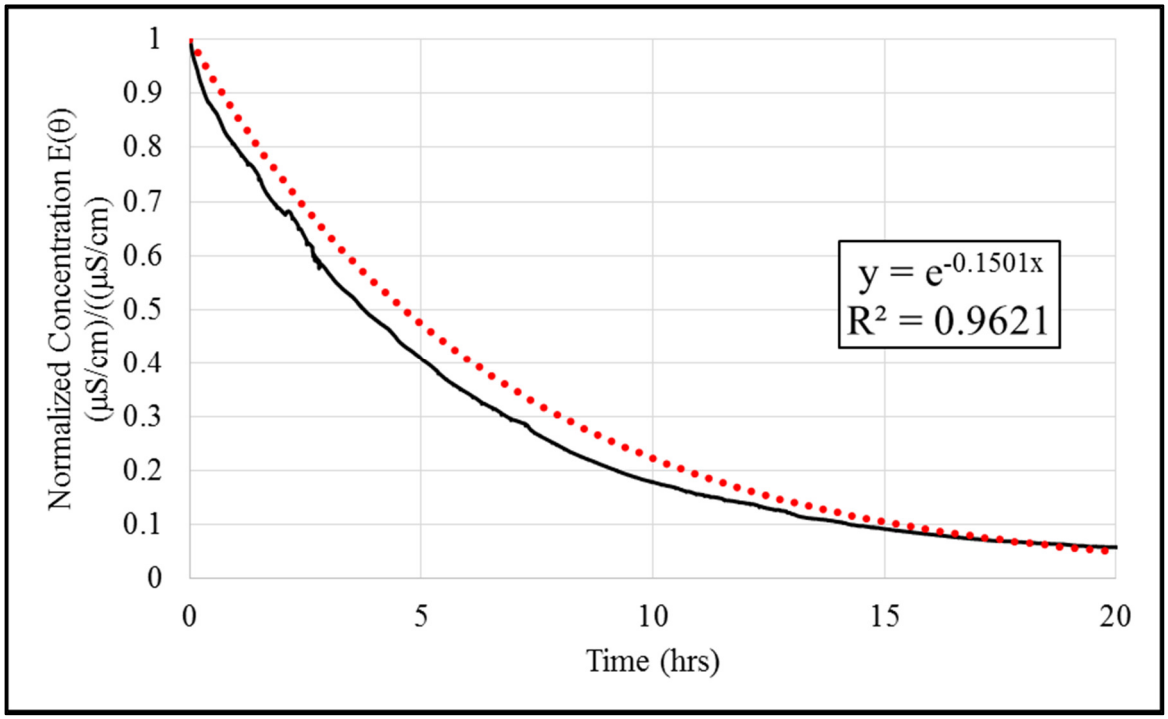


Figure 4.52: Normalized concentration distribution of 6 hour turnover period for the bench-scale upflow pool compared to exponential decay model

By subtracting the right side of equation 4.1 from 1, the percentage of the pool volume that has been circulated at any point in time is predicted.

$$n_t = (1 - \exp\left(-\frac{Q_s}{V_t}t\right)) * 100\% \quad (4.2)$$

Where: $n_t$ = pool circulation efficiency at time t
$Q_S$ = flowrate of pool system (L/hr)
$V_t$ = total volume of system (L)
t = time (hr)

For example, the standard pool operation of the bench-scale Junior Olympic pool with the characteristics shown in Table 4.13, has effectively circulated 63% of the pool volume in 6 hours.

$$1 - \exp\left(-\frac{14.46\ L/hr}{87L} * 6hrs\right) * 100\% = 63.1\% \quad (4.3)$$

Alternately, this formula can be manipulated to provide the necessary time to reach a certain level of recirculation. It is important to consider the efficiency of the treatment system when calculating the time needed to reach a certain level of removal. By including the treatment system efficiency, a realistic and useful value for time is provided to reach a desired removal percentage.

$$T_{n\%\ Removal} = \frac{-\ln((1 - n) * t_e)}{Q_s} * V_t \quad (4.4)$$

Where: $T_{n\%\ Removal}$ = time required to reach $n\%$ removal (hr)
$n$ = desired removal %
$t_e$ = treatment system efficiency %
$Q_s$ = system flowrate (L/hr)
$V_t$ = total volume (L)

The recirculation efficiency minimizes the difference in treatment system efficiency. As shown in Table 4.14, there is very little difference between a treatment systems with 99.99% removal and a treatment system with 90% removal, in the time it takes them to reach 99.9% removal of a contaminant in the pool volume. The impact of the recirculation efficiency dominates the removal timescale, reducing the difference in the time needed for treatment systems to reach a removal goal. In a pool incident in which $1x10^9$ *Cryptosporidium* oocyst are released treatment systems of 90%, 99.9% and 99.99% efficiency, obtain 3 $\log_{10}$ (99.9%) removal within 5.5 hours, or 0.9 turnovers of each other as shown in Figure 4.53. The difference between treatment systems of 90%, 99.9% and 99.99% efficiency in reaching 6 $\log_{10}$ (99.9999%) removal is 10 hours over a 4 day period as shown in Table 4.15. Dramatic reductions in removal times are realized between treatment systems with 25% and 90% efficiency. Improving the removal rates of sand and cartridge filters from 25% to 90% would decrease the time to reach 99.9% (3 $\log_{10}$) removal approximately 3-fold (from nearly 7 days to just over 2 days) and would decrease the number of turnovers needed by 20 turnovers.

Table 4.14: Comparison of treatment system efficiency times to reach 3 $\log_{10}$ removal

| Treatment system efficiency | 25.0% | 90.0% | 99.0% | 99.99% |
|---|---|---|---|---|
| Hours required | 165 | 51 | 48 | 45.5 |
| Days required | 6.88 | 2.13 | 2.00 | 1.90 |
| Turnovers required | 27.5 | 8.5 | 8 | 7.6 |

Table 4.15: Comparison of treatment system efficiency times to reach 6 $\log_{10}$ removal

| Treatment system efficiency | 25.0% | 90.0% | 99.0% | 99.99% |
|---|---|---|---|---|
| Hours required | 327 | 102 | 93 | 91.8 |
| Days required | 13.63 | 4.25 | 3.88 | 3.83 |
| Turnovers required | 54.5 | 17 | 15.5 | 15.3 |

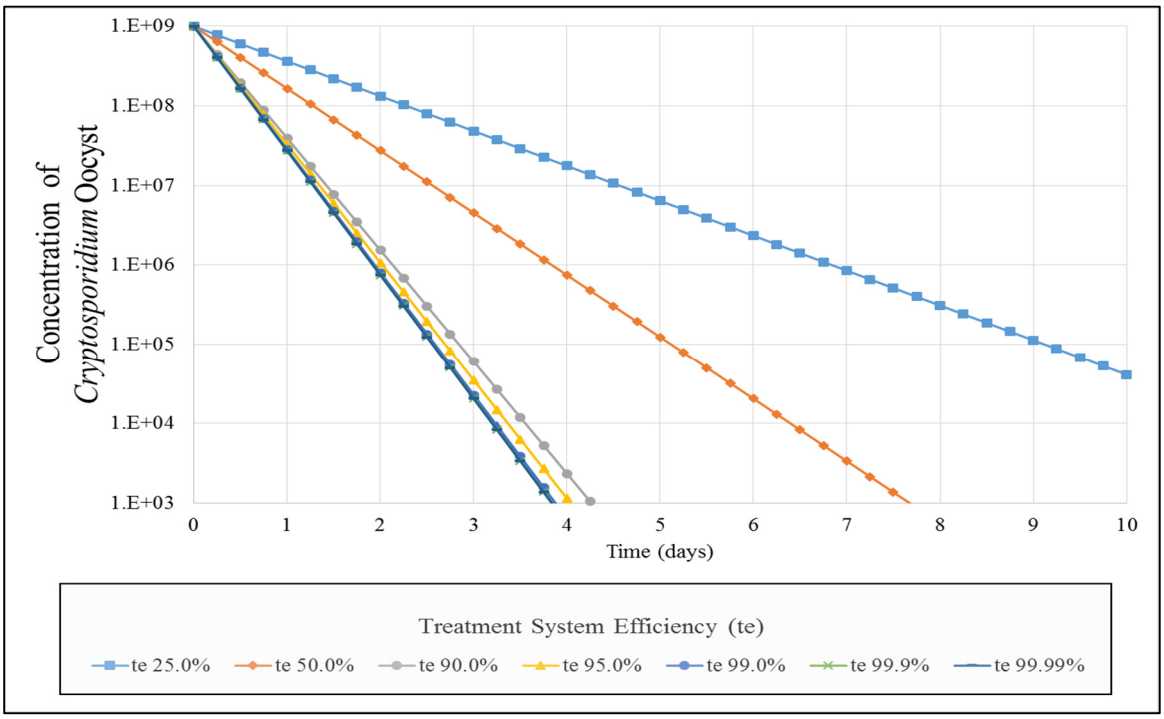


Figure 4.53: Comparison of *Cryptosporidium* concentration removal per days at varied removal efficiencies

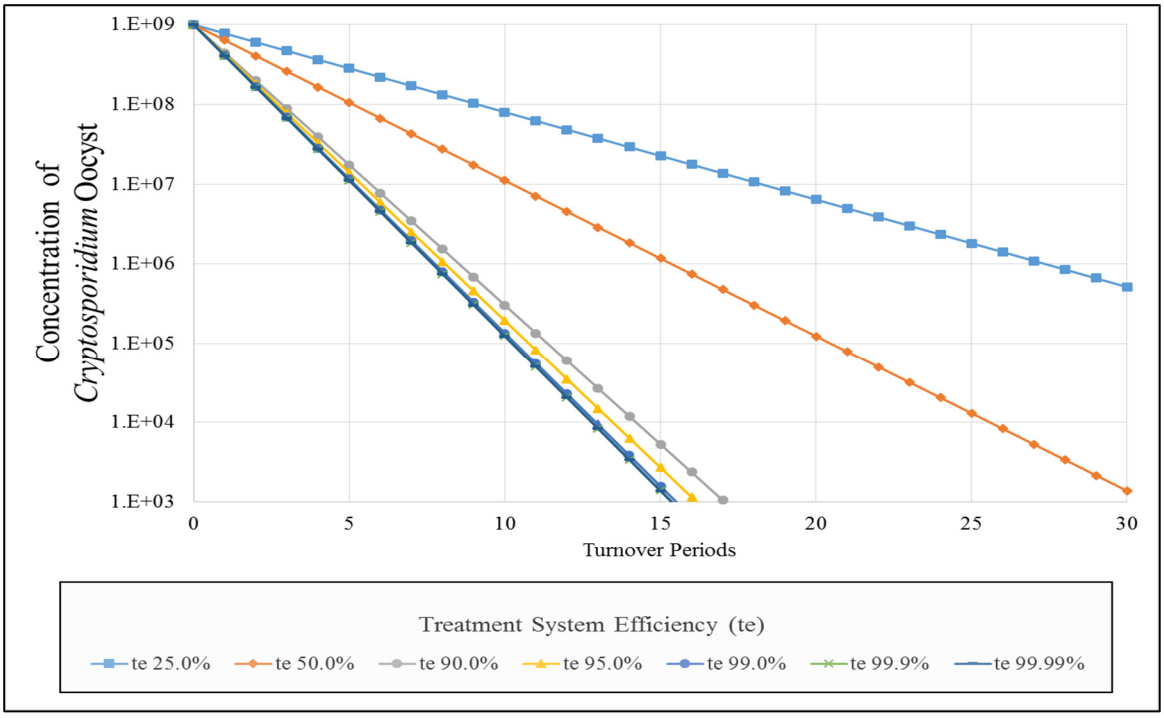


Figure 4.54: Comparison of *Cryptosporidium* concentration removal per turnover period at varied removal efficiencies

# CHAPTER 5: SUMMARY

The ultimate goal of this research was to quantify the efficiency of swimming pools in recirculating water through the treatment system. Two bench-scale pool systems were examined to quantify hydraulic efficiency. Turnover period, flowrate, flow pattern and inlet configuration were modified in an attempt to alter the efficiency of the pools. As shown in Figure 5.1, in all experiments the system efficiency was not significantly changed. Removal efficiency was consistent with the Gage and Bidwell model. Gage and Bidwell predicted removal of 63%, 86% and 95% for the $1^{st}$, $2^{nd}$ and $3^{rd}$ turnovers, which agree closely with experimental values for the 11 experiments shown in Figure 5.2, Figure 5.3, and Figure 5.4. While pool design, turnover time, and hydraulic conditions varied significantly, the range in the experimental data at each number of turnovers was less than approximately 3% and included the predictions represented on flags in each of the figures.

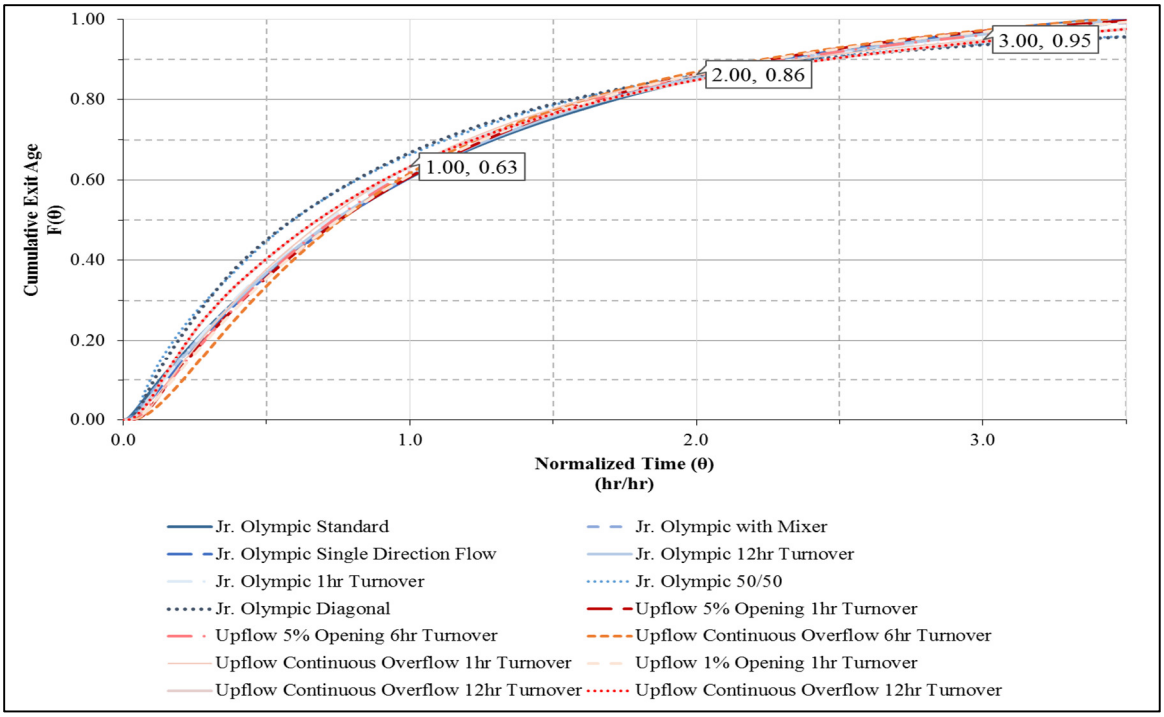


Figure 5.1: Combined cumulative exit age for experimental modes

Practically, the design of inlets and outlets has little impact on the recirculation system or contaminant removal rates. The efficiency of the treatment system is constrained by the pool recirculation efficiency and there is no significant benefit of treatment systems with greater than 90% (1 $\log_{10}$) removal. While treatment system removal efficiencies over 90% are unlikely to show significant performance increase, improving the removal efficiency of sand and cartridge filters up to 90% would provide valuable performance gains. Reducing the turnover period appears to be the most practical method of obtaining increased contaminant removal rates. The pool contaminant removal rate can be modeled using an exponential curve. The shape of the curve can predicted using the model $y = 1 - \exp\left(-\frac{Q}{V}\alpha t\right)$. A fitting parameter (α) value of 1.00 ± 0.11 accurately predicted the contaminant removal.

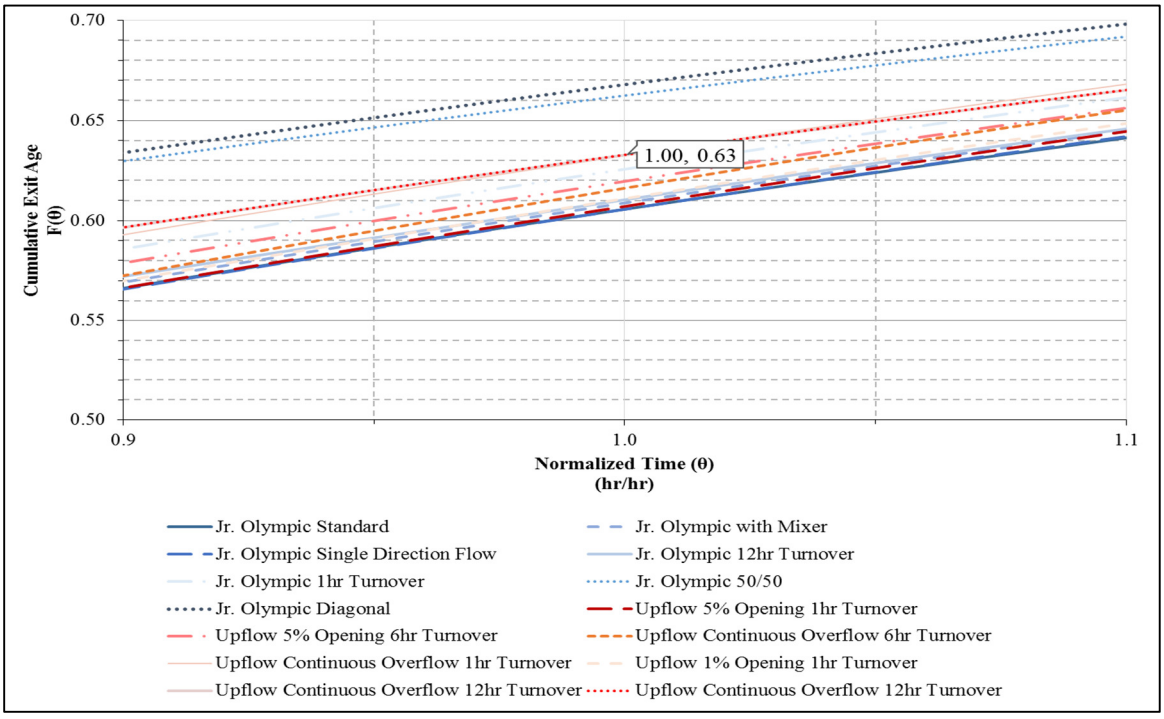


Figure 5.2: Combined cumulative exit age at 1 turnover

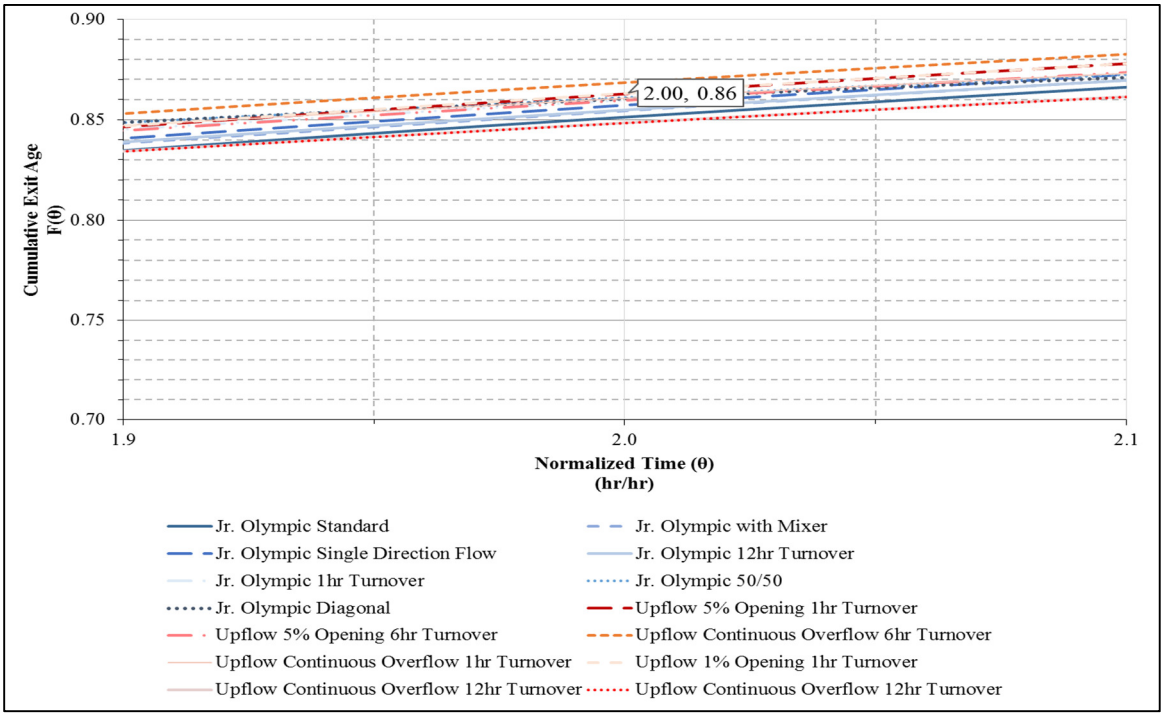


Figure 5.3: Combined cumulative exit age at 2 turnovers

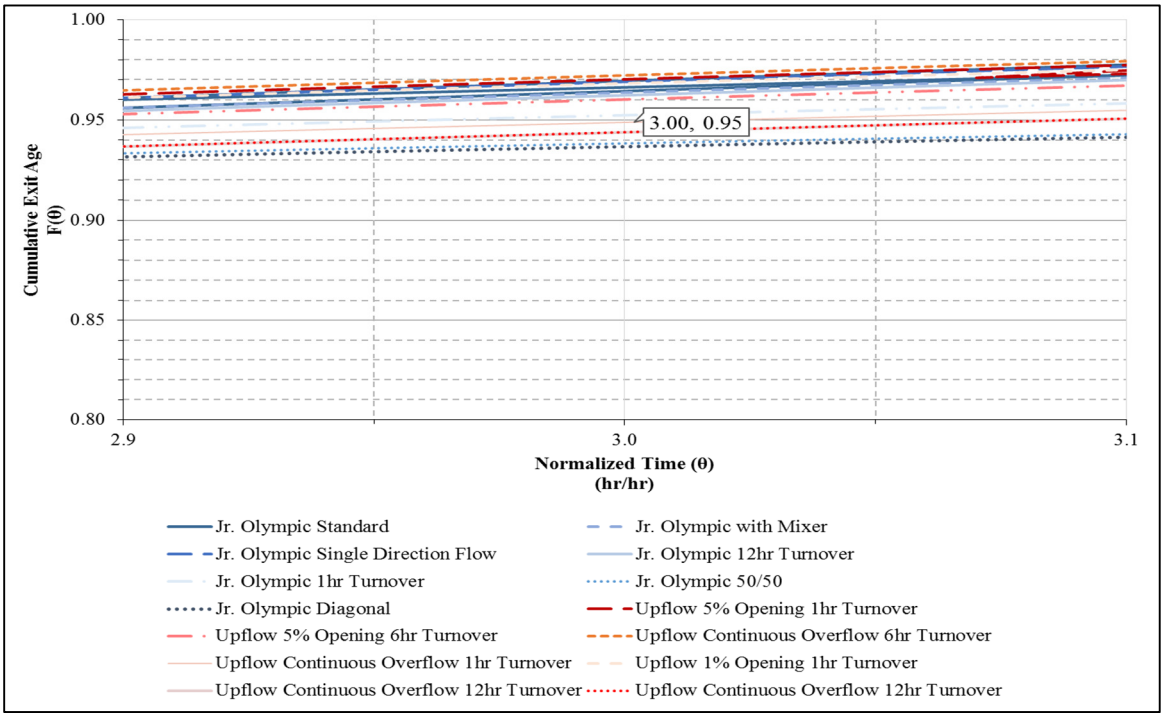


Figure 5.4: Combined cumulative exit age at 3 turnovers

Based on the initial slope of the salt tracer (Figure 5.5), the chlorine distribution time can be defined. In all cases, over 99.0% of salt was distributed throughout the system within 12% of a turnover. Salt tracer distribution times were much longer than dye study distribution times as pools were typically dyed within 4.5 minutes. The difference in times is due to methodology in the test. A pool was considered dyed when there was no easily observed difference in water color. The dye method included operator bias and did not account for areas that appear dyed due to shading. Visual dye observation also did not consider areas of the pool that are un-observable. Salt tracer studies provided a reliable and accurate representation of chemical distribution as steady state can be recorded without operator bias. Practically, chlorine distribution can be thought of as completely distributed within 12% of the pool system turnover time.

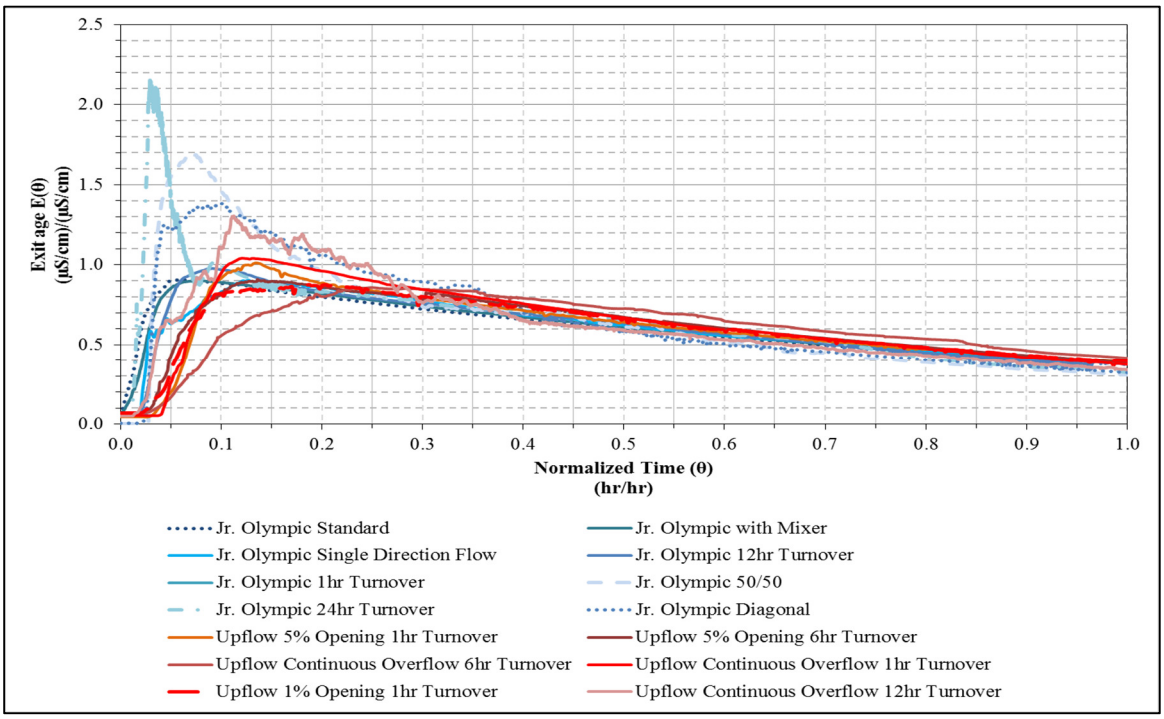


Figure 5.5: Combined initial slope of the exit age distribution

Practically, the hydraulic efficiency of the system creates a bottleneck of the overall treatment system. The inefficiency in getting water into the treatment system negates the benefit of treatment systems with higher efficiencies. However, by combining the relationship between the hydraulic efficiency and treatment system efficiency, it is possible to make accurate predictions of the necessary time needed to reach any given contaminant removal goals.

# CHAPTER 6: CONCLUSIONS AND RECOMMENDATIONS

## 6.1 Conclusions

### 6.1.1 Bench-scale Swimming Pool

A. The hydraulic efficiency of the Junior Olympic bench-scale pool and the Upflow bench-scale pool with bottom inlets in removing salt tracer from the system per turnover period could not be significantly altered by changing flowrates, patterns, or proportions and was consistent with work presented by Gage and Bidwell in 1926.

B. In all cases, 60 to 66% of the salt tracer was removed during the first turnover period. In 11 of 14 cases 60 to 64% was removed during the first turnover, 85 to 87% was removed during the second turnover period, and 94 to 97% during the third turnover period. This was consistent with Gage and Bidwell's prediction of removals values of 63%, 86%, and 95.

C. The removal of salt (or the efficiency of returning contaminants to the treatment system) follows an exponential decay model (removal efficiency = $1\text{-}e^{-Q/V*\alpha t}$) which can be predicted with the system volume, flowrate and a single fitting parameter ($\alpha$) of $1.00 \pm 0.11$.

D. In all cases (n=6), during 6 hour turnover with recirculation, the conductivity of the salt in the water returning to the treatment system reached 90% of the eventual peak conductivity within 35 minutes. Practical chlorine distribution in swimming pools appears to occur during the initial 10% of the turnover period.

E. During qualitative dye studies performed for a 6 hour turnover period, the dye saturated the pool volume under 2% of the turnover period, or 7 minutes. Dye study values were determined based on visual observation of peak concentration and saturation.

F. Design and operational changes had little effect on recirculation efficiency of the pools tested. Combined efficiencies of the filtration and disinfection system of greater than 90% (1 $\log_{10}$) have only small (less than approximately 10%) impacts on contaminant removal rates with 3 $\log_{10}$ removals requiring 45.5 to 51 hours for systems rated at 99.99% down to 90%, respectively.

G. Sizeable performance improvements would be gained by increasing the removal efficiency of sand and cartridge filters (currently averaging 25%-50% removal of *Cryptosporidium* sized particles) up to 90% with 3 $\log_{10}$ removal times decreasing from greater than 7 days to approximately 2 days.

H. For pools with treatment systems averaging at least 90% reduction, reducing turnover time appears to be the most practical means of increasing the rate of contaminant removal because of the inherent limitations in the efficiencies of pools to return water to any side-stream treatment systems.

## 6.2 Lessons Learned

I. In bench-scale swimming pool modeling, the salt solution density plays a critical role in obtaining accurate results.

II. Salt tracer solutions should be within 0.1% of the pool water density.

III. Placement of conductivity sensors must be done in order to minimize air entrapment.

IV. Effluent conductivity sensors should be inverted to prevent air buildup in sensor housing.

V. Extremely low pool flowrates should minimize tube length to prevent loss of suction.

VI. Water tension must be factored into designs for bench-scale continuous overflow pools.

## 6.3 Recommendations for Future Research

Additional research is recommended to compare bench-scale pool results with full scale pools. Research could be done on local full scale pools with the same design. The primary objective of this study should be to validate the bench-scale models, and quantify the full scale pool. This should be done in conjunction with computational fluid dynamics (CFD). A complete comparison of bench-scale and full scale pools coupled with CFD may provide a wide-ranging framework for describing the majority of pool designs. Pool regulators, owners, and operators would benefit from a comprehensive description of recirculating efficiency and its impact on treatment system efficiency.

# REFERENCES


Amburgey, J. E., Fielding, R., & Arrowood, M. (2009). *Filtration removals and swim diaper retention of Cryptosporidium in swimming pools.* Paper presented at the Proc., 2009 Swimming Pool and Spa Int. Conf.

Amburgey, J. E., Goodman, J. M., Aborisade, O., Lu, P., Peeler, C. L., Shull, W. H., Hill, V. R. (2012) Are Swimming Pool Filters Really Removing *Cryptosporidium*?

Boehmer, T., Alden, N., Ghosh, T., & Vogt, R. (2009). Cryptosporidiosis from a community swimming pool: outbreak investigation and follow-up study. *Epidemiology and infection, 137*(11), 1651-1654.

Chappell, C. L., Okhuysen, P. C., Langer-Curry, R., Widmer, G., Akiyoshi, D. E., Tanriverdi, S., & Tzipori, S. (2006). *Cryptosporidium hominis*: experimental challenge of healthy adults. *The American journal of tropical medicine and hygiene, 75*(5), 851-857.

Chen, C., Cheng, G. G., Sun, H. B., Hou, Z. B., Wang, X. C., & Zhang, J. Q. (2012). Effects of Salt Tracer Amount, Concentration and Kind on the Fluid Flow Behavior in a Hydrodynamic Model of Continuous Casting Tundish. *Steel Research International, 83*(12), 1141-1151. doi: 10.1002/srin.201200086

Cloteaux, A., Gerardin, F., & Midoux, N. (2011). Numerical Simulation and Modelling of a Typical Swimming Pool for Disinfection By-Products Assessment.

Cloteaux, A., Gérardin, F., & Midoux, N. (2013). Influence of Swimming Pool Design on Hydraulic Behavior: A Numerical and Experimental Study. *Engineering, 5*(05), 511.

Crittenden, J. C., Trussell, R. R., Hand, D. W., Howe, K. J., & Tchobanoglous, G. (2012). *MWH's Water Treatment: Principles and Design: Principles and Design*: John Wiley & Sons.

Croll, B. T., Hayes, C. R., & Moss, S. (2007). Simulated *Cryptosporidium* removal under swimming pool filtration conditions. *Water and Environment Journal, 21*(2), 149-156. doi: 10.1111/j.1747-6593.2006.00065.x

Danckwerts, P. V. (1953). Continuous flow systems. Distribution of residence times (Reprinted from Chem Engng Sci, vol 2, pg 1-13, 1953). *Chemical Engineering Science, 50*(24), 3857-3866. doi: 10.1016/0009-2509(96)81811-2

Fogler, H. S. (2005). *Elements Of Chemical Reaction Engineering Author: H. Scott Fogler, Publisher: Prentice Hall Pages: 1080 Pub*.

Gage, S. D., Ferguson, H. F., Gillespie, C., Messer, R., Tisdale, E., Hinman Jr, J. J., & Green, H. W. (1926). SWIMMING POOLS AND OTHER PUBLIC BATHING PLACES*. *American Journal of Public Health, 16*(12), 1186-1201.

Goodgame, R. W., Genta, R. M., White, A. C., & Chappell, C. L. (1993). Intensity of infection in AIDS-associated cryptosporidiosis. *Journal of Infectious Diseases, 167*(3), 704-709.

Hayes, C., Croll, B., Wright, C., Rowlands, D., Anex, C., & Henley, H. (2009). *Removal of Cryptosporidium oocysts by filtration in the treatment of swimming pool waters.* Paper presented at the proceeding of the Third International Swimming Pool and Spa Conference, March.

Helenius, I. J., Rytila, P., Metso, T., Haahtela, T., & Venge, P. (1998). Respiratory symptoms, bronchial responsiveness, and cellular characteristics of induced sputum in elite swimmers. *Allergy, 53*(4), 346-352. doi: 10.1111/j.1398-9995.1998.tb03904.x

Kjellstrand, R., Mattsson, A., Niklasson, C., & Taherzadeh, M. J. (2005). Short circuiting in a denitrifying activated sludge tank. *Water Science and Technology, 52*(10-11), 79-87.

Levenspiel, O. (1972). Chemical reaction engineering: Wiley Eastern Limited.

Liu, M. (2011). Prediction of tracer concentration and mixing in CFSTRs with mean age distribution. *Industrial & Engineering Chemistry Research, 50*(9), 5838-5851.

MacMullin, R., & Weber, M. (1935). The theory of short-circuiting in continuous-flow mixing vessels in series and the kinetics of chemical reactions in such systems. *Transactions of American Institute of Chemical Engineers, 31*(2), 409-458.

Okhuysen, P. C., Chappell, C. L., Crabb, J. H., Sterling, C. R., & DuPont, H. L. (1999). Virulence of three distinct Cryptospovidium parvum isolates for healthy adults. *Journal of Infectious Diseases, 180*(4), 1275-1281.

Centers for Disease Control and Prevention. (2014). *The Model Aquatic Health Code*. Atlanta, Georgia.

Stamou, A. I. (2008). Improving the hydraulic efficiency of water process tanks using CFD models. *Chemical Engineering and Processing: Process Intensification, 47*(8), 1179-1189.

Teefy, S. (1996). *Tracer studies in water treatment facilities: a protocol and case studies*: American Water Works Association.

Terashima, M., Iwasaki, M., Yasui, H., Goel, R., Suto, K., & Inoue, C. (2013). Tracer experiment and RTD analysis of DAF separator with bar-type baffles. *Water Science & Technology, 67*(5), 942-947.

Tsai, D. D. W., & Chen, P. H. (2013). Differentiation criteria study for continuous stirred tank reactor and plug flow reactor. *Theoretical Foundations of Chemical Engineering, 47*(6), 750-757. doi: 10.1134/s0040579513060122

Yoder, J. S., Wallace, R. M., Collier, S. A., Beach, M. J., Hlavsa, M. C., Control, C. f. D., & Prevention. (2012). Cryptosporidiosis surveillance—United States, 2009–2010. *MMWR Surveill Summ, 61*(5), 1-12.

# APPENDIX A: RTD CALCULATION

Given Parameters

Volume = 87 L
Flow Rate = 241 mL/min
Tracer Molarity = .02M KCl

Calculation of RTD

Mean Residence Time:

$$\bar{t} = \frac{\int_0^\infty Ct\ dt}{\int_0^\infty C\ dt} \qquad \text{(a.1)}$$

Where: $\bar{t}$ = mean residence time (hr)
C = conductivity exiting reactor at time t (µS/cm)
t = time since addition of tracer (hr)

$$\bar{t} = \frac{1131.652}{185.9112} \qquad \bar{t} = 6.087 \text{ hr}$$

Normalized Concentration:

$$C_N = \frac{\int_0^\infty C\ dt}{\bar{t}} \qquad \text{(a.2)}$$

Where: $C_N$= normalized concentration
C = conductivity exiting reactor at time t, µS/cm
t = time since addition of tracer (hr)
$\bar{t}$ = mean residence time (hr)

$$C_N = \frac{185.9112}{6.087} \qquad C_N = 30.54\ \mu\text{S/cm}$$

Normalized Time:

$$\theta = \frac{t}{\bar{t}} \tag{a.3}$$

Where: θ = normalized time, (dimensionless)
t = time since addition of tracer (hr)
$\bar{t}$ = mean residence time (hr)

$$\theta = \frac{t}{6.087}$$ See Table a.1

Exit Age Distribution:

$$E(\theta) = \frac{C}{C_N} \tag{a.4}$$

Where: E (θ) = exit age distribution
$C_N$= normalized concentration
C = conductivity exiting reactor at time t, µS/cm

Cumulative Exit Age Distribution:

$$F(\theta) = E(\theta)d(\theta) \tag{a.4}$$

Where: F (θ) = cumulative exit age distribution
E (θ) = exit age distribution
θ = normalized time, (dimensionless)

Time Variance and Standard Deviation:

$$\sigma_t^2 = \frac{\int_0^\infty (t-\bar{t})^2 C\, dt}{\int_0^\infty C\, dt} \tag{a.5}$$

$$\sigma_t = \sqrt{\sigma_t^2} \tag{a.6}$$

Where: $\sigma^2_t$= variance with respect to t
$\sigma_{t=}$ standard deviation
t = time since addition of tracer (hr)
$\bar{t}$ = mean residence time (hr)
C = conductivity exiting reactor at time t, µS/cm

$$\sigma_t^2 = \frac{4539.39}{185.9112} \qquad \sigma_t^2 = 24.41698\ hr^2$$

$$\sigma_t = \sqrt{24.41698} \qquad \sigma_t = 4.94\ hr$$

Normalized Variance:

$$\sigma_\theta^2 = \frac{\sigma_t^2}{\bar{t}^2} \tag{a.7}$$

Where: $\sigma_\theta^2$= variance with respect to normalized time
$\sigma_t^2$= variance with respect to t
$\bar{t}$ = mean residence time (hr)

$$\sigma_\theta^2 = \frac{24.41698}{37.05} \qquad \sigma_\theta^2 = .66$$

# APPENDIX B: ALTERNATE EXPERIMENTS

In some experiments, lessons were learned regarding the performance of tracer studies. Salt tracer density became extremely important. Initial experiments were performed with a KCl solutions with a concentration of 1.0M. This created visible currents of heavy salt tracer that did not mix with the pool volume. Instead, these currents of dense solution would flow and collect at the bottom of the pool, being sucked into the drains. This created a short-circuit effect, visible in Figure B.1 In other experiments, pump management and attention to tubing was important in avoiding dosing inaccuracies. While performing an experiment with a standard 6 hour turnover the salt injection line was removed from the solution and then reinserted. This created a 30 second gap in the salt tracer delivery. This "dual dosing", created two spikes in the system, shown in Figure B. 2. Contact with the pool water during the performance of an experiment also created peaks in conductivity. Manipulating any part of the pool system where skin came in contact with the water could introduce extra salt into the system. As shown in Figure B.3, two spikes after the main peak were created by manipulating the balance tank with bare hands, while the system was in operation. Sensor calibration, reset, and malfunction also contributed to exit age distributions that were rejected, as shown in Figure B.4.

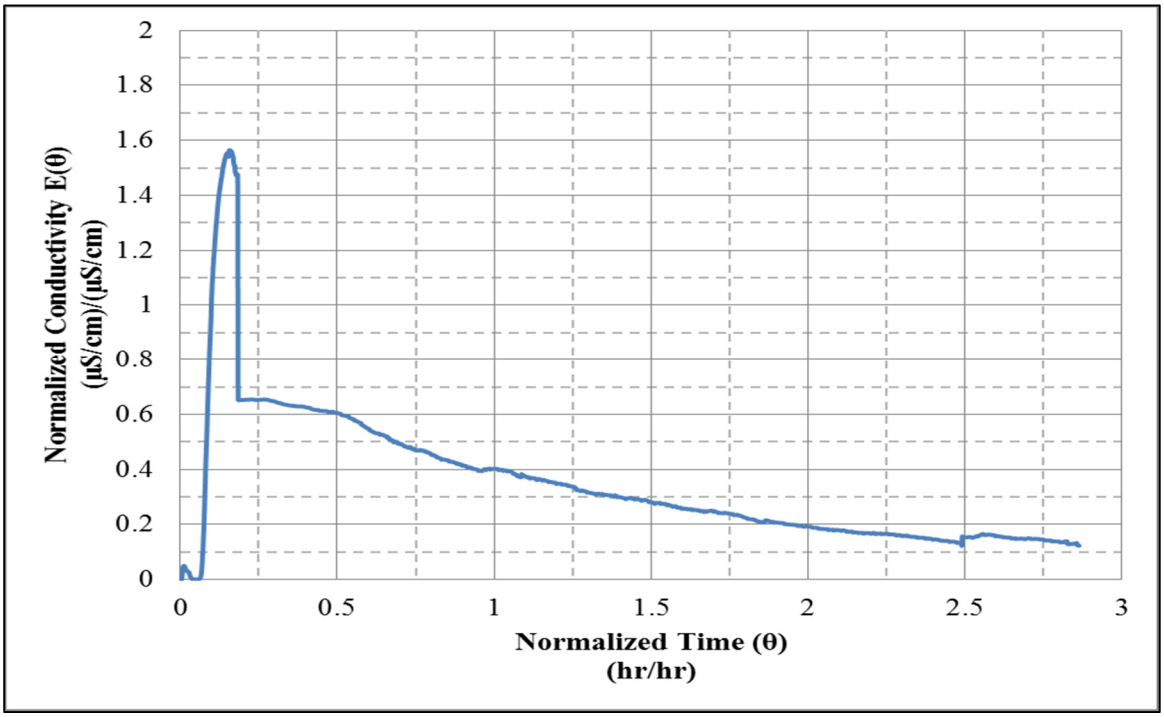


Figure B.1: Exit age distribution with salt density current present

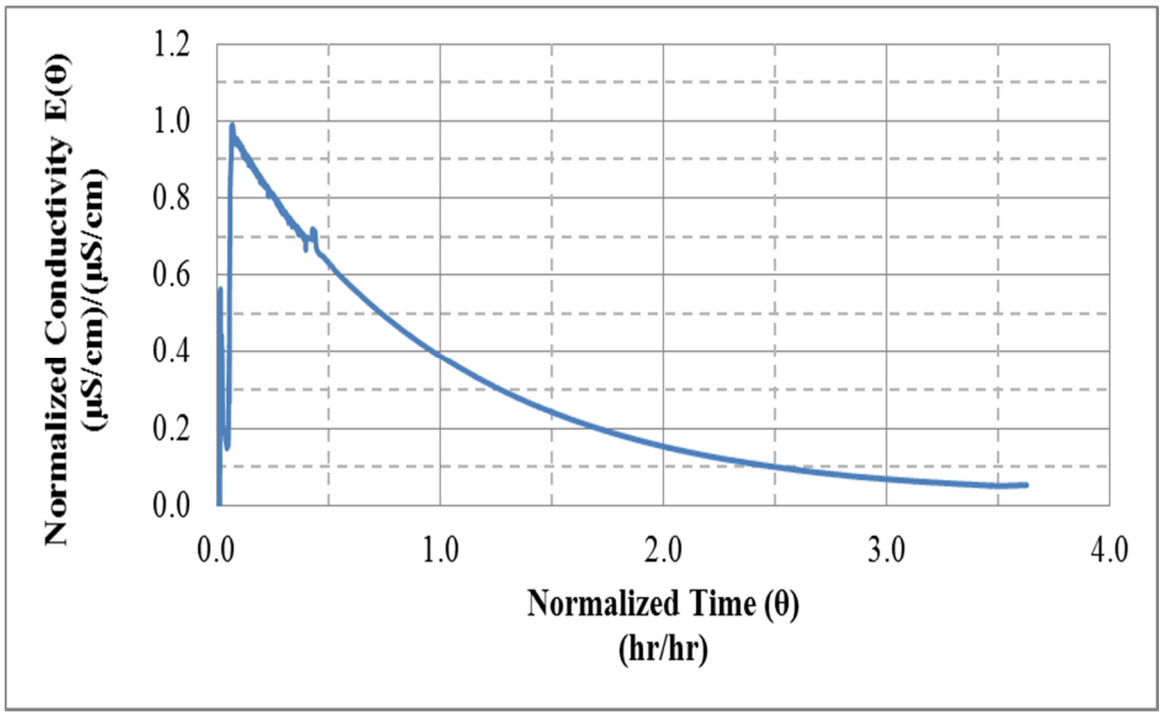


Figure B.2: Exit age distribution with two separate initial peaks

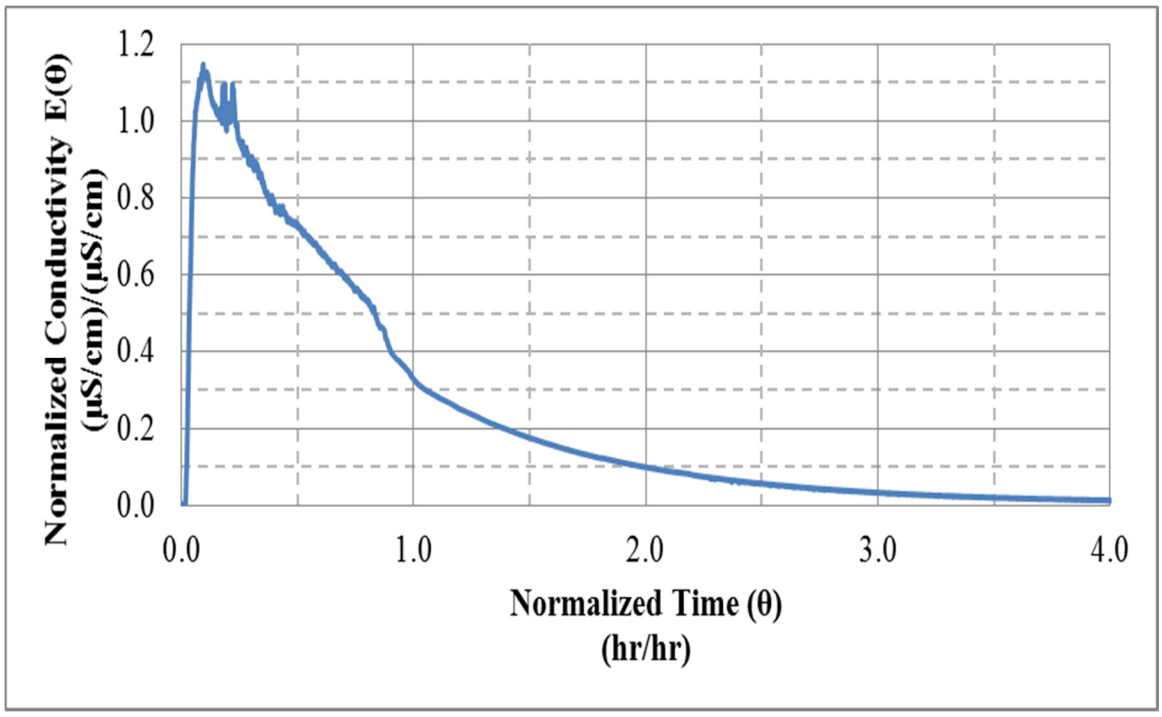


Figure B.3: Exit age distribution with spikes created by skin contact

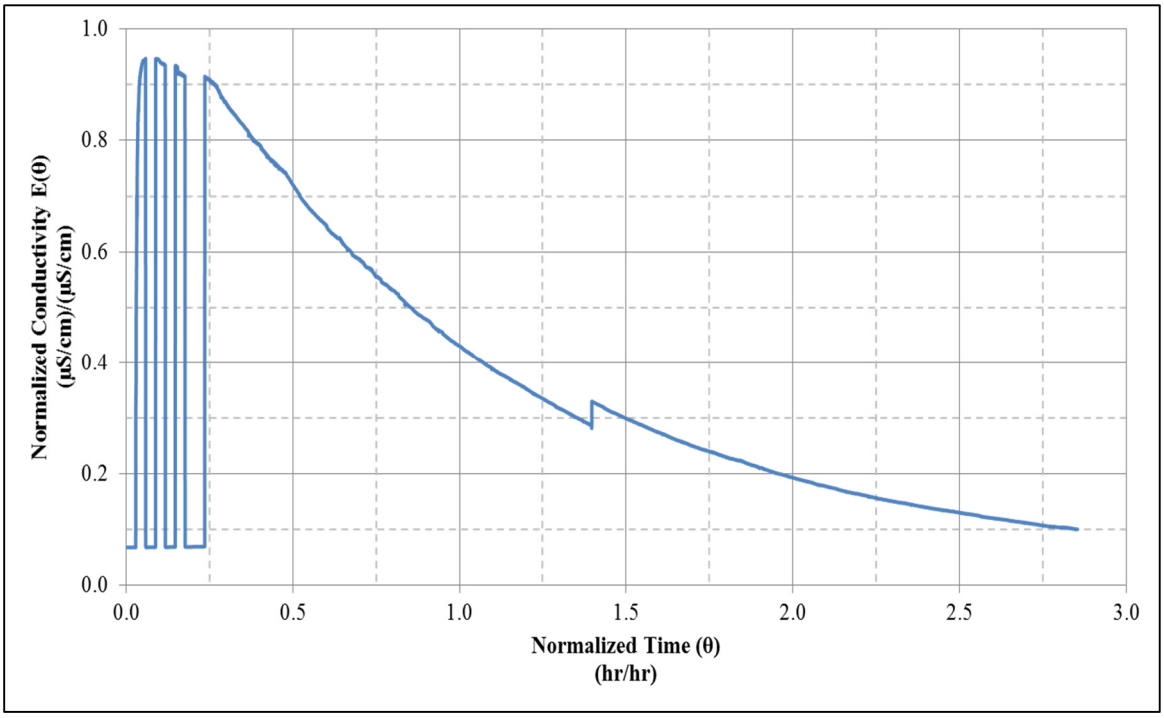


Figure B.4: Exit age distribution with conductivity senor reset

# APPENDIX C: MIXING AND FROUDE CALCULATIONS

Camp and Stein RMS Velocity Gradient:

$$\bar{G}_{Jet} = \sqrt{\frac{P_{Jet}}{\mu V}} \quad \text{(C.1)}$$

Where: $\bar{G}_{Jet}$ = jet Camp and Stein RMS velocity gradient ($s^{-1}$)

$P_{Jet}$ = power of mixing input from jet ($W$)

$\mu$ = dynamic viscosity of water at 25 ºC ($\frac{kg}{ms}$)

V = pool volume ($m^3$)

Total Pool Mixing Value

$$\bar{G}_{Total} = \sqrt{\frac{P_{Total}}{\mu V}} \quad \text{(C.2)}$$

Where: $\bar{G}_{Total}$ = total Camp and Stein RMS velocity gradient ($s^{-1}$)

$P_{Total}$ = total power of mixing ($W$)

$\mu$ = dynamic viscosity of water at 25 ºC ($\frac{kg}{ms}$)

V = pool volume ($m^3$)

Table C.1: Mixing value comparison

| | Bench-scale Junior Olympic Pool | Full-scale Junior Olympic Pool |
|---|---|---|
| $V$ ($m^3$) | 0.087 | 1218.9 |
| $\mu$ ($\frac{kg}{ms}$) | 8.90 x$10^{-4}$ | 8.90 x$10^{-4}$ |
| $P_{Jet}$ (W) | 5.97 x$10^{-7}$ | 0.17 |
| $P_{Total}$ (W) | 1.43E-05 | 4.17 |
| $\bar{G}_{Jet}$ ($S^{-1}$) | 0.09 | 0.40 |
| $\bar{G}_{Total}$ ($S^{-1}$) | 0.43 | 1.96 |

Froude Number:

$$F = \frac{v_{jet}}{\sqrt{g L_{jet}}} \tag{C.3}$$

Where: $F$= Froude Value
$v_{jet}$= velocity of inlet (m/s)
$g$= gravity (m/s$^2$)
$L_{jet}$ =width of jet opening (m)

$$v_{jet} = \frac{Q_{jet}}{A_{jet}} \tag{C.4}$$

Where: $v_{jet}$= velocity of inlet (m/s)
$Q_{jet}$= flowrate of inlet (m$^3$/s)
$A_{jet}$= area of inlet (m$^2$)

Table C.2: Froude number comparison

| | Bench-scale Junior Olympic Pool | Full-scale Junior Olympic Pool |
|---|---|---|
| $V_{Jet}$ (m/s) | 0.0331 | 0.2139 |
| $L_{Jet}$ (m) | 0.0025 | 0.1016 |
| $g$ (m/s2) | 9.81 | 9.81 |
| $F$ (unitless) | 0.2099 | 0.2100 |

# APPENDIX D: REACTOR MODEL COMPARISON

## D.1: Model Comparison

Various models were fitted to the experimental data to produce the most accurate quantification of the model pools. The parameters of these models are shown in Table D.1. Parameters for dead volume, bypass velocity and plug flow volume are compared in Figure D.1 and Figure D.2. Plug flow reactors with dispersion (PFD) were also modelled as shown in Figure D.3 and Figure D.4. The vessel dispersion number, (**D**/*u*L), is used to fit the PFD model and is calculated by dividing the dispersion coefficient (**D**), by the average velocity (*u*) and flow length (L). Vessel dispersion numbers range from 0 for plug flow up to infinity for mixed flow. A value of 0.05 was used for intermediate dispersion while a **D**/*u*L of 0.2 indicates a large amount of dispersion (Fogler, 2005). Figure D.5 and Figure D.6 compare experimental data with a CSTR in series model. In this model, there is no backflow between reactors. Finally, a CSTR with interchange model was fitted as shown in Figure D.7 and Figure D.8. Using this model, CSTRs continuously interchanged contents. Ultimately, the extra complexity of these models was unnecessary, as an ideal CSTR model was able to accurately predict efficiency.

Table D.1: Model parameters (Fogler, 2005)

| Model | Parameter | Value | Parameters | Value |
|---|---|---|---|---|
| Bypass | Bypass velocity ($\upsilon_b$) percent | 10% | | |
| Dead Volume | Dead volume ($V_d$) percent | 10% | | |
| Plug Flow | Plug volume ($V_p$) percent | 10% | | |
| Plug flow with Dispersion | Vessel dispersion number (**D**/*u*L) | 0.05 | | |
| CSTR in Series | Reactor number (n) | 1,2,3 | | |
| CSTR with interchange | Flow interchange percent (β) | 20% | Volume interchange percent (α) | 70% |

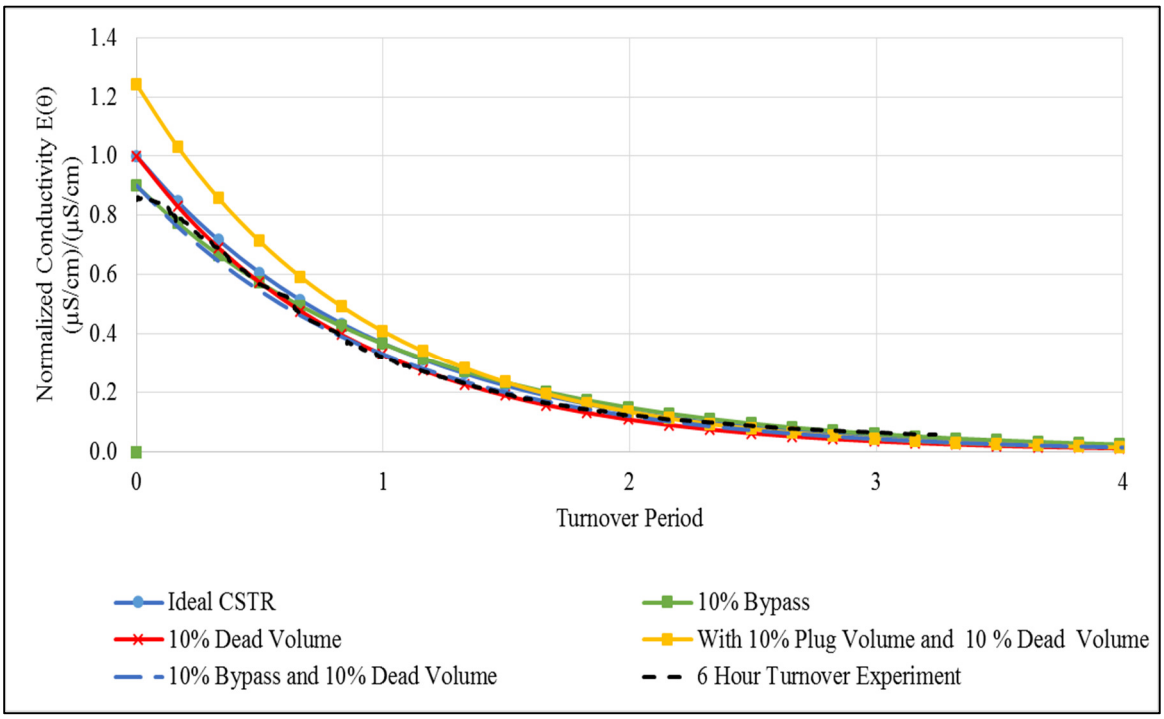


Figure D.1: Junior Olympic model compared to CSTR models with bypass, dead volume, and plug flow volumes

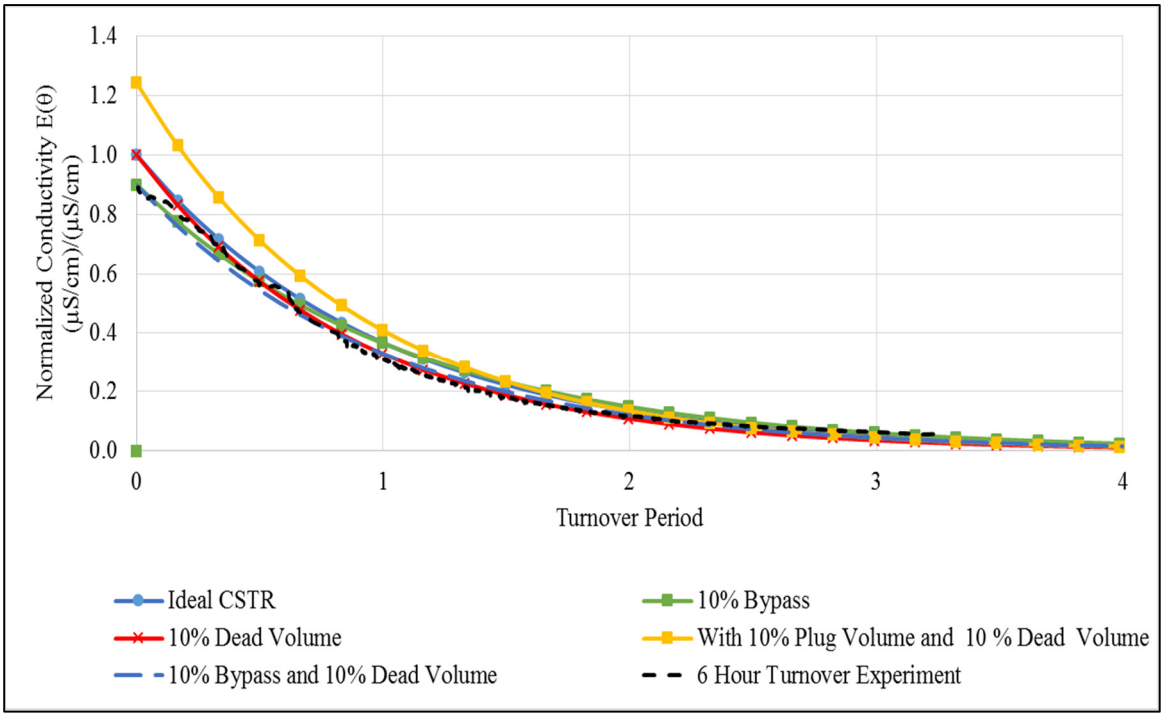


Figure D.2: Upflow model compared to CSTR models with bypass, dead volume, and plug flow volumes

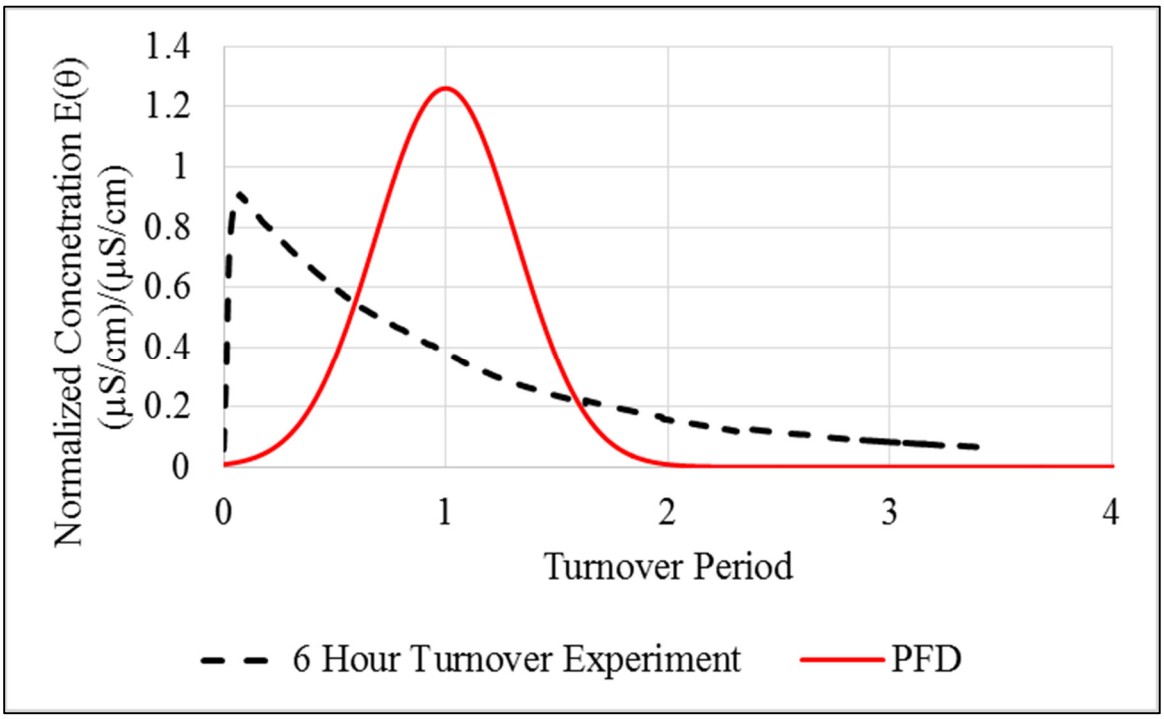


Figure D.3: Junior Olympic pool compared to model of plug flow reactor with dispersion

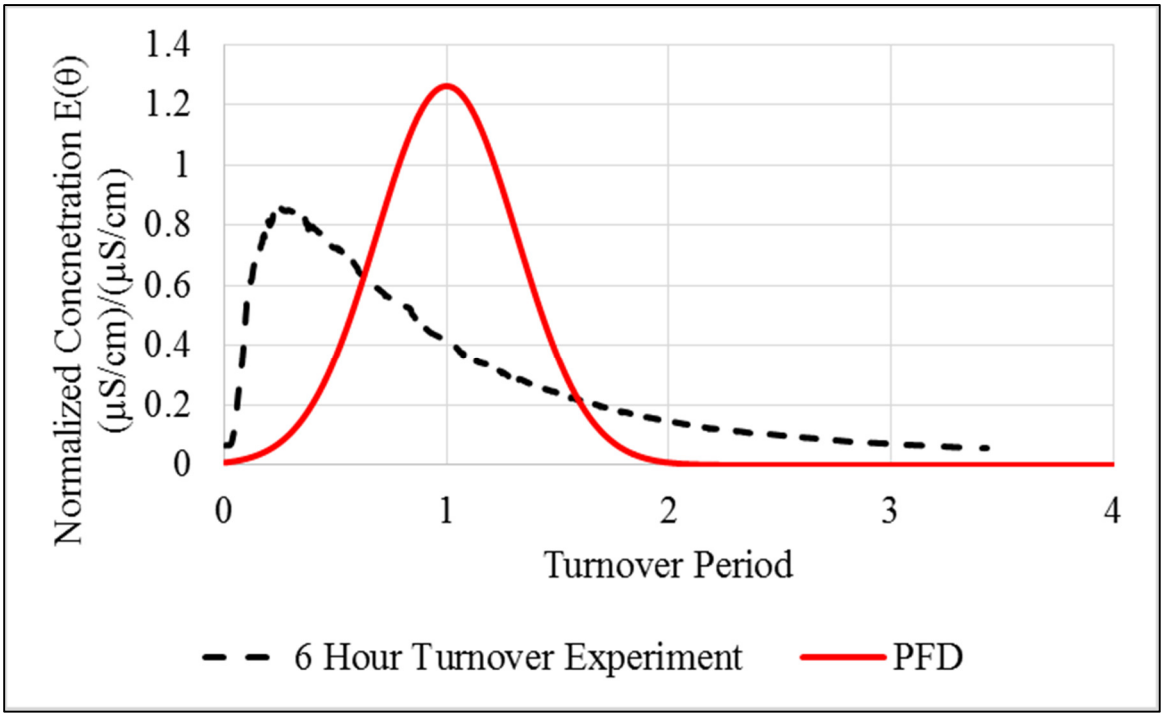


Figure D.4: Upflow pool compared to model of plug flow reactor with dispersion

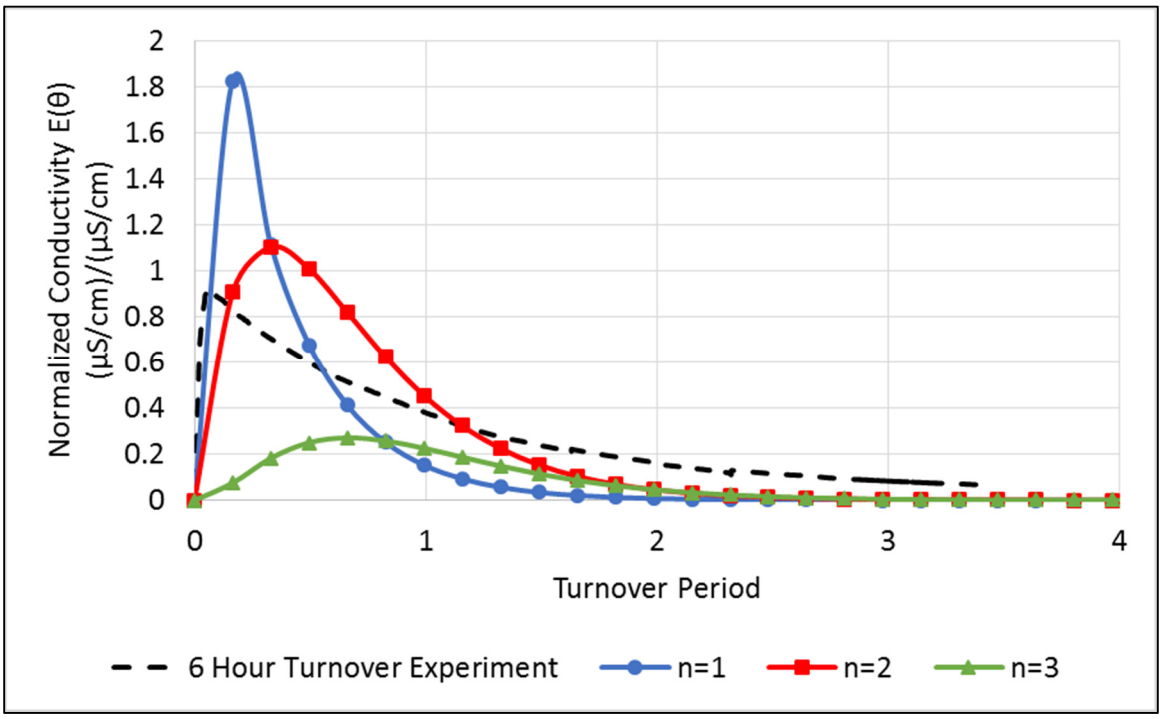


Figure D.5: Junior Olympic pool compared to CSTRs in series with (n) reactors

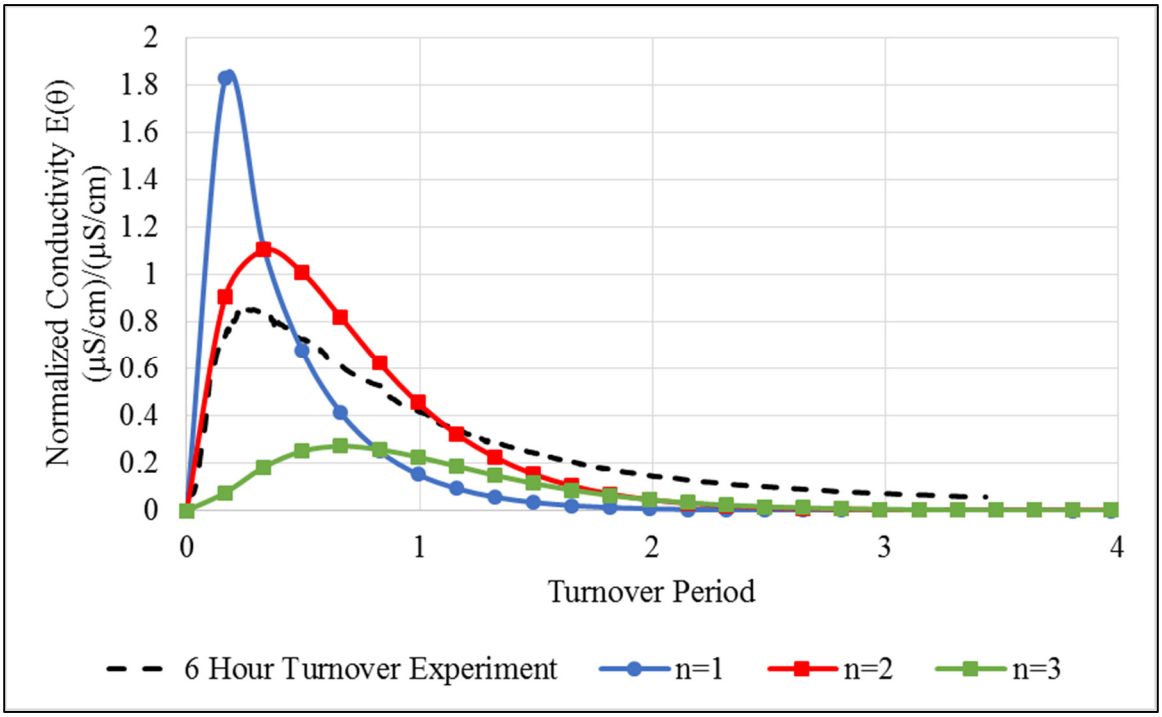


Figure D.6: Upflow pool compared to CSTRs in series with (n) reactors

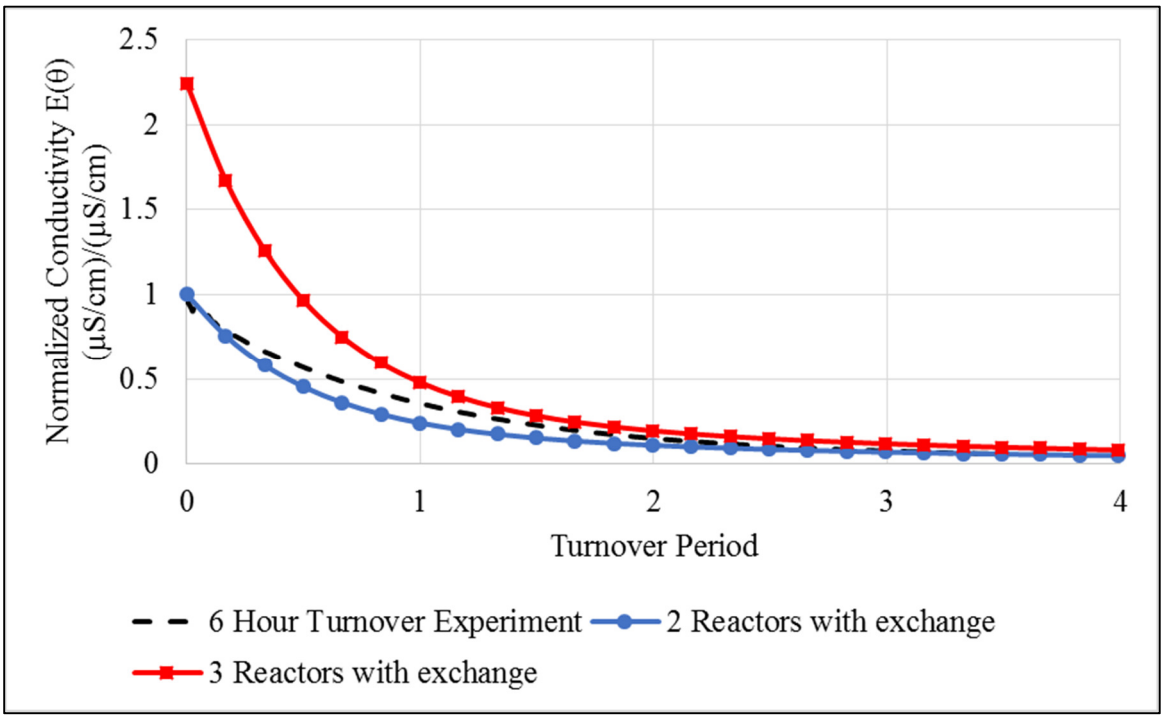


FIGURE D.7: Junior Olympic pool compared to CSTRs with interchange

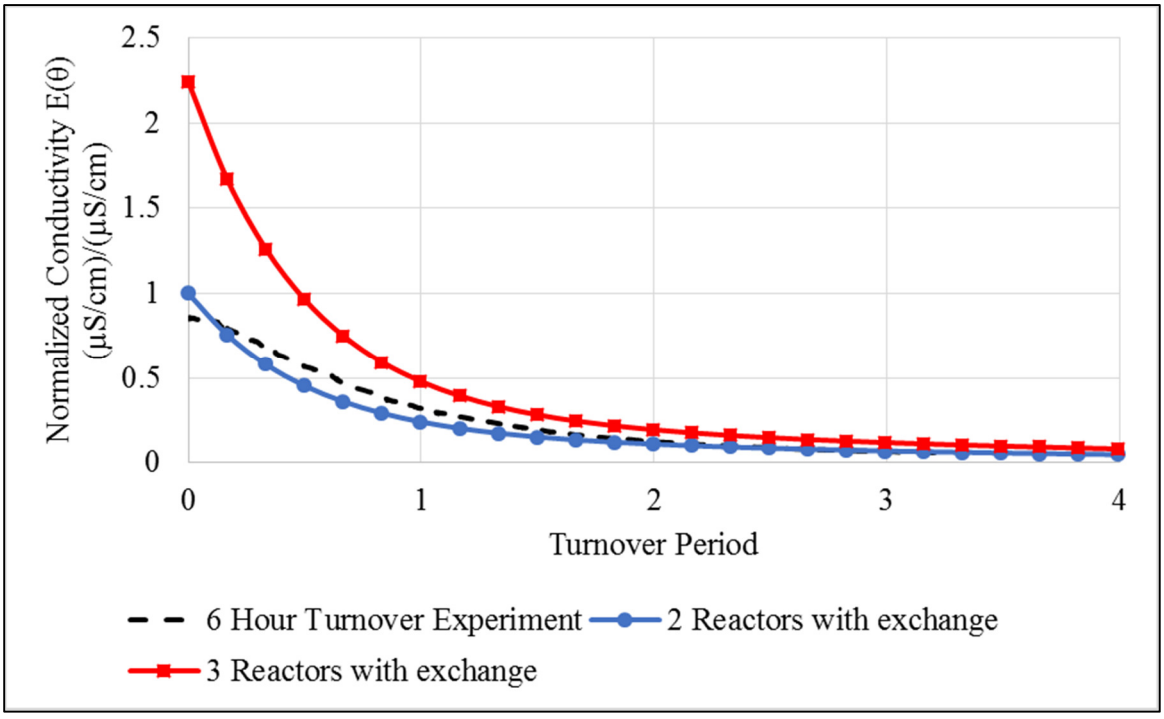


FIGURE D.8: Upflow pool compared to CSTRs with interchange